An-Najah National University

Faculty of Graduate Studies

CuO FILMS PREPARED BY COMBINED ELECTROCHEMICAL AND CHEMICAL BATH DEPOSITIONS

By

Sondos Waleed "Mohammad Ali" Omareyyeh

Supervisors

Dr. Ahed Zyoud
Prof. Hikmat Hilal

This Thesis is Submitted in Partial Fulfillment of the Requirements for the Degree of Master of Chemistry, Faculty of Graduate Studies, An-Najah National University, Nablus - Palestine.

2022

CuO FILMS PREPARED BY COMBINED ELECTROCHEMICAL AND CHEMICAL BATH DEPOSITIONS

By

Sondos Waleed "Mohammad Ali" Omareyyeh

This Thesis was Defended Successfully on 16/6/2022 and approved by

Dr. Ahed Zyoud Supervisor	Signature
Prof. Hikmat Hilal Co-Supervisor	Signature
Dr. Zafer Hawwash External Examiner	Signature
Dr. Samer Shaksheer Internal Examiner	Signature

Dedication

To those who gave me years of care and tenderness to;

My parents

My beloved sisters & brothers

My first booster; My Husband

My Husband Family

All those who pave the way to science

All my professors

All friends

Acknowledgments

First of all, thanks are Allah for enabling me to complete this work. Also, I want to express gratitude to both supervisors Prof. Hikmat S. Hilal and Dr. Ahed Zyoud for help and guidance at any time I needed them until I finished my work, may allah reward them well.

Thanks also for the technical staff in chemistry lab at An-Najah National University, especially Mr. Nafiz Dweikat for devotion and care.

Very special thanks for my friends; Heba Ghannam and Majd Sbeah for their support and help during our work.

Finally, I thank my family, my husband and his family for support and encouragement.

Sondos W. "M.A" Omareyyeh

Declaration

I, the undersigned, declare that I submitted the thesis entitled:

CuO FILMS PREPARED BY COMBINED ELECTROCHEMICAL AND CHEMICAL BATH DEPOSITIONS

I declare that the work provided in this thesis, unless otherwise referenced, is the researcher's own work, and has not been submitted elsewhere for any other degree or qualification.

Student's Name: Sondos Waleed Omaraygah

Signature: 

Date: 16/6/2022

List of Contents

List of Tables

List of Figures

List of Schemes

CuO FILMS PREPARED BY COMBINED ELECTROCHEMICAL AND CHEMICAL BATH DEPOSITIONS

By
Sondos Waleed "Mohammad Ali" Omareyyeh
Supervisor
Dr. Ahed Zyoud
Prof. Hikmat S. Hilal

Abstract

Background: Thin film electrodes are emerging in solar energy technology to produce electricity from light. CuO is one example of common semiconductors that did not yield high photoelectrochemical (PEC) performance. This is a problem to solve.

Objectives: The present study aims at producing CuO thin film electrodes with high PEC performance. CuO thin films will be deposited onto FTO/glass substrate by electro-chemical deposition (ECD), chemical bath deposition (CBD) and combined EC/CB deposition techniques. The resulting electrodes will be assessed in photoelectrochemical process, after being modified by annealing and by cooling rate control (fast and slow cooling).

Methodology: Three techniques have been used to deposit CuO thin film on fluorine doped tin oxide (FTO) Glass substrate. These techniques are; chemical-bath deposition (CBD), electrochemical deposition (ECD) and combined electrochemical and chemical bath (ECD/CBD) deposition technique. The prepared films were characterized by various methods including; X-ray diffraction (XRD), scanning-electron microscope (SEM), electronic absorption spectra and photoelectrochemical measurements. Effect of annealing temperature, cooling rate and deposition time have also been studied. The CuO films exhibit p-type conductivity as shown by photoelectrochemical characteristics (PEC) study.

Results: The prepared films exhibit low photoelectrochemical behaviors. Higher PEC characteristics were gotten from CBD method, but they need annealing at temperatures higher than 150℃ in order to remove the resulting $Cu(OH)_2$. Annealing at high temperatures affect CuO films negatively, since CuO has a very small band gap (1.3-

2.1 eV). Combined ECD/CBD technique does not improve CuO thin film characteristics which against our predictions. The prepared films show good stability measurements.

Conclusions: The prepared films exhibit low photoelectrochemical behaviors**.** CBD method is the best method to prepare CuO films with higher PEC characteristics, but needs annealing to remove resulting $Cu(OH)_2$. Because the CuO has very small band gap, it is sensitive to annealing at high temperature. Higher temperatures affect the films negatively. On the other hand, ECD method gives CuO films with more uniform structures with no $Cu(OH)_2$ product, but do not have improved PEC characteristics. Films deposited by combined ECD/CBD did not show improved PEC characteristics. Annealing ECD/CBD films negatively affects their SEM micrographs, due to sensitivity of the ECD layer to annealing.

Suggestions: CuO thin films can be prepared with more modifications, e.g: coating with multiwalled carbon nano tubes (MWCNT) is recommended. More annealing temperatures should be studied to optimize film characteristics. Electrochemical deposition may be repeated several times to enhance film performance. Doping the prepared CuO films with other dopants is recommended. Depositing combined EC/CB CuO thin film on other type of substrates. For example, Indium tin oxide (ITO) substrate.

Keywords: Thin films, chemical bath deposition (CBD), electrochemical deposition (ECD), combined EC/CB deposition, annealing.

Chapter One
Introduction

1.1 Solar energy

Energy is important to our life. It ensures our life quality and supports the economy[1]. Fossil fuels including oil, coal, natural gas and gasoline; have been used as the main source of energy for a long time [2]. But they also have several disadvantages. In addition to being nonrenewable, they produce CO_2 when burned and cause global climate change and air pollution, which is estimated to link to millions of deaths every year. Fossil fuels are also the main cause of ozone layer depletion as they release chemical compounds containing gaseous chlorine or bromine [3, 4].

As a result of shortage in fossil fuel sources and their serious hazard to the environment, the world tends toward a new life style that protects the environment and covers human needs at the same time. Renewable energy sources were the best alternative choice. Renewable energy comes from natural processes that are replenished constantly such as sun light, wind, geothermal heat and the movement of water. All these sources are cleaner and healthier than fossil fuels [5, 6].

Solar energy is the most plentiful, sustainable source of energy. One thousand times more energy reaches the earth's surface from sun than energy that is released today by fossil fuels[1]. Sun provides 150000 terawatt of power to the earth, 50% is reflected to the outer space by the atmosphere, and the other 50% reaches the earth surface. Very little portion of the solar radiations, that reaches the earth surface, is enough to cover our energy demand [7].

Solar energy is expected to become the main source in light to electricity conversion due to several advantages including; it is freely available and the most clean source of energy, it is an unlimited source, it does not need expensive distribution networks and finally it is a quiet source of energy and does not cause any danger to plants and animals [8]. On the other hand, solar energy technology has some disadvantages such as, the manufacturing cost, it needs large areas of land for solar energy installations. Scientists are working to avoid these problems and solar energy is still promising as a long lasting and renewable source of energy [5, 6].

Sunlight can be converted to electric power using the solar cells. Light that strikes the solar cell produces photovoltage and photocurrent as generated electric power. Solar energy technology converts solar light to electricity using semiconductor materials [8].

1.2 Semiconductors and Energy Band Gap ($E_{b.g}$).

Semiconductors (SCs) are materials that have conductivity between conductors and insulators. Semiconductors have an important role in our life today. For example, it plays an essential role in equipment control in air conditioners, improving cars safety and laser treatment in medical care. Semiconductors have been used in many fields, including light emitters, mobile phones, optical sensors, power devices and solar cells [9, 10].

Energy band gap, the difference in energy between valence band (VB) and conduction band (CB). Band Gap values are used to distinguish between conductors, semiconductors and insulators. Conductors do not have energy band gap, while insulators have very wide band gaps. Semiconductors have medium band gap values that allow electron thermal excitation from the valence band to the conduction band even at room temperature [10, 11], Scheme (1.1) (a).

1.3 Types of semiconductors.

There are two main types of semiconductors (SCs), intrinsic SCs and extrinsic SCs[12].

1.3.1 Intrinsic Semiconductors.

It is a pure semiconductor without any impurities (dopants). Intrinsic semiconductors behave like insulators at zero Kelvin. With higher temperatures, some electrons leave the conduction band going to the valence band leaving holes behind. In this type number of holes & electrons are equal [13], Scheme (1.1) (b)

Scheme 1.1

(a) Band gaps. [11]. (b) Intrinsic semiconductor Energy band gap diagram[14].

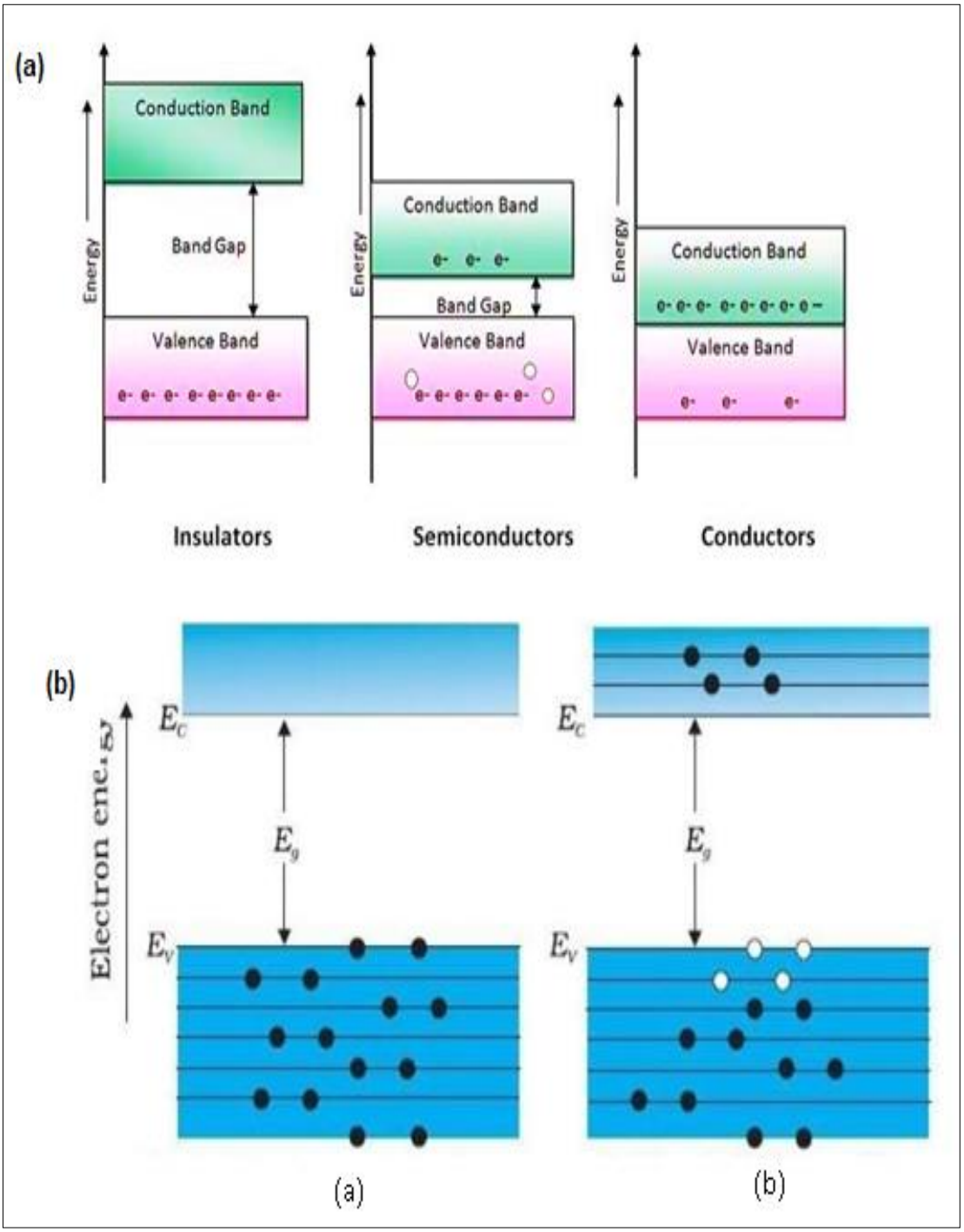

Scheme 1.1(a) shows *Band gaps of insulators, semiconductors and conductors.* (b) *Intrinsic semiconductor Energy band gap diagram a) at zero Kelvin, b) at higher temperatures.*

1.3.2 Extrinsic semiconductors

These contain small amounts of impurities (dopants). There are two types of extrinsic semiconductors [12]:

1.3.2.1 n-type

Contains a dopant from group V elements, they act as electron donor. For example, atoms of phosphorus are used as electron-donors for Si crystals, their energy level is close to the CB edge of silicon, so its valence electrons jump to the conduction band. In this case, the conduction is by electrons and called negative type (n-type)[15], Scheme (1.2a).

1.3.2.2 p-type

Contains a dopant from group III of the periodic table, they act as electron acceptor. For example, boron atoms are used as electron acceptors for silicon crystals, their energy levels are close to Si valence band. Therefore, Si valence band electrons go to dopant atoms, and the holes remain in the VB. Conduction here is positive type and called (p-type) [15], Scheme (1.2b).

Scheme 1.2

Extrinsic semiconductors, a) n-type SCs, b) p-type SCs [16].

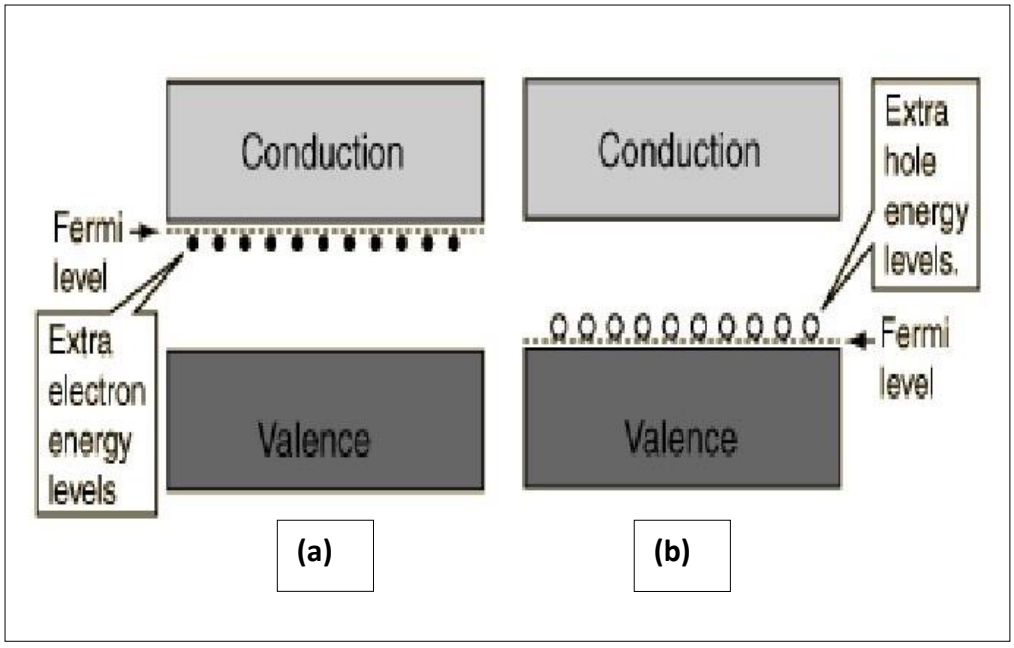

1.4 Types of solar systems

Two main methods can be used for light-to-electricity conversion, photovoltaic (PV) and photo-electrochemical (PEC) solar cells [17].

1.4.1 Photovoltaic (PV) solar cells.

Solar energy can be converted to electric power through PV effect. The solar cell involves two semiconductor types, p-type and n-type, bound together in a (p-n) junction. When photons excite the solar cell, electrons move from VB to CB and the holes are created in the CB. Electrons go down to positive potentials, and holes move up to negative potentials to make charge separations. Barrier potential in the cell produces photovoltage, which drives a current through the circuit [17, 18]

Scheme 1.3

Electron and hole pair formation by absorbing photons with energy equal or larger than the energy band gap (E_{bg}) [19].

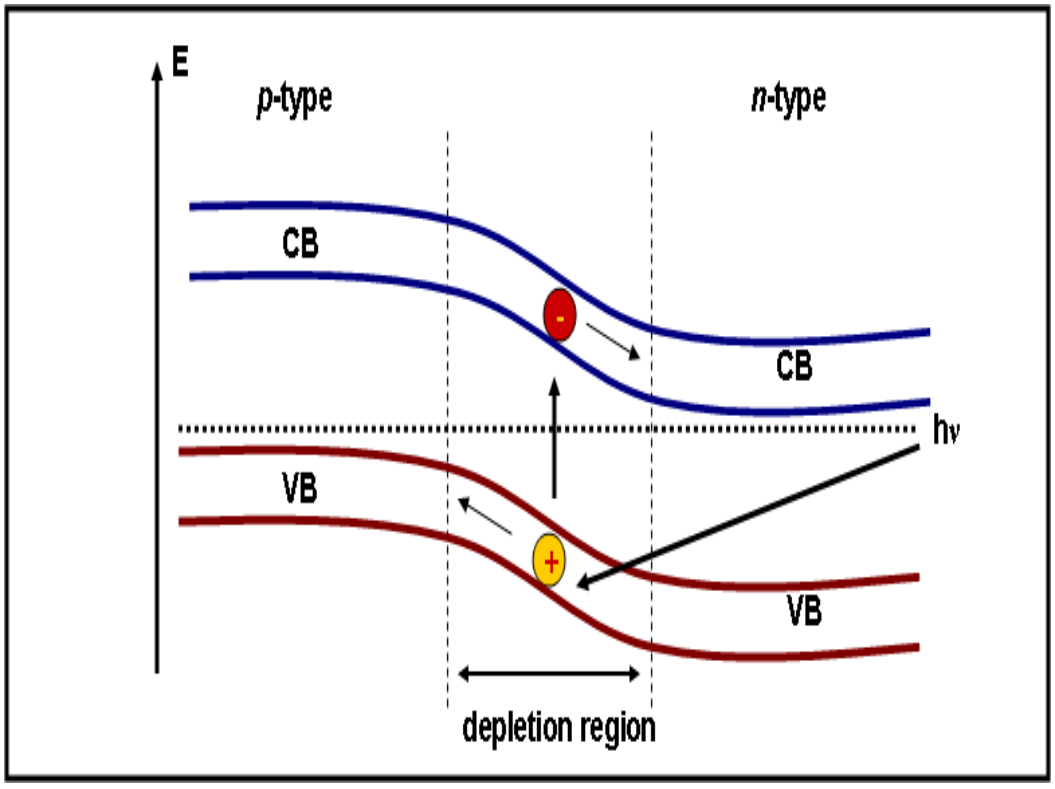

PV systems can be manufactured from one crystal of same semiconducting material, such as Si crystals. In these systems, the same crystal is doped from one side as p-type and on the other side as n-type. Such class of p-n junction is called homojunction.

Alternatively, two types of materials can be used, on as n-type and the other as p-type, and the junction is then called heterojunction. Both heterojunctions and homojunctions are being used in modern technologies, particularly in solar cells. Currently, PV systems have reached very high light-to-electricity conversion values of up to 20% in practice. Up to 40% values can be theoretically achieved[20].

One main shortcoming for PV systems is the high production cost. Manufacturing PV systems is commonly made using ultrahigh vacuum conditions. Costly equipment are commonly used. Moreover, relatively large amounts of starting materials are used in the preparation, which makes the process non-friendly to the environment [21]. Therefore, scientists are looking for alternative technologies to PV systems.

1.4.2 Photoelectrochemical (PEC) Solar Cells

Photoelectrochemical (PEC) cells follow the same basic principles of PV systems. The PEC cells transform light to electricity by SC-Electrolyte interface. Instead of using all-solid p-n junctions, as in PVs, the PEC cell involves a mono-crystal of one semiconductor type in direct contact with a liquid solution that involves a redox couple [22]. At the solid/liquid interface, one side behaves as n-type and the other behaves as p-type. Various types of monocrystalline semiconducting materials have been studied including Si, porous Si, GaAs, GaP and others. If the semiconductor is n-type, the liquid solution behaves as p-type, whereas in the solid is p-type the liquid behaves as n-type.

In the p-type semiconductors, Fermi level is below the electrolyte Fermi level, so electrons go from the electrolyte to the SC until equilibrium is reached. In n-type semiconductors, Fermi level is above the electrolyte Fermi level so electrons move from SC to electrolyte to reach equilibrium [23, 24].

Compared to PV systems, mono-crystalline based PEC systems have the advantage of being easy to prepare. However, the mono-crystalline PEC systems still demand very highly pure crystals which needs high production costs. The electrodes are relatively thick which needs large starting chemicals for preparation. This adds to the preparation costs and to the environmental impact [25].

Scheme 1.4

Schematic energies for p- and n-type semiconductor electrodes in electrolytic solutions

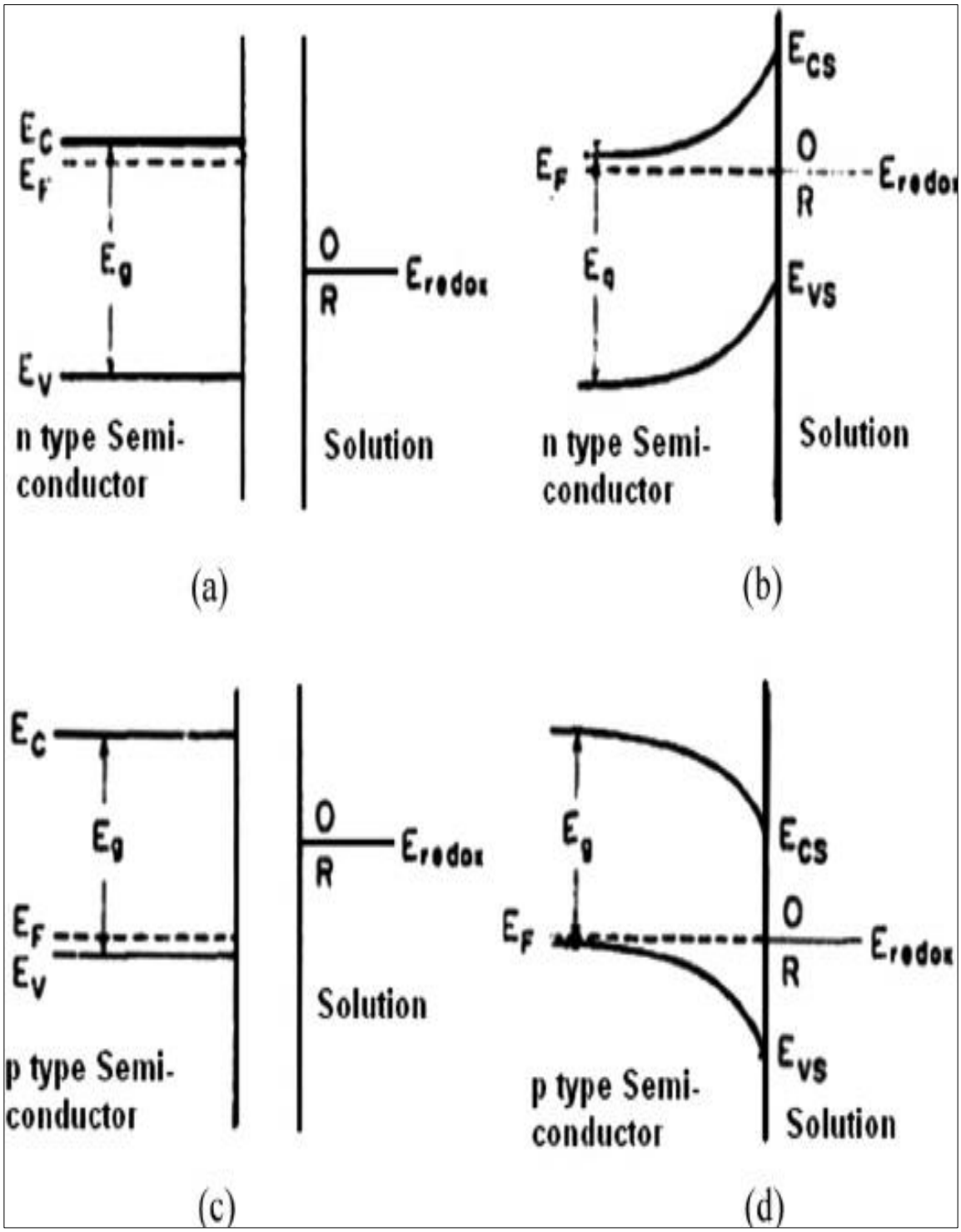

1.5 Dark-current production in PEC cell

Dark current occur when electrons move from the redox couple to the p-type semiconductor valence band, or from the conduction band to the electrolyte in n-type semiconductors. At equilibrium a potential difference is formed by VB and CB bending. Electrons must have enough energy to overcome the barrier. Applying negative potentail helps electrons to overcome this barrier and move from n-type SC electrode CB to electrolyte. [26-28].

1.6 Photocurrent generation in PEC cell

Photocurrent is generated when light passes through the electrochemical cell, then absorbtion of photons with energy larger than $E_{b.g}$ occures creating electrons and holes. Photocurrent occures when the electrode has a depletion (Space Charge) layer and the minority carriers (electrons in the p-type and holes in the n-type) moves toward the inter face between electrode and electrolyte [29-31].

Scheme 1.5

(a) Dark current in n-type semiconductor [23]. (b) Photocurrent generation in n- and p-type semiconducting electrodes [26].

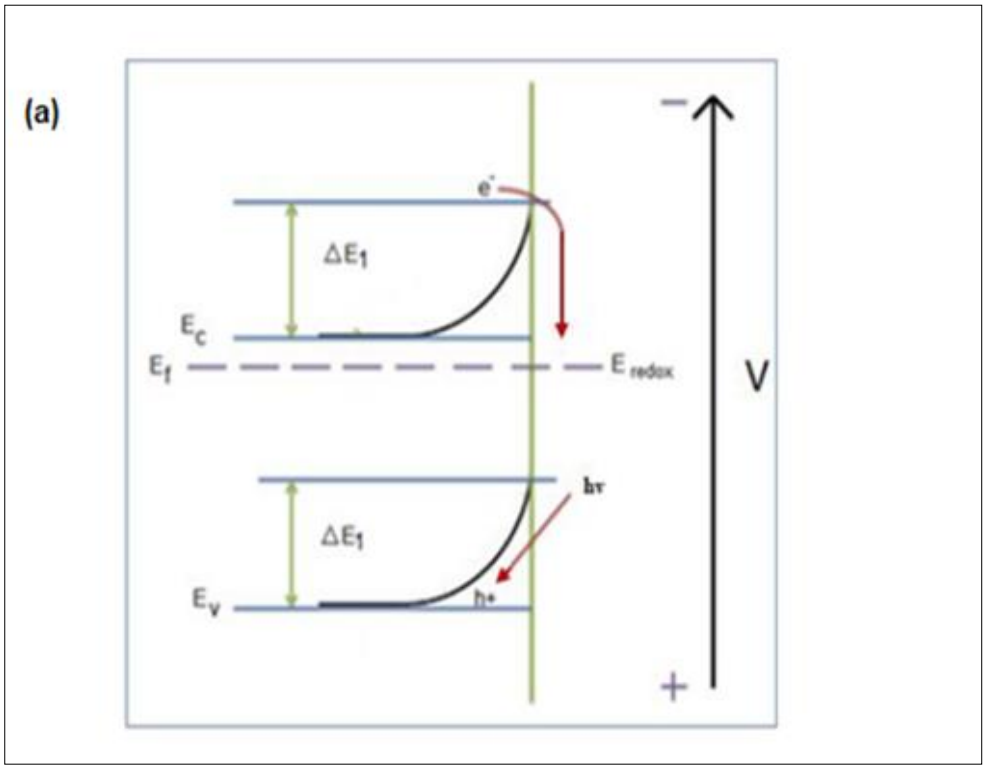

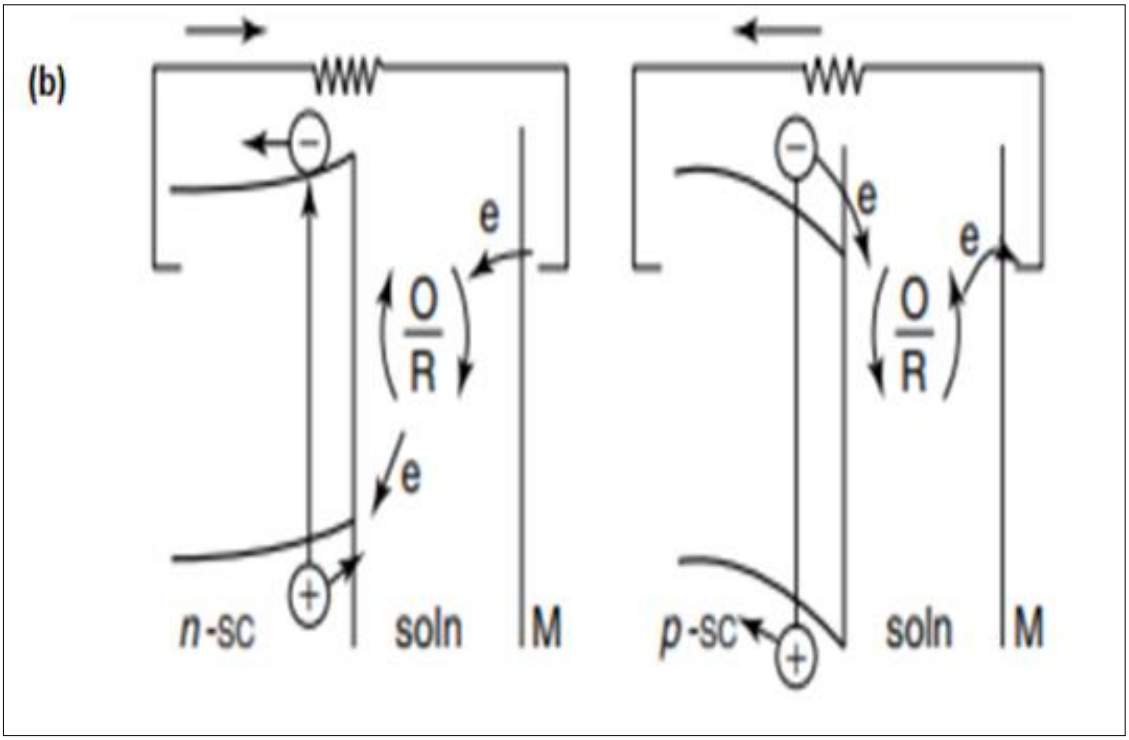

1.7 Semiconductor materials used in solar cells

Popular semiconductores that are used in solar cells can be categorized in to[32]:

a- Elements (e .g. Si and Ge).

b- III-V Compounds (e.g. GaAs, GaP and InP) .

c- II-VI compounds (e.g. CdS, CdSe and CdTe).

d- Ternary compounds (e.g. $CuInS_2$ and $CdIn_2Se_4$).

e- Transition Metal Di- chalcogenides (e.g. $MoSe_2$ and ZrS2).

f – Zinc phosphides (e.g. ZnP_2)

g- Oxide semiconductors (e.g. TiO_2, WO_3 and ZnO).

CuO is an example of oxide semiconductores that can be used in solar cells[33].

1.8 Thin film technology

Thin films have been used in semiconductor materials instead of monocrystalline semiconductor electrode. In PV systems, the electrode system thickness in typically 0.2-0.4 mm thick, while in thin films the film thickness is in the nano-scale only. Therefore, thin films demand low amounts of starting materials which lowers production costs and minimizes environmental impact. Despite that, thin film electrodes have lower efficiency.

In this techonolgy thin layer of semiconductor is deposited on a substrate, like fluorine-doped tin oxide (FTO), or tin-doped indium oxide (ITO). To fabricte thin films, many simple techniques can be used, such as chemical bath deposition (CBD) and electro-chemical deposition (ECD) [34, 35].

Inorganic semiconducting materials are commonly employed as thin films, including CdS, CdSe, ZnSe, ZnS, CuSe and others. Thin films can be used in place of mono-crystalline electrodes in PEC cells. Thin film electrodes can therefore be prepared very easily by simple methods[36-40].

Both n- and p-type thin film semiconductor electrodes can be prepared by the simple CBD and ECD methods. The film itself involves polycrystalline particles which are in the nano-scale, normally 5-50 nm in diameter. The thin film thickness itself may vary between 100 nm to 800 nm or more[41, 42].

1.9 CuO thin film

Copper oxide is a semicoducting material with good electrical and optical characteristics, inexpensive, non toxic and prepared easily. CuO lattice has a monoclinic structure. It exhibits a p-type conductivity because of the prescence of holes in the VB, the repoted optical band gaps of p-type CuO are between 1.3-2.1 eV [41, 43-46].

Copper oxide thin films have several applications including photoelectrochemical cells, gas sensors, super conductors, photocatalyst and photovoltaic devices [47-50]. Many methods were used to prepare CuO thin films. Examples are: thermal oxidation, chemical conversion, electrodeposition, chemical bath deposition and others [41, 51].

The choice for CuO is not arbitrary. The material does not involve highly toxic elements. Copper is not a costly element as well. CuO can be prepared by simple deposition methods such as CBD and ECD.

Scheme 1.6

Monoclinic crystal structure of CuO. [44]

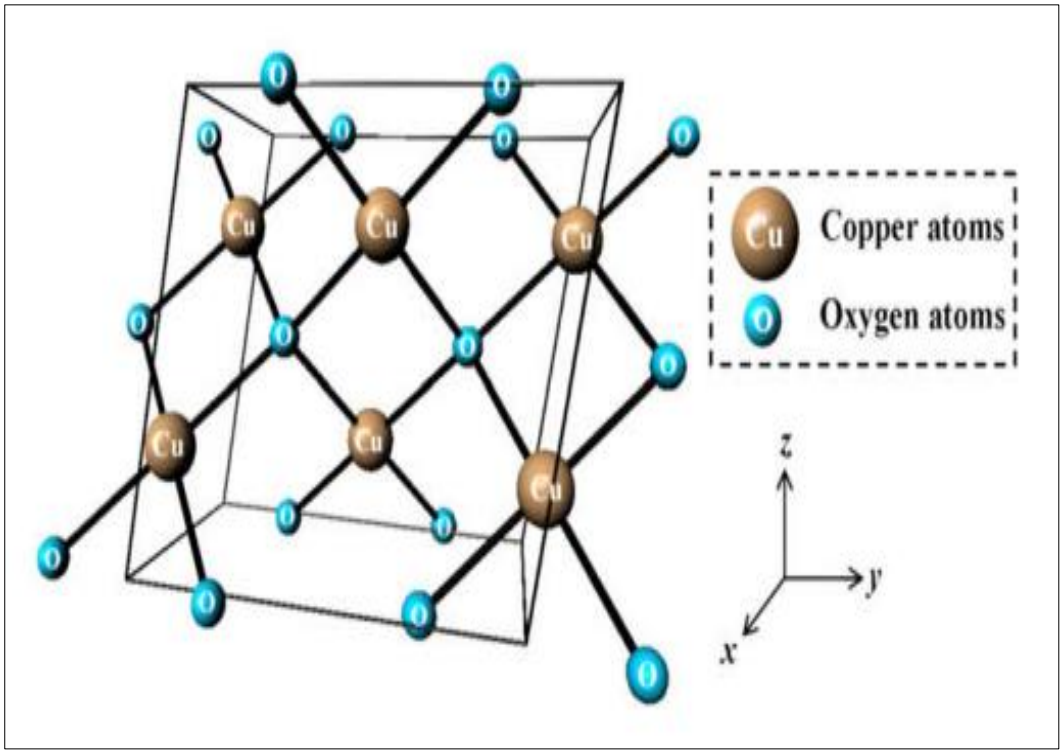

1.10 CuO thin film deposition techniques

Literature shows that CuO films have been deposited by several methods including, spray pyrolysis technique, sol-gel dip coating technique, chemical vapor deposition technique, vacuum evaporation, thermal oxidation, sputtering process, electron-beam evaporation, chemical solution deposition (CSD), chemical path deposition and electrochemical deposition[52, 53].

In this research CuO well be deposited by chemical bath deposition and electrochemical deposition techniques in addition to another new technique which is the combined electrochemical and chemical path deposition technique.

1.10.1 Chemical path deposition (CBD) technique

Chemical path deposition involves controlled precipitation of a compound from the solution on a selected substrate. This technique has several advantages including; it is a simple and inexpensive technique, multi compound chalcogenide thin film with a wide range of stoichiometry can be deposited, low material consumption, large area of deposition is possible and it is a safe method to handle[54].

In this technique, several parameters can be adjusted to control film thickness and composition. This parameters include; temperature, pH value of the solution, precursor concentration and others. The film that is produced by this technique will have a large area with good thickness which will be good to increase light absorption in solar cells[55].

However, CBD technique is not the most efficient for thin film deposition. It can be employed for a semiconductor electrode that is deposited with another technique like electrochemical deposition, to enhance the efficiency[56].

1.10.2 Electrochemical deposition (ECD) technique

It is the process of producing a thin and tightly adherent coating on a conductor substrate by the action of electric current inside the electrolytic cell. Three electrodes are needed, working electrode (WE), counter electrode (CE) and reference electrode (RE). All are placed in to electrolyte that is aqueous solution contains ions of desired deposition[57].

Current causes ions to move towards electrodes and the deposition occurs when reduction takes place on WE. Reduction requires electron transfer from CE which is achieved by oxidation of ions or neutral molecules. RE is used to monitor potential and current changes during deposition. Altering the conditions of electrochemical deposition controls the shape and size of electrocatalysts[57, 58].

Electrochemical deposition technique has so many advantages, including surface smoothness, good performance of protection against corrosion, low environmental pollution, ease of processing and thickness control and ease of condition control such concentrations, pH and temperature[59].

Therefore this technique was used here to deposit CuO thin film on to fluorine doped tin oxide substrate. It is expected to give a layer of CuO that has good contact with the substrate.

1.10.3 Combined EC/CB deposition technique

This technique have been used for the first time in this research. In the combined technique, thin layer of CuO is deposited electrochemically on the substrate. After that another layer of CuO is deposited by chemical path deposition to produce a film with two layers having a good contact with the substrate and good thickness at the same time.

1.11 Semiconductor film electrode modification:

To improve semiconductor film electrode PEC performance, the film properties must be improved accordingly. Examples of film properties are: thickness, band gap, particle size, connection between particles and adherence to susbstrate surface. Such properties are normally controlled by modification processes. Examples of such processes are:

1.11.1 Surface coating:

Applying thin layer coatings on the film may stabilize it chemically and mechanically. Modification can be made using chemical bonds or just by attachment[60].

1.11.2 Annealing:

Annealing allows sintering between smaller particles to yield larger ones. When the size increases the band gap values decreases. This may help in PEC performance enhancement.

Moreover annealing the film creates more disorder (imperfections) while under heat. After cooling to room temperature, the imperfections should go away and the atoms in the unstable positions go back to stable positions, therefore, annealing should improve film crystallinity which improves other properties. Therefore, researchers normally anneal their prepared films[61].

However, in case of metal chalcogenides, with relatively small band gaps, annealing must be made at moderate temperatures of about 300 ºC or lower. Otherwise, the film

material may degrade during annealing. In case of film electrodes with very large band gaps, things are different and higher annealing temperatures (of 800 ºC or higher) are needed. Therefore, materials such as CuO films should be annealed at temperatures only[62].

1.11.3 Cooling rate control:

As stated above, the heated semiconductor electrode involves imperfections while under heat. By cooling such imperfections should be removed as the atoms in the unstable positions immigrate to stable positions. However, if the heated material is cooled quickly, the unstable atoms may not have enough time to go back to their stable positions. Slow cooling is therefore needed. In slow cooling, enough time is allowed to the unstable atoms to go back to the stable positions. This is applicable to highly stable semiconductors with larger band gap values.

In case of heated unstable semiconductors, with low band gap values, slow cooling may not be recommended, especially when heated at upper allowed temperature. This is because the semiconductor material is kept at higher temperature for longer times, which may cause unwanted chemical and physical in the crystal[62].

1.11.4 Multilayer deposition:

In some cases, the film is deposited in prepared as multi layered film. This may improve crystallite sizes, optical properties and other properties[63].

1.11.5 Controlling the Redox couple:

Certain semiconducting materials demand certain redox couple to function efficiently. This depends on band structure and band gap value for the semiconductor, and its alignment with the redox couple potential (E_{redox}). Typically, the E_{redox} must exist within the forbidden band gap of the semiconductor electrode. Common redox couples are used such as: $K_3Fe(CN)_6/K_4Fe(CN)_6/LiClO_4$, S/$Na_2S$/KOH, KI/$I_2$, $FeCl_2/FeCl_3$ and other systems. The redox couple may be used inside various solvents such as water, CH_3CN, but the aqueous systems are preferred for environmental purposes[64].

1.12 Objectives

The present study aims at producing CuO thin film electrodes with high PEC performance. CuO thin films will be deposited onto FTO/glass substrate by electro-chemical deposition (ECD), chemical bath deposition (CBD) and combined EC/CB deposition techniques. The resulting electrodes will be assessed in photoelectrochemical process, after being modified by annealing and by cooling rate control (fast and slow cooling).

Technical objectives are :

1- Preparing CuO thin films by ECD, CBD and combined EC/CB deposition techniques onto FTO/glass substrate.
2- Annealing the prepared films at different temperatures with both fast and slow cooling.
3- Characterizing the produced CuO film electrodes by different methods
4- Investigating the various prepared films in PEC processes in a comparative manner.
5- Examining the prepared film stability to photodegradation under PEC experimental conditions.

1.13 Hypothesis and assumptions

This work will be used to test the following assumptions:

1- ECD preparation method makes good contact between CuO thin film and FTO/glass substrate.
2- CBD preparation method gives thick layer of CuO on the substrate.
3- Combined EC/CB deposition method should give a film of good contact with substrate and good thickness at the same time.
4- Annealing the prepared films is expected to enhance the PEC efficiency of the film electrodes prepared here, by lowering the imperfection in the crystallites.

1.14 Novelty of this work

1- Combined ECD/CBD deposition of CuO thin films has not been earlier reported. The ECD/CBD method has been described in preparing CdS and CdSe thin film

electrodes. However, CuO electrodes were not prepared by the combined preparation method, to our knowledge.

2- Effects of controlling annealing temperature and cooling rate on CuO film electrodes in PEC processes will be studied for the first time here.

Chapter Two

Experimental

2.1 Materials

2.1.1 Chemicals

$CuSO_4.5H_2O$, tartaric acid, lactic acid, NaOH, acetone, isopropyl alcohol and FTO/glass, were brought from Sigma Aldrich in pure states.

2.1.2 Equipment

2.1.2.1 Electronic spectrophotometer

Electronic absorption (solid state) spectra for CuO films were measured on a Shimadzu UV-1601 spectrophotometer, at room temperature in the wave length range 200 to 800 nm.

2.1.2.2 X-ray diffractometer (XRD)

Crystallinity of CuO thin films was studied on a PAN alytical X'Pert PRO XRD machine using a CuKa (λ=1.5418 Å) source (UAE University, Al-Ain, UAE). The XRD patterns were compared with literature JCPD cards.

2.1.2.3 The PEC cell

A PC controlled "Corr Test electrochemical work station Potentiostat/Galvanostat" was employed to measure PEC characteristics. CuO films were employed for the working electrodes (WE). The counter electrode involved a Pt sheet, and the internal reference electrode was a saturated calomel electrode (SCE). The three electrodes were inserted inside the redox couple solution. $K_3Fe(CN)_6/K_4Fe(CN)_6/LiClO_4$ system was used as the redox couple, with concentrations $K_3Fe(CN)_6$ (0.1 M), $K_4Fe(CN)_6$ (0.1 M) and $LiClO_4$) (0.1 M).

Illumination has been made with a 50-Watt halogen solar-simulator lamp having radiation range ~450-800 nm. The radiation intensity at the electrode surface was measured to be about 0.0086 $W.cm^{-2}$.

Scheme 2.1

Scheme for PEC experiment.

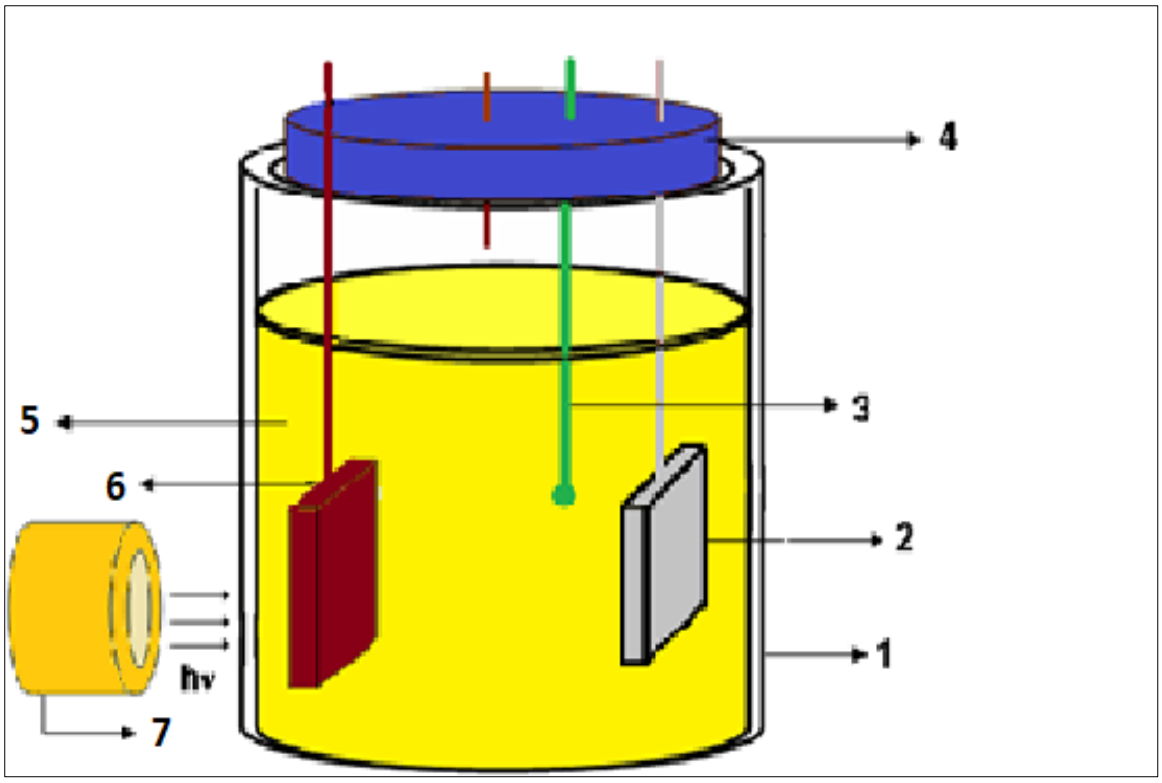

Scheme 2.1 illustrates PEC experiment. 1) beaker;2) platinum counter electrode; 3) reference electrode; 4) rubber stopper; 5) Iron-redox couple; 6) CuO working electrode and 7) light source.

2.1.2.4 Scanning electron microscope (SEM)

SEM micro-images for the CuO thin films were measured on Field Emission Scanning Electron Microscope, JEOL JSM-6700F FE-SEM, with energy-dispersive X-ray spectra (EDS). The SEM micrographs were measured in the laboratories of UAE University, Al-Ain, UAE.

2.2 Pretreatment of FTO/glass substrate

Highly conducting and transparent FTO/glass substrates were cleaned carefully, to support the CuO thin-films, by thorough washing with detergent solution. Then the substrates were washed with distilled water (DW), cleaned with acetone for 10 minutes in ultrasonic cleaning bath, and then another 10 minutes with isopropyl alcohol. Finally, they were rinsed with DW and then air dried.

2.3 CuO thin film preparations.

CuO films were deposited by three techniques: CBD, ECD and combined ECD/CBD.

2.3.1 Chemical bath deposition of CuO thin films

A 0.2 M CuSO4.5H2O solution was prepared by adding 1.24 g CuSO4.5H2O to 25 ml distilled water. After 5 minutes, 25 mL of 1.5M lactic acid was added and stirred till dissolution and complete mixing. Sodium hydroxide (NaOH) was added until the pH reached ~ 12. After that, the cleaned FTO/glass substrate was dipped vertically inside the mixture. Then, CBD proceeded at 90 ºC for 15 minutes with slow stirring in open atmosphere. After deposition, the slide was taken out of the bath, rinsed with DW and air dried.

During deposition, the color changes from indigo blue to sky blue, Scheme (2.4a). Earlier procedures [65] was followed here with some modifications.

Scheme 2.2

Experimental setup for chemical bath deposition technique.

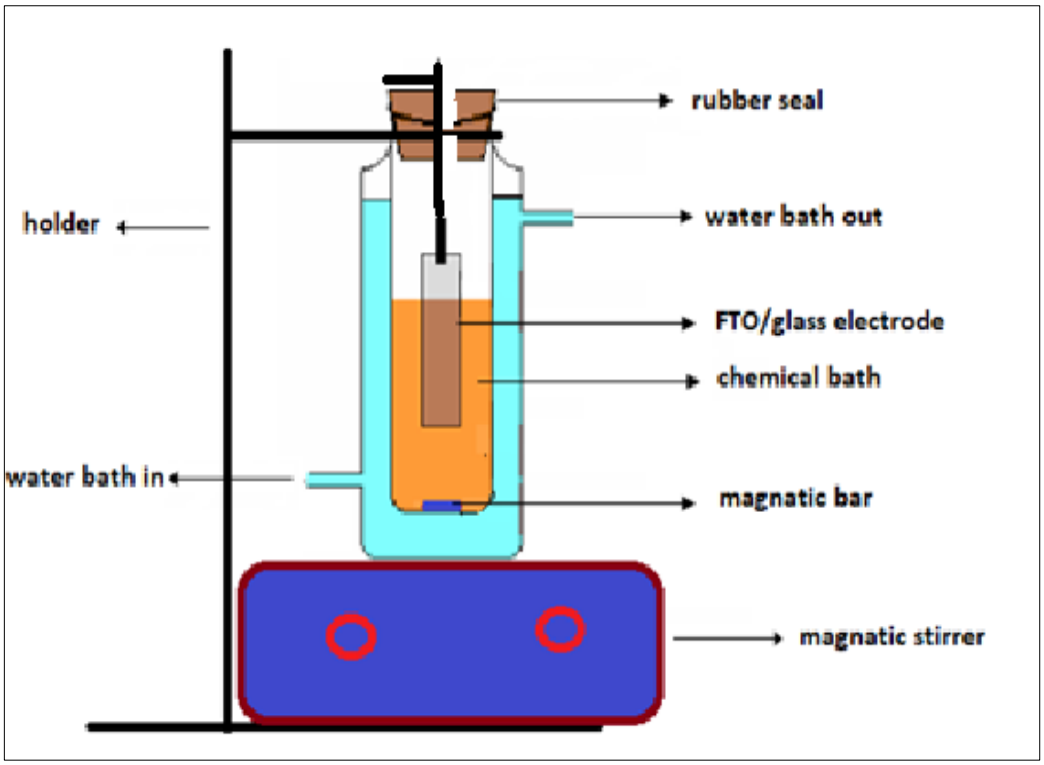

2.3.2 Electrochemical deposition of CuO films

The electrochemical cell that was used to deposit CuO consisted of FTO/glass slide as a working electrode (WE), Pt sheet as a counter electrode (CE) and a standard-calomel electrode as a reference (RE), Scheme (2.3). All were immersed in aqueous electrolyte containing 0.06M $CuSO_4.5H_2O$ and 0.06 M tartaric acid. Solution pH was made ~11 by adding NaOH. Depositions were performed by direct current (DC)-stripping at constant working potential of -0.65 V (vs. SCE) at room temperature in open atmosphere.

Scheme 2.3

The experimental set-up for the ECD-deposition of CuO film.

Numbers in this scheme illustrates: 1) potentiostat; 2) internal refernce electrode, 3)CuO thin film; 4) platinum counter electrode; 5) glass coverand 6) ECD cell.

The procedure was repeated with several time intervals (2min, 4min, 6min, 8min and 10 min). The coated substrate was taken from the electrochemical cell, rinsed with DW and air dried. The procedure used in this technique was taken from [42, 66], with making some modifications. The electrochemically deposited films have yellow color, Scheme (2.4b).

2.3.3 Combined ECD/CBD preparation of CuO thin films.

The chemical bath deposition procedure described above was applied to the best electrochemically deposited films to produce films with two layers. One layer with a

good contact with the FTO/glass substrate resulted from the electrochemical deposition procedure, the second layer is a thick layer appropriate for light to electricity conversion.

2.4 Modification of CuO thin films

Annealing temperature and cooling rate were controlled to modify the deposited CuO thin films.

2.4.1 Annealing process

The deposited films were heated using a furnace with thermostat. The annealing was conducted at four different temperatures (150 ˚C; 200 ˚C; 250 ˚C and 300 ˚C) throughout 60 min.

Annealing at temperature 200 ˚C and higher, converts the color of the deposited films to black, Scheme (2.4c).

Scheme 2.4

(a) Chemically bath deposited films. (b) Electrochemically deposited films. (c) Films after annealing.

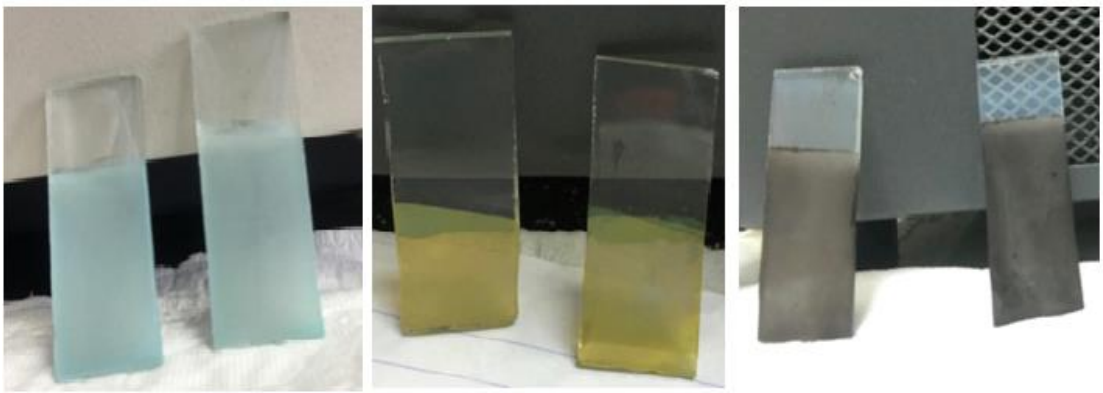

2.4.2 Cooling rate

2.4.2.1 Fast cooling

After 1 h of heating, the heater was turned off, and the film was immediately and carefully taken out of the furnace and cooled under air (within less than 10 min).

2.4.2.2 Slow cooling

After 60 min annealing, the heating was stopped and the films were left inside the furnace until it cooled to room temperature slowly with cooling rate 0.6 ˚C/min.

2.5 Current Density vs. potential (J-V) plots

Plots of current density vs. applied potential (J-V) were constructed using the Corr Test electrochemical workstation Potentiostat/Galvanostat with a 50-Watt halogen lamp for photo-experiments. $K_3[Fe(CN)_6]/K_4[Fe(CN)_6]/LiClO_4$) redox couple was employed. Another redox couple $KI/I_2/KOH$ was attempted by gave very poor J-V plots and was therefore ignored in this work. Values of short-circuit current density (J_{sc}) were calculated by dividing the measured short-circuit current (I_{sc}) by the electrode area.

2.6 Stability measurements of CuO thin films.

The electrode stability was measured by using Corr Test electrochemical workstation under PEC conditions. Zero-volt potential (vs. calomel electrode) was used, with steady radiation intensity of ~0.0086 W/cm^2. Values of I_{sc} were divided by the area immersed in solution to obtain J_{sc} values. Measurements were done at room temperature using $K_3[Fe(CN)_6]/K_4[Fe(CN)_6]/LiClO_4$) as a redox couple.

Chapter Three

Results and discussion

CuO films were prepared onto FTO/Glass using ECD, CBD and ECD/CBD combined methods. Various parameters were studied, to improve the deposited film properties, such as deposition time, annealing (at different temperatures under ambient environment -21% oxygen- gas for 60 min) and cooling rate (slow and fast cooling).

The prepared thin films were characterized using XRD, SEM, optical spectra, J-V plots, conversion efficiency in addition to stability. The XRD patterns were measured to confirm the composition and structure for each prepared film. Confirmation of CuO and any other compounds such as Cu_2O and $Cu(OH)_2$ has been studied using XRD patterns. The Patterns were also used to calculate the crystallite sizes for various films prepared at various temperatures. The electronic absorbance spectra have been used to calculate the band gap values for various films.

The SEM has been used to study the surface morphology of various films. In addition to studying small particles, larger aggregates and their sizes have also been studied for various films.

The J-V plots have been studied under illumination to measure all PEC characteristics. All values of J_{SC}, V_{OC}, FF and conversion efficiency have been calculated based on the measured J-V plots for various films.

Comparative study between ECD-CuO, CBD-CuO and ECD/CBD-CuO thin films has been made.

3.1 Characteristics of chemical-bath deposited CuO/FTO glass thin film

3.1.1 XRD measurements.

Figure 3.1 shows XRD patterns for electrochemically deposited CuO thin films that are not annealed or annealed at different temperatures (150˚C, 200˚C, 300˚C) then cooled either quickly or slowly.

Figure 3.1

XRD patterns for CBD-CuO films that are annealed then (1) rapidly cooled, (2) slowly cooled.

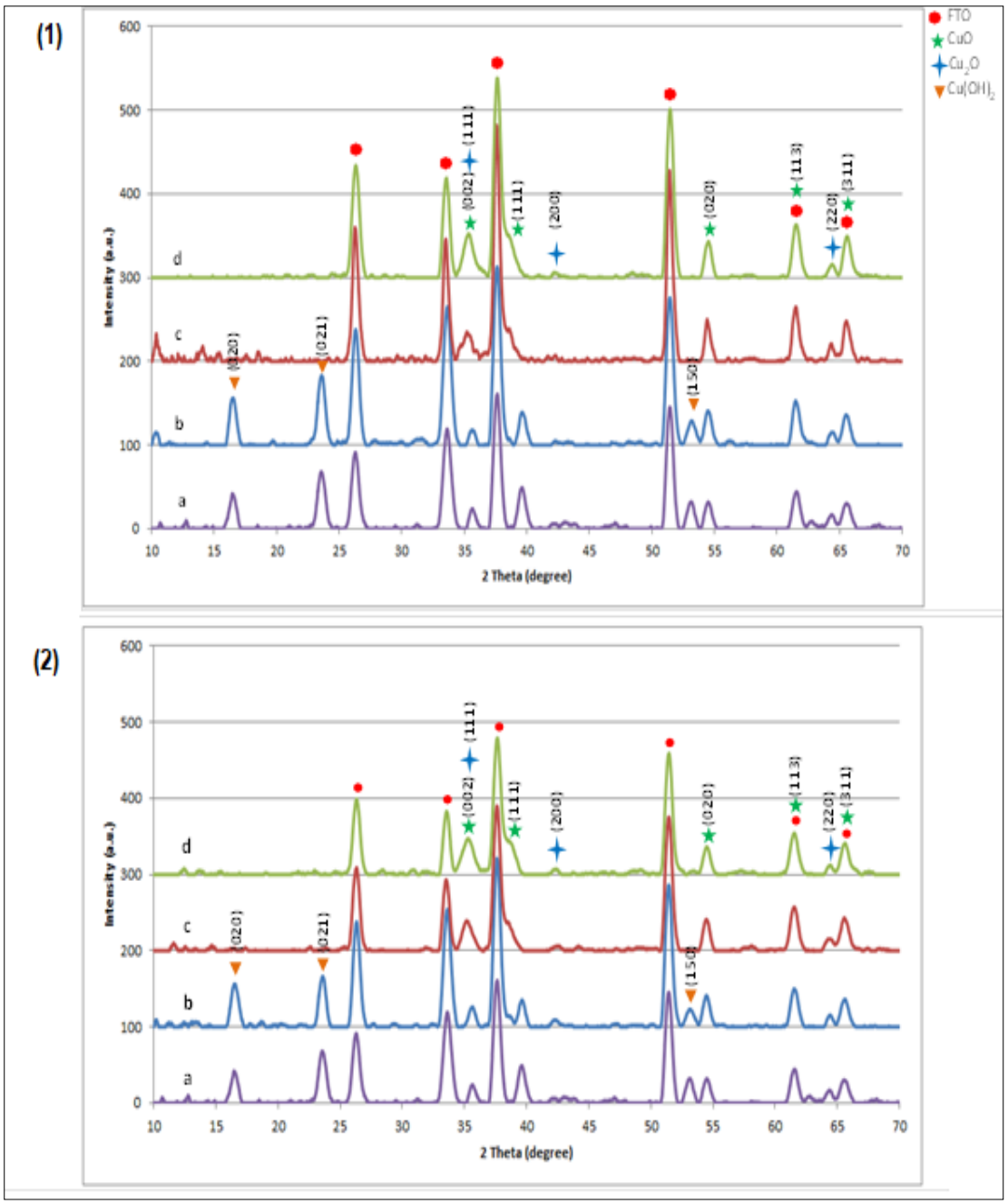

This Figure shows (1) XRD patterns for CBD-CuO films. A) not annealed, b) 150℃ annealed and quickly cooled, c) 200℃ annealed and quickly cooled, d) 300℃ annealed and quickly cooled. (2) XRD patterns measured for CBD-CuO thin films. A) not annealed, b) 150℃ annealed and slowly cooled, c) 200℃ annealed and slowly cooled, d) 300℃ annealed and slowly cooled.

Figure 3.1(1) describes XRD patterns for ECD-CuO thin films annealed using different temperatures, then quickly cooled. Both annealed and non-annealed films show crystallinity. Monoclinic phase for CuO nanoparticles can be seen from two main peaks 35.6˚ (002) and 38.6˚ (111), cubic phase for Cu_2O nanoparticles is observed from the two peaks 36.4˚ (111) and 42.2˚ (200), orthorhombic crystal phase for $Cu(OH)_2$ is observed from the peaks 16.5˚ (020), 23.5˚ (021) and 53.11˚ (150), the other peaks refer to FTO substrate[67-70].

We see that the non-annealed and 150℃ annealed films show $Cu(OH)_2$ particles. On the other side, films annealed at higher temperatures show CuO and Cu_2O particles with no $Cu(OH)_2$ phase. So the chemical bath deposition procedure that was examined in this research deposits $Cu(OH)_2$ crystals on the FTO glass thin film, which must be annealed at temperature higher than 150℃ in order to convert to CuO [70, 71].

Figure 3.1(2) summarizes XRD patterns for CBD-CuO thin films that were annealed at different temperatures and then slowly cooled. There is pattern similarity for fast cooling occurs here with slow cooling in terms of annealing temperature effect. $Cu(OH)_2$ is converted to CuO and Cu_2O at higher temperatures.

Table (3.1) shows the average particle size of each type of crystals. The average crystallite sizes were measured using the XRD data and Scherrer equation, $D = k\lambda/\beta\cos\theta$. D is average crystallite size (Å); λ is X-ray wavelength (Cu K_α, $\lambda = 1.5406$ Å); β is full-width at half-maximum (FWHM, in radians); while θ is angle of diffraction.

With fast cooling, it is noticed that the average crystallite-size values of CuO and Cu_2O increased with increased temperature until 200˚C, but decrease at 300˚C. So very high temperature may decompose CuO and Cu_2O particles. This is consistent with earlier literature, where higher annealing temperatures should be avoided in cases of low-to-medium band gap semiconductors [62]. The average particle size of $Cu(OH)_2$ decreases with annealing then phase completely yields CuO and Cu_2O.

In case of slowly cooled films. It is shown that the average crystallite size increased with annealing until 150˚C, after that it begins to decrease. So, exposure to high temperature for a long time degrades off CuO and Cu_2O particles. It is also consistent

with references that showed that heating semiconductor causes lattice sintering. But with semiconductors of low-to-medium band gap range, very high temperatures should be avoided. Moreover, Table 3.1 show that the average crystallite sizes of CuO and Cu_2O in case of slow cooling are smaller than fast cooling. This is because the semiconductor is exposed at higher temperature for longer times in slow cooling. The results are consistent with earlier literature [62, 72].

The average particle size for $Cu(OH)_2$ decreases with annealing because it begins to convert to CuO and Cu_2O at temperatures above 150 ºC. However, at 150 ºC or lower the $Cu(OH)_2$ remain, and exhibit larger sizes with slow cooling than with fast cooling. With slow cooling the $Cu(OH)_2$ are exposed for longer time to undergo sintering and size increase. Since $Cu(OH)_2$ has high energy band gap of 4.5 eV [73], it undergoes more sintering at 150 ºC when slowly cooled.

Table 3.1

Particle size measured for CBD-CuO/FTO/glass thin films, annealed at different temperatures, quickly and slowly cooled.

Sample	Annealing temperature (°C)	Average particle size for CuO	Average particle size for Cu_2O	Average particle size for $Cu(OH)_2$
A	Non-annealed	14.48	14.75	13.09
B	150 quickly cooled	14.92	19.25	12.66
C	200 quickly cooled	13.03	20.06	-
D	300 quickly cooled	12.30	19.29	-
E	150 slowly cooled	14.67	14.53	12.95
F	200 slowly cooled	12.53	12.87	-
G	300slowly cooled	12.03	12.07	-

3.1.2 Electronic absorption spectra

3.1.2.1 Annealing temperature and cooling rate effects on film electronic spectra.

Figure (3.2) shows the electronic absorption spectra of CBD-CuO thin films heated at various temperatures (150, 200, 250 and 300℃) and then cooled either rapidly or slowly. The figure show that the absorption spectra exhibit red shift upon annealing. But annealing at higher temperatures (250℃ and 300℃) gives lower absorbance, which indicate negative effect of high temperature annealing on the films.

In both cases, fast and slow cooling, the non annealed film gives the highest absorption pattern. Absorption decreases with increasing annealing temperature this also indicates negative effect of higher temperatures at chemically bath deposited films.

Table (3.2) below summarizes the optical band gap values for the prepared CuO thin films. The values for band gap were calculated by Tauc method using absorbance data plotted with respect to the energy. This can be illustrated in the relation $(\alpha h\nu)^{1/n} = A(h\nu - E_{bg})$, where h is Planck's constant, ν is the photon frequency, α is the absorption coefficient, E_{bg} is the band gap, A is a proportionality constant and n represent the nature of the electronic transition [74]. In addition, the wave length was calculated using the relation λ_{bg} (nm) = 1240/E_{bg}(eV) [75].

Normally band gap value decreases with increasing annealing temperature due to sintering and increasing crystallite sizes. In our work we noticed lowering in particle sizes at higher temperature by XRD. However, as higher temperature changes $Cu(OH)_2$ (with E_{bg} ~4.2 eV), into CuO (with smaller band gap), the lowering in the band gap upon higher annealing temperature can be explained. Also, band gap values in case of slow cooling are smaller than fast cooling. This means that the particle size becomes larger with longer heating time. Higher temperature causes more sintering. Slow cooling means exposure to temperature for longer time which also means more sintering. Appendix B shows Tauc plots for each type of films that have been prepared in this research.

Figure 3.2

Optical absorption spectra for CBD-CuO films that are annealed then (1) rapidly cooled, (2) slowly cooed.

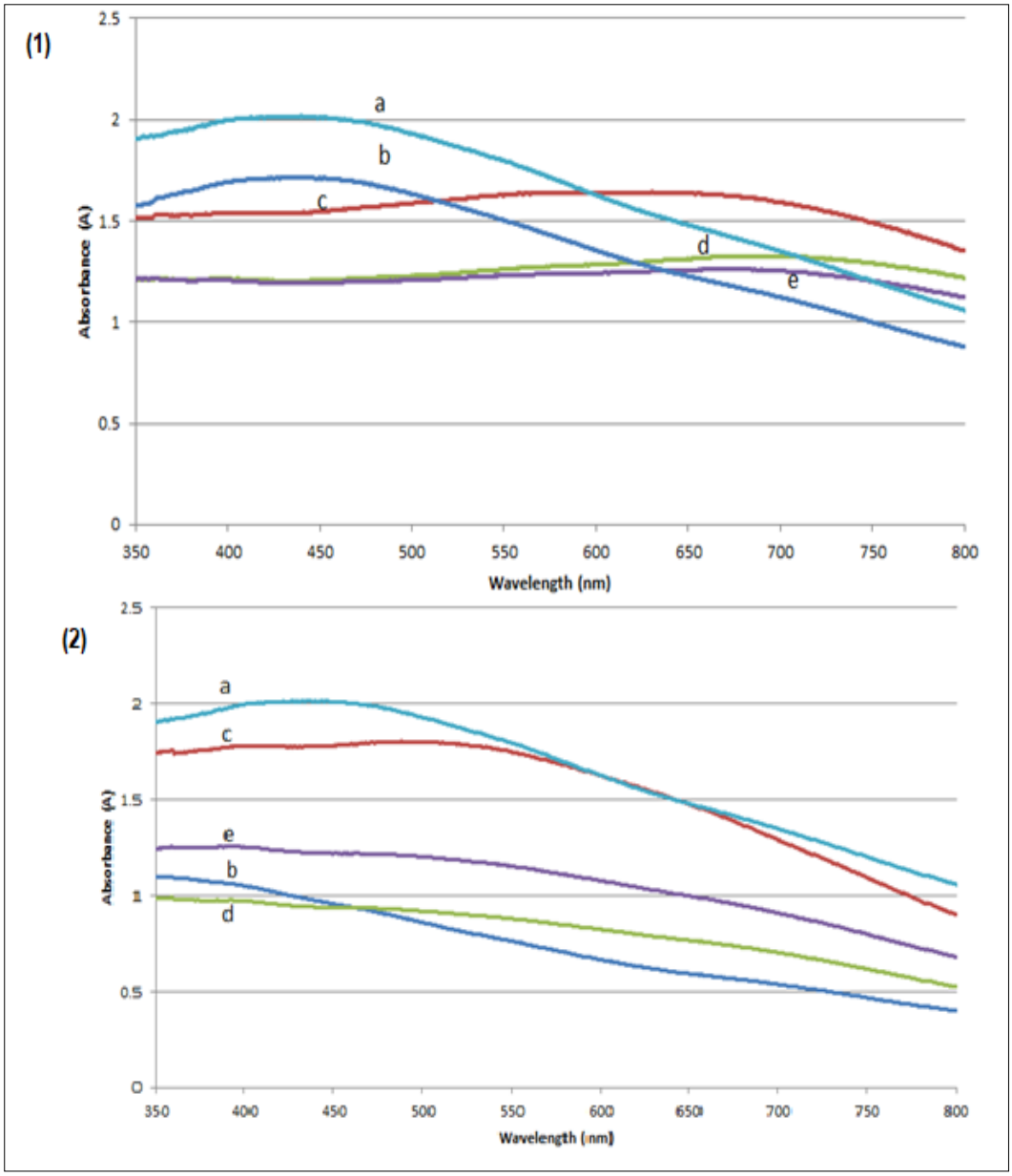

This figure shows (1) Optical spectra measured for CBD-CuO film electrodes prepared on FTO/glass. a) not annealed; b) 150℃ annealed and quickly cooled; c) 200℃ annealed and quickly cooled; d) 250℃ annealed and quickly cooled; e) 300℃ annealed and quickly cooled. (2) Absorption spectra for CBD-CuO films prepared onto FTO/glass. (a) not annealed; b) 150℃ annealed and slowly cooled; c) 200℃ annealed and slowly cooled; d) 250℃ annealed and slowly cooled; e) 300℃ annealed and slowly cooled.

Table 3.2

Optical-band gaps for CBD-CuO/FTO/glass films annealed at different temperatures, quickly cooled and slowly cooled. Measurements are based on Tauc method.

Sample	Annealing temperature (˚C)	E_{bg} (eV)	λ_{bg} (nm)
1a	Not annealed	1.75	709
1b	150 quickly cooled	1.70	729
1c	200 quickly cooled	1.60	755
1d	250 quickly cooled	1.50	827
1e	300 quickly cooled	1.45	855
2b	150 slowly cooled	1.68	738
2c	200 slowly cooled	1.55	800
2d	250 slowly cooled	1.42	873
2e	300 slowly cooled	1.40	886

3.1.3 SEM images for CBD-CuO/ FTO/glass thin films

Figure (3.3) shows SEM images for CBD-CuO thin film that is annealed at 300℃ either fast or slow cooled. The figure shows rod aggregates with nearly 1500 nm length and 500 nm width.

Figure 3.3

SEM micrographs measured for CBD-CuO/FTO/glass films annealed at 300℃; a) rapidly cooled; b) slowly cooled.

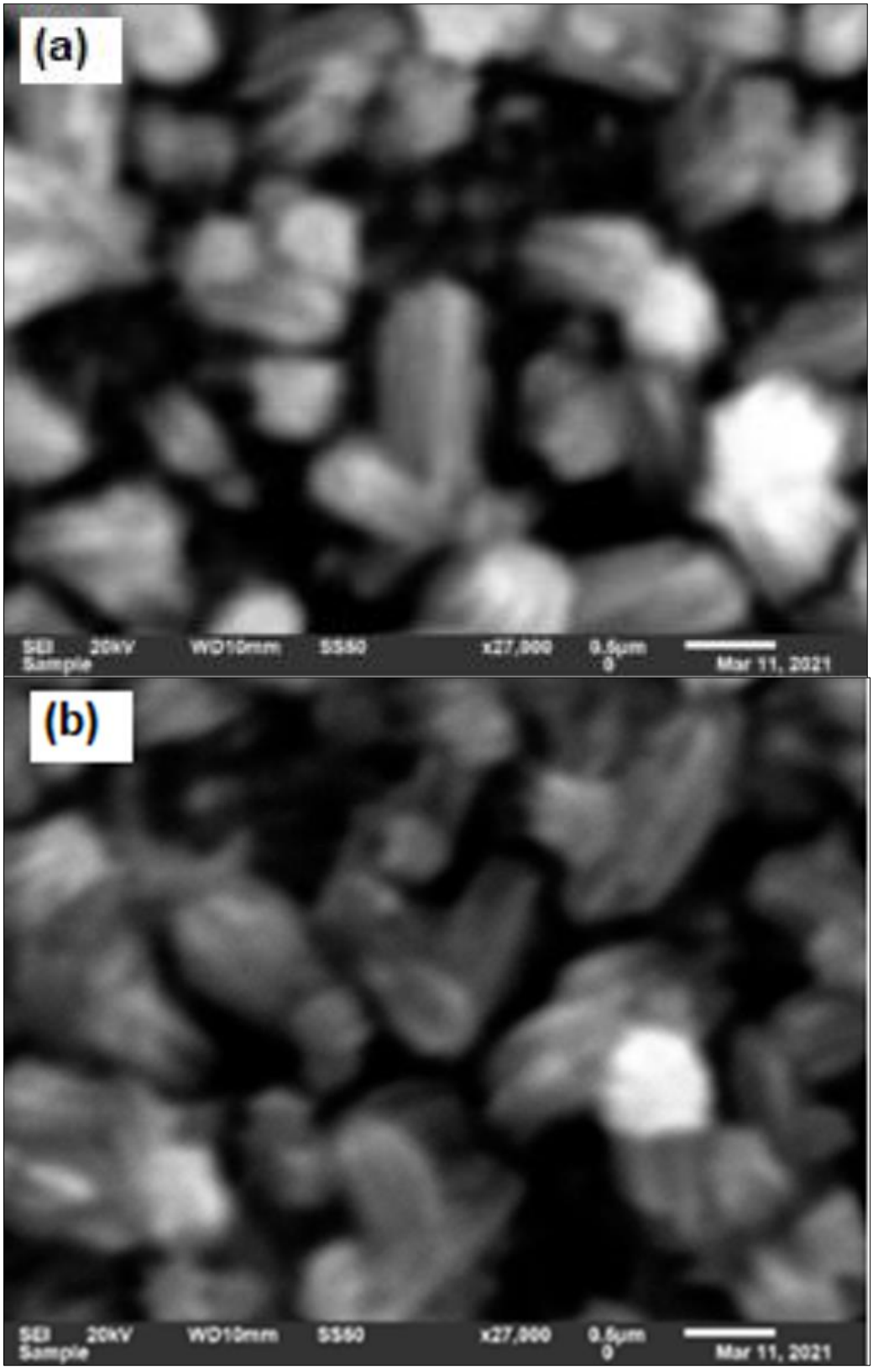

The SEM images are measured with low resolution. Therefore, the nano-scale crystallites in the film cannot be observed inside the films. However, the nano-scale crystallites have already been observed using the XRD patterns as described above. Therefore, it can be concluded that the CBD-CuO/FTO electrodes (both slowly and quickly cooled) involve small nano-size crystallites (from XRD) that exist inside larger agglomerates (from SEM). Each agglomerate involves a number of large columnar particles stacked together, while each column involves smaller nano-scale crystallites.

3.1.4 Photo electrochemical (PEC) characteristics for CBD-CuO FTO/glass thin films.

PEC characteristics, such as photo J-V plots, values of J_{SC} and values of efficiency, have been measured at room temperature. Photo J-V plots show negative value for the J_{SC} and positive value for V_{OC}, which means that the semiconductor is p-type in all films. The results agree with literature [72].

Based on literature, the values for short circuit photocurrent J_{SC} measured at zero applied potential for p-type semiconductor electrodes should be negative. In n-type semiconductor electrodes, the values for the J_{SC} must be positive. In the present study, the negative values for the J_{SC} indicate that the CuO is a p-type semiconductor.

3.1.4.1 Effects of annealing-temperature and of cooling rate on the J-V plots of CBD-CuO thin films

Figure (3.4) show photo J-V plots for CBD-CuO thin films that are annealed at various temperatures (150, 200, 250 and 300℃), then rapidly or slowly cooled, respectively. Table (3.3) show the photo electrochemical characteristics for the films mentioned. CuO thin film that is annealed at 150˚C then quickly cooled has the highest V_{OC} (0.102), J_{sc}(-0.58) and efficiency (0.17 %) values. In general, these values are not especially high, but are good for a start up. CuO is not expected to give high current in solar cells according to these results. However, this is not new for CuO films. In some cases they did not show any PEC activity. In other cases, they showed only low PEC values [43, 76, 77]. Further future surface modification may help enhance CuO film electrochemical characteristics.

Figure 3.4

Photo J-V plot for CBD-CuO FTO/glass films that are annealed then (1) rapidly cooled. (2) slowly cooled.

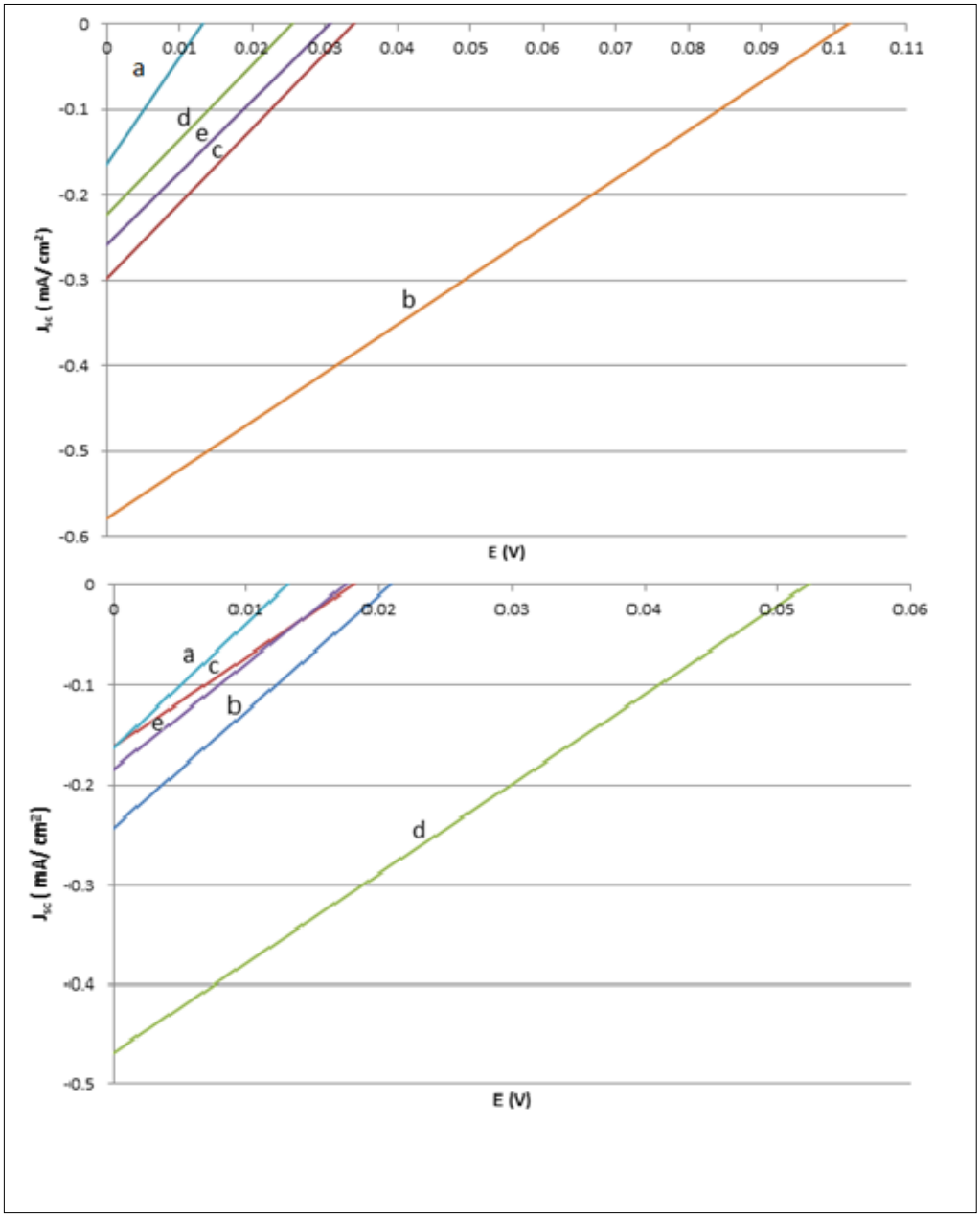

This figure shows (1) Photo J-V plot for CBD-CuO FTO/glass electrodes that are a) not annealed, b) 150℃ annealed and quickly cooled, c) 200℃ annealed and quickly cooled, d) 250℃ annealed and quickly cooled, e) 300℃ annealed and quickly cooled. (2) Photo J-V plot for CBD-CuO FTO/glass electrodes that are a) not annealed, b) 150℃ annealed and slowly cooled, c) 200℃ annealed and slowly cooled, d) 250℃ annealed and slowly cooled, e) annealed at 300℃, slowly cooled.

Table 3.3

PEC characteristics for CBD-CuO/FTO films annealed at various temperatures, rapidly cooled and slowly cooled.

Sample	Annealing temp. (˚C)	V_{OC} (V)	J_{SC} (mA/cm^2)	η %	FF%
1a	Not annealed	0.013	-0.16	0.006	26.92
1b	150 quickly cooled.	0.102	-0.58	0.170	25.35
1c	200 quickly cooled.	0.034	-0.30	0.030	26.08
1d	250 quickly cooled.	0.025	-0.22	0.010	26.00
1e	300 quickly cooled.	0.031	-0.26	0.025	27.42
2b	150 slowly cooled.	0.021	-0.24	0.018	30.95
2c	200 slowly cooled.	0.018	-0.16	0.007	22.22
2d	250 slowly cooled.	0.052	-0.47	0.072	25.20
2e	300 slowly cooled.	0.017	-0.18	0.009	26.14

FF = Fill factor = [(maximum observed power density)/J_{sc}×V_{oc}] ×100%; J_{SC} = short-circuit current density; V_{OC} = open-circuit voltage; η (%) = conversion efficiency = [(maximum observed power density)/ (reach-in power density)]×(100%).

3.2 Characteristics of electrochemically deposited CuO/FTO glass thin film.

XRD measurements, SEM images, electronic absorption spectra and photo electrochemical characteristics for electrochemically deposited films that are non annealed or annealed at different temperatures then cooled either quickly or slowly can be illustrated as shown below.

3.2.1 XRD measurements

XRD patterns for the electrochemically prepared CuO films that have been annealed at 150 ˚C, 200 ˚C and 300 ˚C then cooled rapidly or slowly are presented in Figure (3.5) below. The figure shows CuO and Cu_2O crystals, but $Cu(OH)_2$ is not observed in case of ECD. In contrast with CBD, ECD gives useful CuO films, free of $Cu(OH)_2$, without annealing.

Table (3.4) shows the average particle size of each type of crystals. The average crystallite sizes were measured using the XRD data and Scherrer equation, $D = k\lambda/\beta\cos\theta$. *D* is average crystallite size (Å); λ is X-ray wavelength (Cu K_α, λ = 1.5406 Å); β is full-width at half-maximum (FWHM, in radians); while θ is angle of diffraction.

As illustrated in the table, the average particle size for electrochemically deposited films increases with increasing temperature. Unlike CBD-CuO films, in case of annealing at 150˚C, the average particle size in case of fast cooling is larger, but annealing at 200 ˚C and 300˚C the average particle size is larger in case of slow cooling. The reason is possibly due to the special stability of the ECD-CuO films compared to CBD-CuO counterparts.

Comparing these results with the average crystallite size in case of CBD films. Table (3.4) shows that the average crystallite size of nano crystals prepared electrochemically is larger than chemically bath deposited ones.

Figure 3.5

XRD patterns for ECD-CuO electrodes that are annealed then (1) rapidly cooled, (2) slowly cooled.

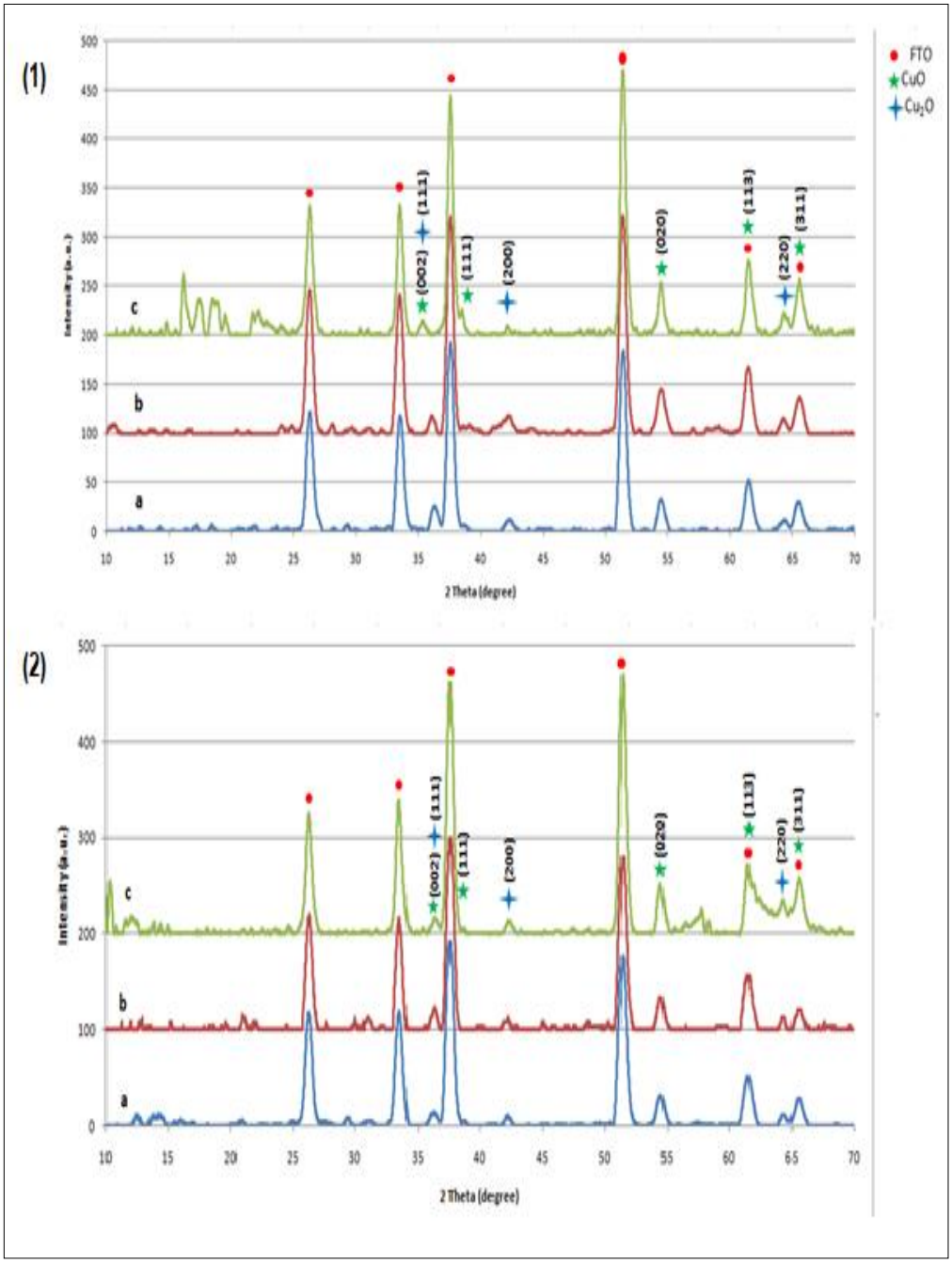

This figure shows (1) XRD patterns for ECD-CuO electrodes. a) 150℃ annealed quickly cooled; b) 200℃ annealed quickly cooled; c) 300℃ annealed quickly cooled. (2) XRD pattern for ECD-CuO films; a) 150℃ annealed slowly cooled; b) 200℃ annealed slowly cooled; c) 300℃ annealed slowly cooled.

Table 3.4

Particle size values calculated for ECD-CuO/FTO/glass films annealed at different temperatures then rapidly and slowly cooled.

Sample	Annealing temperature (ºC)	Average crystallite size for CuO	Average crystallite size for Cu_2O (nm)
1a	150 rapidly cooled	14.82	17.44
1b	200 rapidly cooled	15.49	15.77
1c	300 rapidly cooled	23.66	20.69
2a	150 slowly cooled	13.48	16.81
2b	200 slowly cooled	17.01	17.63
2c	300 slowly cooled	17.37	17.90

3.2.2 Electronic absorption spectra

3.2.2.1 Deposition time effect on optical spectra for ECD-CuO/FTO/glass films

The optical spectra for ECD-CuO films in different deposition times are described in Figure (3.6) (1). Highest absorption spectrum was observed for the film prepared in 10 minutes, indicating thicker film with deposition time. Chemically bath deposited films show higher absorption spectra than electrochemically deposited films as shown above. This is because the CBD film is thicker than the ECD film.

Figure 3.6

Absorption spectra for ECD-CuO films (1) prepared in different times. (2) annealed then rapidly cooled (3) annealed then slowly cooled.

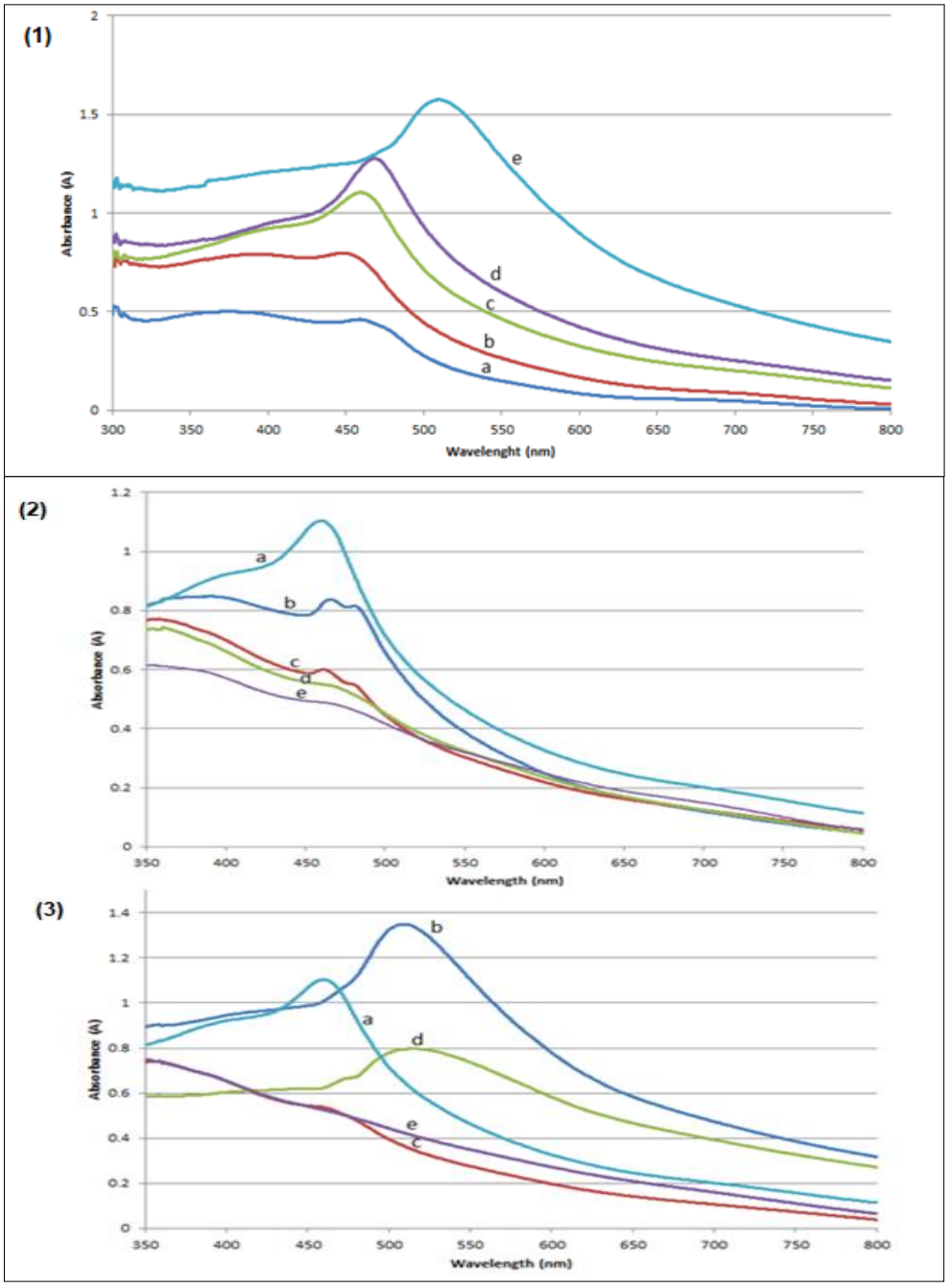

This figure shows (1) Optical absorption spectra observed for ECD-CuO/FTO/glass films prepared in different times, a) 2; b) 4; c) 6; d) 8 and e) 10 min. (2) Absorption spectra for ECD-CuO films a) not annealed, b) 150℃ annealed and quickly cooled, c) 200℃ annealed and quickly cooled, d) 250℃ annealed and quickly cooled, e) 300℃ annealed and quickly cooled. (3) Absorption spectra for ECD-CuO film electrodes a)

not annealed, b) 150℃ annealed and slowly cooled, c) 200℃ annealed and slowly cooled, d) 250℃ annealed and slowly cooled, e) 300℃ annealed and slowly cooled.

Table (3.5) shows values for optical band-gap for ECD-CuO films. The band gap values for the prepared films are in the range (2.0 – 2.4 eV). Band gap values decreases with time because crystallites grow more with time. Larger particle sizes are expected with longer time.

Table 3.5

Energy band gaps for ECD-CuO/FTO/glass prepared films in various times.

Sample	Deposition time (min)	E_{bg} (eV)	λ_{bg}(nm)
A	2	2.40	517
B	4	2.40	517
C	6	2.40	517
D	8	2.30	540
E	10	2.00	620

3.2.2.2 Annealing temperature and cooling rate effects on absorption spectra.

Optical absorption spectra for ECD-CuO thin films annealed at various temperatures (150, 200, 250 and 300℃) with both fast and slow cooling patterns are shown in Figure (3.6)(2&3)above.

In case of fast cooling, the non-annealed film gives better absorption spectrum than the annealed films. However, with slow cooling the film that is annealed at 150℃ gives the best absorption spectrum.

Band-gap values for these films are shown in Table (3.5) below. The band gap value ranges from (1.6 – 2.4 eV). The band gap value decreased at higher temperature. This is because the crystallite size becomes larger with increasing annealing temperature. Slow cooling also gives smaller band gap values than fast cooling, due to longer time at higher temperature in slow cooling.

Table 3.6

Values of optical band gaps for ECD-CuO/FTO/glass annealed at different temperatures, rapidly and slowly cooled.

Sample	Annealing temperature (ºC)	E_{bg} (eV)	λ_{bg} (nm)
1a	Not annealed	2.40	517
1b	150 rapidly cooled	2.30	539
1c	200 rapidly cooled	2.25	551
1d	250 rapidly cooled	2.20	564
1e	300 rapidly cooled	2.10	590
2b	150 slowly cooled	2.00	620
2c	200 slowly cooled	1.75	709
2d	250 slowly cooled	1.70	729
2e	300 slowly cooled	1.60	775

3.2.3 SEM images for ECD-CuO/FTO/glass thin films

Figure (3.8) describes SEM images for ECD-CuO thin films annealed at 300 ˚C either rapidly or slowly cooled. The Figure shows spherical aggregates of CuO nanoparticles that have a radius of nearly 340 nm. SEM images for chemically bath deposited films shows rod aggregates with diameters that are larger than the spherical aggregates in case of electrochemically deposited films.

Figure 3.7

SEM micrographs for ECD-CuO thin films annealed at 300 ˚C and a) rapidly cooled, b) slowly cooled.

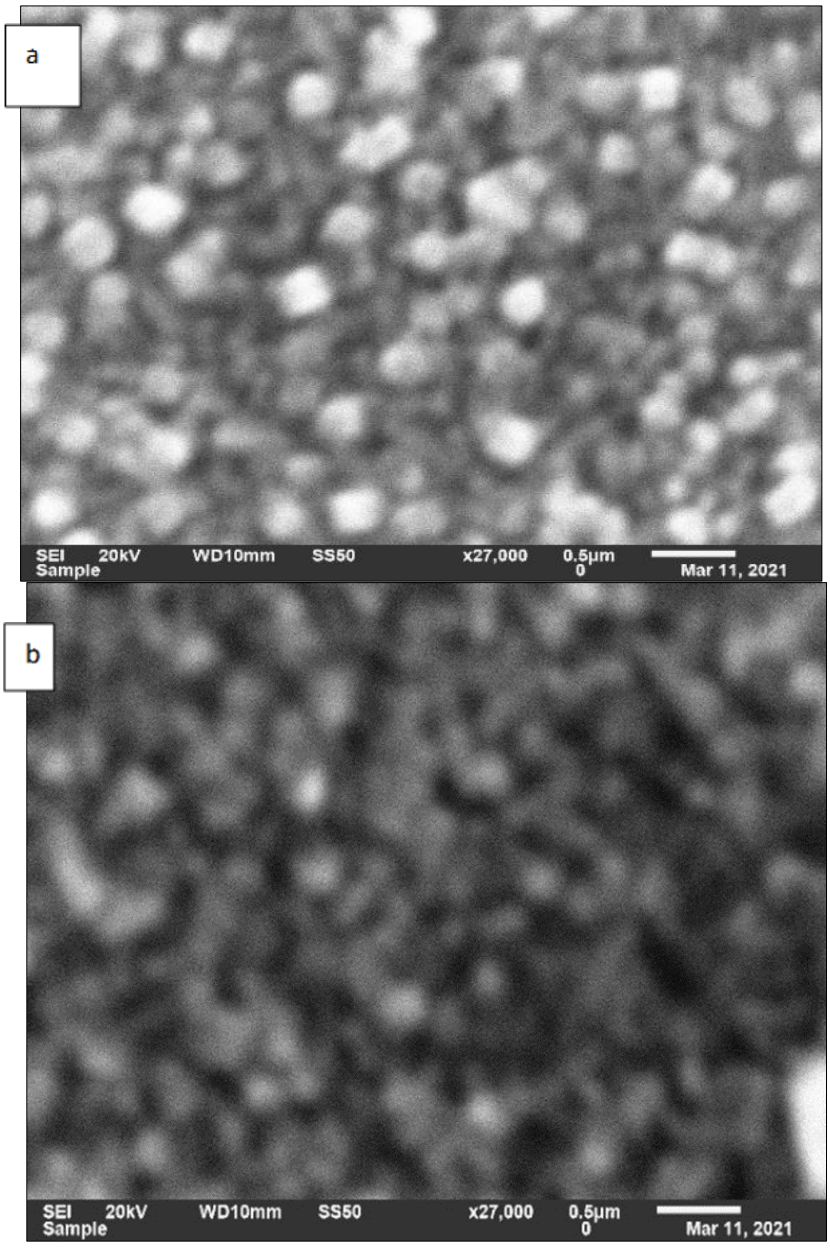

The SEM images here are also measured with low resolution. So, the nano-scale crystallites in the film cannot be observed inside the films. But they have already been observed using the XRD patterns as described above. Therefore, it can be concluded that the ECD-CuO/FTO electrodes (both slowly and quickly cooled) involve small nano-size particles (from XRD) that exist inside larger agglomerates (from SEM). Each agglomerate involves a number of large spheres stacked together, while each sphere involves smaller nano-scale crystallites.

3.2.4 Photo electrochemical (PEC) characteristics for ECD-CuO thin films

Photo J-V plots were measured and photo electrochemical characteristics have been calculated. Values for J_{SC}, V_{OC}, FF and conversion efficiency were calculated from the J-V plots for all electrodes.

3.2.4.1 Deposition time effect on photo J-V plots of ECD-CuO/FTO/glass thin films.

Figure (3.8)(1) describes photo J-V plots of electrochemically deposited CuO films that are prepared in various times (2, 4, 6, 8 and 10 min), without annealing.

The Photo electrochemical (PEC) characteristics for these films are presented in Table (3.7). The electrochemically prepared CuO film that is deposited for 6 minutes gives the highest efficiency value. But again here, the J_{sc} values are not so good for use in solar cells, as described above.

Studying the time effect is not expected to improve the PEC of electrochemically deposited films. The film that was deposited for 6 minutes have been prepared several times and annealed at different temperatures then cooled quickly and slowly in order to study the effect of annealing temperature and cooling rate as shown in the next section.

Figure 3.8

Photo J-V plots measured for ECD-CuO films, (1) prepared in different times, (2) annealed then quickly cooled. (3) *annealed then slowly cooled.*

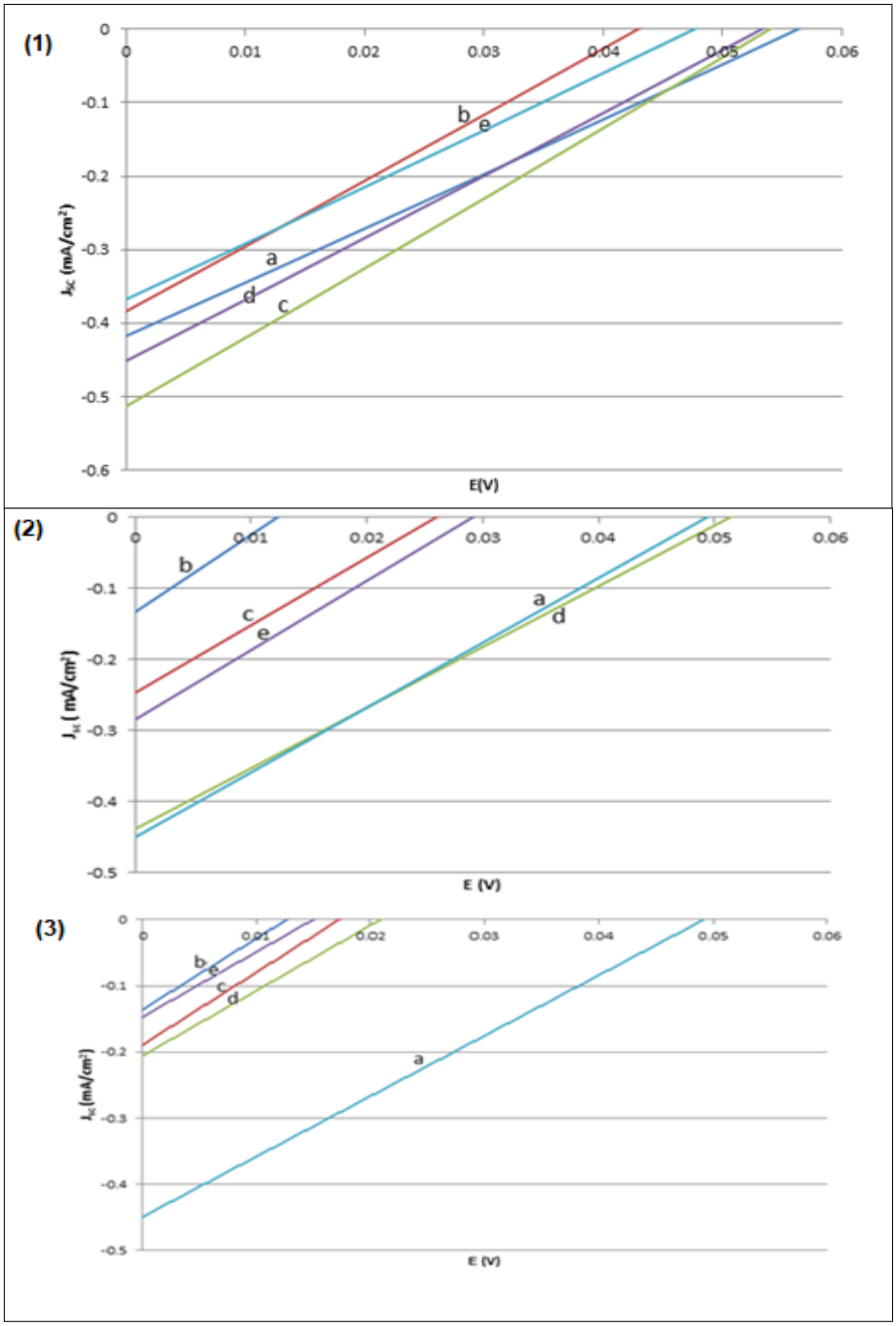

This figure illustrates (1) Photo J-V plots measured for ECD-CuO films prepared in different times: a) 2 min, b) 4 min, c) 6 min, d) 8 min, e) 10 min. (2) Photo J-V plots of ECD-CuO/FTO/glass electrodes, a) not annealed, b) 150℃ annealed and quickly cooled, c) 200℃ annealed quickly cooled, d) 250℃ annealed and quickly cooled, e) 300℃ annealed and quickly cooled. (3) Photo J-V plots for ECD-CuO/FTO/glass

electrodes, a) not annealed, b) 150℃ annealed and slowly cooled, c) 200℃ annealed and slowly cooled, d) 250℃ annealed and slowly cooled, e) 300℃ annealed and slowly cooled.

Table 3.8

PEC values for CuO/FTO films electrochemically deposited at various times.

Electrode	Deposition time (min)	V_{OC} (V)	J_{SC} (mA/cm^2)	η %	FF%
A	2	0.056	-0.42	0.075	27.55
B	4	0.043	-0.39	0.045	23.32
C	6	0.054	-0.52	0.082	25.00
D	8	0.053	-0.45	0.072	26.20
E	10	0.048	-0.37	0.054	26.01

FF = Fill factor = [(maximum observed power density)/J_{sc}×V_{oc}] ×100%; J_{SC} = short-circuit current density; V_{OC} = open-circuit voltage; η (%) = conversion efficiency = [(maximum observed power density)/ (reach-in power density)]×(100%).

3.2.4.2 Annealing-temperature and cooling-rate effects on photo J-V plots of ECD-CuO/FTO/glass films.

PEC values for CuO thin films that are annealed at various temperatures (150, 200, 250, 300℃) with fast and slow cooling rates are illustrated in figure (3.8)(2&3) above. Table (3.9) summarize the results of the two graphs.

The non-annealed film gives the highest efficiency value in both cases. The film that is annealed at 250℃ and rapidly cooled gives higher efficiency than slowly cooled electrode. That is because the slow cooling exposes the film to high temperature for longer time which affects its characteristics and lowers its PEC performance.

Table 3.9

PEC values for ECD-CuO/FTO films heated at various temperatures, rapidly and slowly cooled.

Sample	Annealing temperature °C	V_{OC} (V)	J_{SC} (mA/cm^2)	η %	FF%
1a	Not annealed	0.049	-0.45	0.067	26.08
1b	150 rapidly cooled	0.012	-0.13	0.004	23.07
1c	200 rapidly cooled	0.026	-0.25	0.018	24.00
1d	250 rapidly cooled	0.051	-0.44	0.067	25.67
1e	300 rapidly cooled	0.029	-0.28	0.024	25.86
2b	150 slowly cooled	0.013	-0.14	0.006	26.92
2c	200 slowly cooled	0.017	-0.19	0.009	24.77
2d	250 slowly cooled	0.021	-0.21	0.014	27.44
2e	300 slowly cooled	0.015	-0.15	0.007	24.88

3.3 Characteristics of combined EC/CB deposited CuO/FTO glass thin film.

CuO thin films were deposited by combined method, first by ECD, followed by CBD. The films were then annealed at various temperatures with fast or slow cooling. Characteristics of the films were studied as shown below:

3.3.1 XRD Measurements

XRD patterns for combined EC/CB-CuO thin films that were annealed at various temperatures (150, 200 and 300℃) and then cooled quickly and slowly are shown in Figure (3.9). It is noticed that the films that are non-annealed or annealed at 150℃ contain $Cu(OH)_2$ particles. At higher annealing temperature $Cu(OH)_2$ is converted to CuO or Cu_2O particles. That is because the CBD layer contains $Cu(OH)_2$ as described above. $Cu(OH)_2$ is converted to CuO with annealing at 200˚C or higher, so the annealing step is important also in case of preparing combined films.

The average particle sizes of each type of particles are illustrated Table (3.10) below. The average crystallite sizes were measured using the XRD data and Scherrer equation, $D = k\lambda/\beta\cos\theta$. *D* is average crystallite size (Å); λ is X-ray wavelength (Cu K_α, λ = 1.5406 Å); *β* is full-width at half-maximum (FWHM, in radians); while θ is angle of diffraction.

In general, the average particle size here decreases with increasing temperature, like the pattern noticed in CBD procedure. Comparing these results with CBD and ECD results, the average particle sizes here are nearly similar to those mentioned above. This is logical because the combined films involve both ECD layer and CBD layer.

Figure 3.9

XRD-patterns for combined EC/CB-CuO films that are annealed then (1) quickly cooled, (2) slowly cooled.

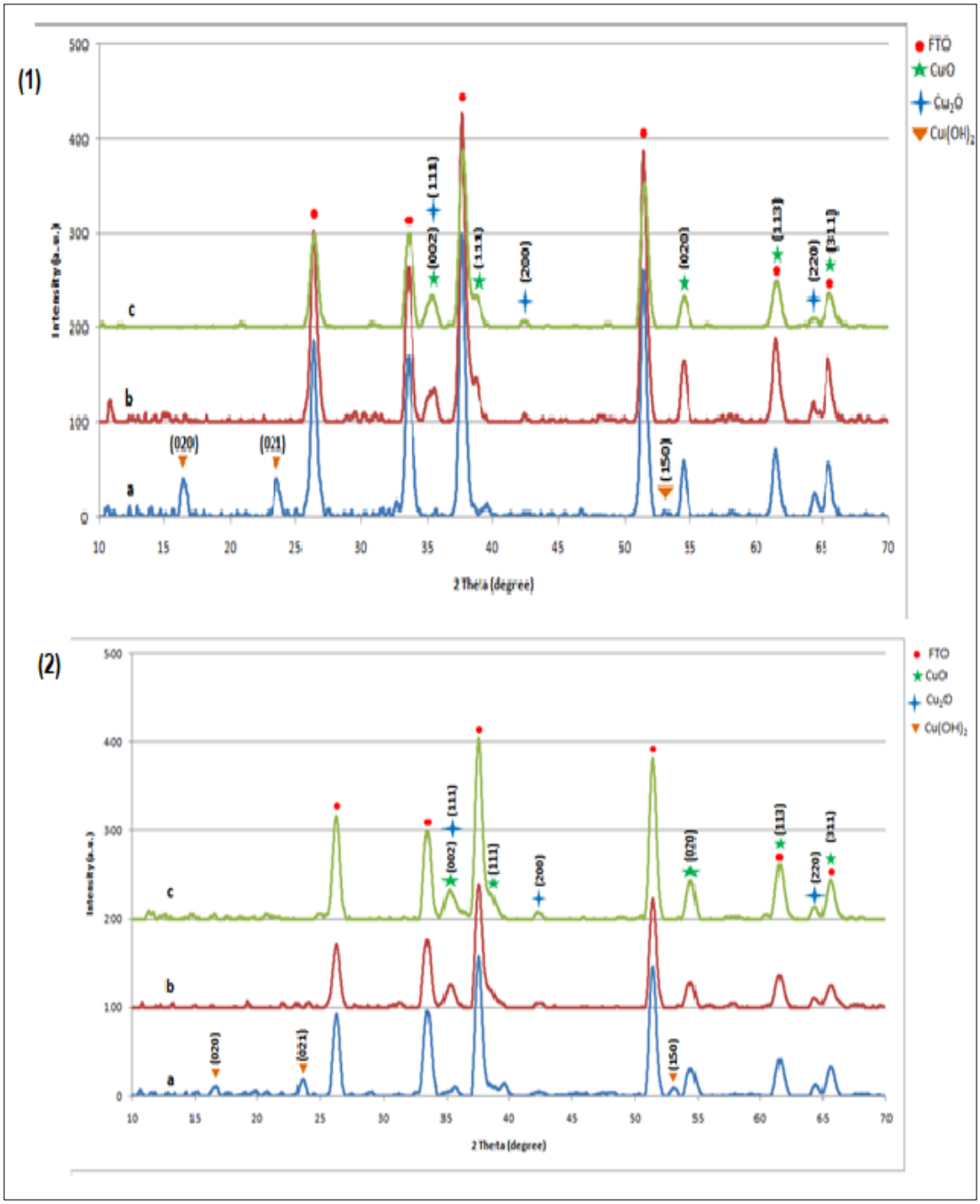

This figure shows (1) XRD-patterns for combined EC/CB-CuO films. a) 150℃ annealed quickly cooled; b) 200℃ annealed quickly cooled; c) 300℃ annealed quickly cooled. (2) XRD patterns for combined EC/CB-CuO thin films. a) 150℃ annealed slowly cooled; b) 200℃ annealed slowly cooled; c) 300℃ annealed slowly cooled.

Table 3.10

Particle size values for combined EC/CB-CuO/FTO/glass thin films annealed at different temperatures then quickly cooled.

Sample	Annealing temperature ºC	Average crystallite size for CuO (nm)	Average crystallite size for Cu_2O (nm)
1a	150, quickly cooled	26.77	17.84
1b	200, quickly cooled	13.85	26.79
1c	300, quickly cooled	11.75	16.08
2a	150, slowly cooled	14.23	18.04
2b	200, slowly cooled	13.66	15.29
2c	300, slowly cooled	12.76	14.40

3.3.2 Electronic absorption spectra Effects of annealing-temperature and cooling-rate on the optical spectra of combined EC/CB-CuO/FTO/glass thin films.

Electronic absorption spectra for combined EC/CB-CuO thin films that annealed at various temperatures then cooled quickly and slowly are illustrated in Appendix A Figures (1) and (2). The electronic absorption in case of combined films is nearly twice the absorption in case of CBD films or the ECD films separately ones. The combined EC/CB deposited films are much thicker since they contain two layers so the absorption must be larger. In both cases, fast and slow cooling the combined film that is annealed at 250℃ showed highest absorption pattern. This could be due to the stability of the ECD layer which is not sensitive to higher temperatures as described above.

The optical band gap values for combined CuO films are summarized in Appendix A Tables (1) and (2). Values of optical band gaps are in the range (1.35 – 1.95 eV) which is lower than the optical band gap values of CBD films and ECD films separately. This means that the particle size in EC/CB systems is larger than in separate depositions.

Table (3) and (4) also show that band gaps of slowly cooled combined films are smaller than rapidly cooled ones. Therefore, more heating time allows more sintering and lager size as mentioned above.

3.3.3 SEM images for combined EC/CB-CuO/FTO/glass thin films

Figure (3) in Appendix A shows SEM images for combined EC/CB deposited CuO films annealed at 300 ˚C, either quickly or slowly cooled. The figure shows two layers, the first inner one represents aggregates of spherical particles for electrochemically deposited CuO film. Above that, there is a layer of rod aggregates, which represents the chemically bath deposited CuO film.

The rod aggregates have a length of 1200 nm and a width of 440 nm. The spherical aggregates have a radius of nearly 450 nm. The aggregate dimensions resemble those described above for separate CBD and ECD films, respectively

Low resolution for SEM images is noticed here also, and the nano-scale in the film cannot be observed. But it has already been observed using XRD patterns. So, we can conclude that combined EC/CB deposited films involve small nano-size particles (from XRD) that exist inside larger agglomerates (from SEM).

3.3.4 Photo electrochemical (PEC) characteristics of combined EC/CB-CuO thin films

Photo J-V plots for combined EC/CB-CuO thin films were measured and photo electrochemical characteristics have been calculated.

3.3.4.1 Annealing-temperature and cooling-rate effects on photo J-V plots of combined EC/CB-CuO/FTO/glass thin films.

PEC properties for combined EC/CB-CuO thin films that are annealed at various temperatures (150, 250 and 300℃) with fast and slow cooling rates are illustrated in Appendix A Figures (4) and (5). Tables (3) and (4) summarize the results of the two graphs.

The results shows that the non annealed film gives the largest efficiency value in both fast and slow cooling cases. However, its efficiency is lower that the best efficiency result from the CBD films. So, combined procedure does not improve the PEC characteristics of CuO thin films.

3.4 Stability measurements for CuO/FTO/glass films under PEC conditions

Stability of some selected CuO films has been measured as shown in Appendix A Figure (6). Zero-volt potential (vs. calomel electrode) was used, with steady radiation intensity of ~ 0.0086 W/cm^2. Measurements were done at room temperature using $K_3[Fe(CN)_6]/K_4[Fe(CN)_6]/LiClO_4$) as a redox couple.

Nearly all selected films have good stability. The most stable one is the CBD film that is anneled 250 ˚C and slowly cooled. The electrochemically deposited film that is annealed at 150 ˚C and rapidly cooled shows the least stability.

3.5 Conclusions

Three techniques were used to deposit CuO thin film on FTO/Glass substrate, using ECD, CBD and combined ECD/CBD deposition technique.

- The prepared films exhibit low photoelectrochemical behaviors
- CBD method is the best method to prepare Cu films with higher PEC characteristics, but needs annealing to remove resulting $Cu(OH)_2$
- Because the CuO has very small band gap, it is sensitive to annealing at high temperature. Higher temperatures affect the films negatively.
- ECD method gives CuO films with more uniform structures with no $Cu(OH)_2$ product, but do not have improved PEC characteristics.
- Films deposited by combined ECD/CBD did not show improved PEC characteristics.
- Annealing ECD/CBD films negatively affects their SEM micrographs, due to sensitivity of the ECD layer to annealing.

3.6 Suggestions for Future Work:

- Preparing CuO thin films with more modifications, e.g: coating with multiwalled carbon nano tubes (MWCNT) is recommended.
- More annealing temperatures should be studied to optimize film characteristics.
- Electrochemical deposition may be repeated several times to enhance film performance.
- Doping the prepared CuO films with other dopants is recommended.

- Depositing combined EC/CB CuO thin film on other type of substrates. For example, Indium tin oxide (ITO) substrate.

List of Abbreviations

Abbreviation	Meaning
E_{bg}	Energy band gap
CB	Conduction band
VB	Valance band
eV	Electron- volt
SCs	Semiconductors
PEC	Photoelectrochemical cell
PV	Photovoltaic
WE	Working electrode
CE	Counter electrode
RE	Reference electrode
E_f	Fermi energy level
E_c	Conduction band energy
E_{redox}	Redox energy level
ECD	Electrochemical deposition
CBD	Chemical band deposition
ECD/CBD	Combined between electrochemical and chemical bath methods
FTO	Fluorine doped tin oxide
V_{oc}	Open-circuit potential
J_{SC}	Short circuit current density
J-V	Current density potential
η	Conversion efficiency
FF	Fill factor
DC	Direct current
XRD	X-ray diffraction
SEM	Scanning electron microscope

References

[1] S.R. Bull, Renewable energy today and tomorrow, Proceedings of the IEEE, 89 (2001) 1216-1226.

[2] G. Nicoletti, N. Arcuri, G. Nicoletti, R. Bruno, A technical and environmental comparison between hydrogen and some fossil fuels, Energy Conversion and Management, 89 (2015) 205-213.

[3] H. Ritchie, M. Roser, Fossil fuels, Our world in data, (2017).

[4] N. Abas, A. Kalair, N. Khan, Review of fossil fuels and future energy technologies, Futures, 69 (2015) 31-49.

[5] J. Mohtasham, Renewable energies, Energy Procedia, 74 (2015) 1289-1297.

[6] U. Shahzad, The need for renewable energy sources, energy, 2 (2012) 16-18.

[7] E.F. Camacho, M. Berenguel, Control of solar energy systems, IFAC proceedings volumes, 45 (2012) 848-855.

[8] A.M. Bagher, M.M.A. Vahid, M. Mohsen, Types of solar cells and application, American Journal of optics and Photonics, 3 (2015) 94-113.

[9] Y. Feng, A. Cheriet, M. Panagopoulou, D. Aureau, A.C. Rowe, C. Henry-de-Villeneuve, M. Rosso, F. Ozanam, Controlling homogeneity of the first lithiation in methylated amorphous silicon, Electrochimica Acta, (2021) 139655.

[10] G. Roumeliotis, III-Nitride Emitters and Converters: Built-in polarization-induced electric fields, built-in potential, and effective doping concentration, (2018).

[11] J.W. Orton, The story of semiconductors, OUP Oxford, 2008.

[12] B.G. Yacobi, Semiconductor materials: an introduction to basic principles, Springer Science & Business Media, 2003.

[13] Z. Pan, J.A. Röhr, Z. Ye, Z.S. Fishman, Q. Zhu, X. Shen, S. Hu, Elucidating charge separation in particulate photocatalysts using nearly intrinsic semiconductors with small asymmetric band bending, Sustainable energy & fuels, 3 (2019) 850-864.

[14] K. Inazu, M. Kitahara, K.-i. Aika, Decomposition of ammonium nitrate in aqueous solution using supported platinum catalysts, Catalysis today, 93 (2004) 263-271.

[15] H.O. Finklea, Titanium dioxide (TiO 2) and strontium titanate (SrTiO 3). Chapter 2, in: Semiconductor electrodes, 1988.

[16] M.S. Tyagi, Introduction to semiconductor materials and devices, John Wiley & Sons, 2008.

[17] M. Grätzel, Photovoltaic and photoelectrochemical conversion of solar energy, Philosophical Transactions of the Royal Society A: Mathematical, Physical and Engineering Sciences, 365 (2007) 993-1005.

[18] R. Li, Latest progress in hydrogen production from solar water splitting via photocatalysis, photoelectrochemical, and photovoltaic-photoelectrochemical solutions, Chinese Journal of Catalysis, 38 (2017) 5-12.

[19] M.m.M.K. Mari′e, Thin Film CdS/FTO/Glass Electrodes Prepared by Combined Electrodeposition/Chemical Bath Deposition: Enhancement of PEC Characteristics by Coating with Metalloporphyrinate/Polysiloxane Matrices, in, An-Najah National University, 2013.

[20] R. Fu, D. Feldman, R. Margolis, M. Woodhouse, K. Ardani, US solar photovoltaic system cost benchmark: Q1 2017, in, EERE Publication and Product Library, Washington, DC (United States), 2017.

[21] R. Venkateswari, S. Sreejith, Factors influencing the efficiency of photovoltaic system, Renewable and Sustainable Energy Reviews, 101 (2019) 376-394.

[22] G. Hodes, I. Howell, L. Peter, Nanocrystalline photoelectrochemical cells: A new concept in photovoltaic cells, Journal of the Electrochemical Society, 139 (1992) 3136.

[23] H. Gerischer, Electrochemical photo and solar cells principles and some experiments, Journal of Electroanalytical Chemistry and Interfacial Electrochemistry, 58 (1975) 263-274.

[24] V. Dusastre, Materials for sustainable energy: a collection of peer-reviewed research and review articles from Nature Publishing Group, World Scientific, 2010.

[25] M. Grätzel, Photoelectrochemical cells, nature, 414 (2001) 338-344.

[26] D. Chauhan, A. Perera, L. Li, L. Chen, E. Linfield, Dark current and photoresponse characteristics of extended wavelength infrared photodetectors, Journal of Applied Physics, 122 (2017) 024501.

[27] S. Ito, P. Liska, P. Comte, R. Charvet, P. Péchy, U. Bach, L. Schmidt-Mende, S.M. Zakeeruddin, A. Kay, M.K. Nazeeruddin, Control of dark current in photoelectrochemical (TiO 2/I−–I 3−) and dye-sensitized solar cells, Chemical Communications, (2005) 4351-4353.

[28] J.P. Omaggio, Analysis of dark current in IR detectors on thinned p-type HgCdTe, IEEE transactions on electron devices, 37 (1990) 141-152.

[29] H. Yaghoubi, Z. Li, D. Jun, R. Saer, J.E. Slota, M. Beerbom, R. Schlaf, J.D. Madden, J.T. Beatty, A. Takshi, The role of gold-adsorbed photosynthetic reaction centers and redox mediators in the charge transfer and photocurrent generation in a bio-photoelectrochemical cell, The Journal of Physical Chemistry C, 116 (2012) 24868-24877.

[30] S. Lemieux, R. Carpentier, Properties of a photosystem II preparation in a photoelectrochemical cell, Journal of Photochemistry and Photobiology B: Biology, 2 (1988) 221-231.

[31] Y.S. Chaudhary, A. Agrawal, R. Shrivastav, V.R. Satsangi, S. Dass, A study on the photoelectrochemical properties of copper oxide thin films, International Journal of Hydrogen Energy, 29 (2004) 131-134.

[32] M.P. Paranthaman, W. Wong-Ng, R.N. Bhattacharya, Semiconductor materials for solar photovoltaic cells, Springer, 2016.

[33] H. Kidowaki, T. Oku, T. Akiyama, A. Suzuki, B. Jeyadevan, J. Cuya, Fabrication and characterization of CuO-based solar cells, Journal of Materials Science Research, 1 (2012) 138.

[34] K. Seshan, Handbook of Thin Film Deposition Techniques Principles, Methods, Equipment and Applications, Second Editon, CRC Press, 2002.

[35] H. Frey, H.R. Khan, Handbook of thin film technology, Springer, 2015.

[36] S. Venkatachalam, D. Mangalaraj, S.K. Narayandass, Characterization of vacuum-evaporated ZnSe thin films, Physica B: Condensed Matter, 393 (2007) 47-55.

[37] J. Cheng, D. Fan, H. Wang, B. Liu, Y. Zhang, H. Yan, Chemical bath deposition of crystalline ZnS thin films, Semiconductor science and technology, 18 (2003) 676.

[38] A. Ashour, Physical properties of spray pyrolysed CdS thin films, Turkish Journal of Physics, 27 (2004) 551-558.

[39] A. Yadav, M. Barote, E. Masumdar, Studies on cadmium selenide (CdSe) thin films deposited by spray pyrolysis, Materials chemistry and physics, 121 (2010) 53-57.

[40] M. Petrović, M. Gilić, J. Ćirković, M. Romčević, N. Romčević, J. Trajić, I. Yahia, Optical Properties of CuSe Thin Films–Band Gap Determination, Science of Sintering, 49 (2017).

[41] J. Sultana, S. Paul, A. Karmakar, R. Yi, G.K. Dalapati, S. Chattopadhyay, Chemical bath deposited (CBD) CuO thin films on n-silicon substrate for electronic and optical applications: Impact of growth time, Applied surface science, 418 (2017) 380-387.

[42] V. Dhanasekaran, T. Mahalingam, R. Chandramohan, J.-K. Rhee, J. Chu, Electrochemical deposition and characterization of cupric oxide thin films, Thin Solid Films, 520 (2012) 6608-6613.

[43] Y. Keriti, R. Brahimi, Y. Gabes, S. Kaci, M. Trari, Physical and photo-electrochemical properties of CuO thin film grown on µc-Si: H/glass. Application to solar energy conversion, Solar Energy, 206 (2020) 787-792.

[44] A. Moura, L. Cavalcante, J. Sczancoski, D. Stroppa, E. Paris, A. Ramirez, J.A. Varela, E. Longo, Structure and growth mechanism of CuO plates obtained by microwave-hydrothermal without surfactants, Advanced Powder Technology, 21 (2010) 197-202.

[45] D. Jundale, P. Joshi, S. Sen, V. Patil, Nanocrystalline CuO thin films: synthesis, microstructural and optoelectronic properties, Journal of Materials Science: Materials in Electronics, 23 (2012) 1492-1499.

[46] D.S. Murali, S. Kumar, R. Choudhary, A.D. Wadikar, M.K. Jain, A. Subrahmanyam, Synthesis of Cu2O from CuO thin films: Optical and electrical properties, AIP advances, 5 (2015) 047143.

[47] S. Masudy-Panah, R. Siavash Moakhar, C.S. Chua, H.R. Tan, T.I. Wong, D. Chi, G.K. Dalapati, Nanocrystal engineering of sputter-grown CuO photocathode for visible-light-driven electrochemical water splitting, ACS applied materials & interfaces, 8 (2016) 1206-1213.

[48] Z. Jin, X. Zhang, Y. Li, S. Li, G. Lu, 5.1% Apparent quantum efficiency for stable hydrogen generation over eosin-sensitized CuO/TiO2 photocatalyst under visible light irradiation, Catalysis Communications, 8 (2007) 1267-1273.

[49] R. Vasiliev, M. Rumyantseva, N. Yakovlev, A. Gaskov, CuO/SnO2 thin film heterostructures as chemical sensors to H2S, Sensors and Actuators B: Chemical, 50 (1998) 186-193.

[50] P. Dai, H.A. Mook, G. Aeppli, S.M. Hayden, F. Doğan, Resonance as a measure of pairing correlations in the high-T c superconductor YBa 2 Cu 3 O 6.6, Nature, 406 (2000) 965-968.

[51] B. Balamurugan, B. Mehta, Optical and structural properties of nanocrystalline copper oxide thin films prepared by activated reactive evaporation, Thin solid films, 396 (2001) 90-96.

[52] T. Maruyama, Copper oxide thin films prepared by chemical vapor deposition from copper dipivaloylmethanate, Solar energy materials and solar cells, 56 (1998) 85-92.

[53] N. Serin, T. Serin, Ş. Horzum, Y. Celik, Annealing effects on the properties of copper oxide thin films prepared by chemical deposition, Semiconductor science and technology, 20 (2005) 398.

[54] X. Obradors, T. Puig, A. Pomar, F. Sandiumenge, S. Pinol, N. Mestres, O. Castaño, M. Coll, A. Cavallaro, A. Palau, Chemical solution deposition: a path towards low cost coated conductors, Superconductor Science and Technology, 17 (2004) 1055.

[55] T.B. Nasr, N. Kamoun, M. Kanzari, R. Bennaceur, Effect of pH on the properties of ZnS thin films grown by chemical bath deposition, Thin solid films, 500 (2006) 4-8.

[56] A. Oliva, R. Castro-Rodrıguez, O. Solıs-Canto, V.c. Sosa, P. Quintana, J. Pena, Comparison of properties of CdS thin films grown by two techniques, Applied surface science, 205 (2003) 56-64.

[57] M. Paunovic, M. Schlesinger, Fundamentals of electrochemical deposition, john wiley & sons, 2006.

[58] X. Zhang, K. Wan, P. Subramanian, M. Xu, J. Luo, J. Fransaer, Electrochemical deposition of metal–organic framework films and their applications, Journal of materials chemistry A, 8 (2020) 7569-7587.

[59] L. Liu, D. Mandler, Using nanomaterials as building blocks for electrochemical deposition: A mini review, Electrochemistry Communications, 120 (2020) 106830.

[60] Y. Nakato, T. Ohnishi, H. Tsubomura, Photo-electrochemical behaviors of semiconductor electrodes coated with thin metal films, Chemistry Letters, 4 (1975) 883-886.

[61] H.S. Hilal, S.K. Salih, I.A. Sa'Adeddin, G. Campet, Effect of annealing and of effect of annealing and of cooling rates on n-GaAs electrode photoelectrochemical characteristics, Active and passive electronic components, 27 (2004) 69-80.

[62] H.S. Hilal, A. Zyoud, M.H. Helal, H. Bsharat, H.H. Helal, C. Ali, Effects of annealing temperature and cooling rate on photo-electrochemical performance of pristine polycrystalline metal-chalcogenide film electrodes, Solar Energy, 183 (2019) 704-715.

[63] J. Shen, Z. Gai, J. Kirschner, Growth and magnetism of metallic thin films and multilayers by pulsed-laser deposition, Surface science reports, 52 (2004) 163-218.

[64] H.-S. Kim, S.-B. Ko, I.-H. Jang, N.-G. Park, Improvement of mass transport of the [Co (bpy) 3] II/III redox couple by controlling nanostructure of TiO 2 films in dye-sensitized solar cells, Chemical Communications, 47 (2011) 12637-12639.

[65] M. Nurfazliana, S.A. Kamaruddin, N. Nafarizal, H. Saim, J. Lias, M.Z. Sahdan, Direct Growth of Copper (II) Oxide (CuO) Nanostructures Films via One-Step Chemical Bath Deposition by pH Variation, in: Applied Mechanics and Materials, Trans Tech Publ, 2015, pp. 637-641.

[66] P. Poizot, C.-J. Hung, M.P. Nikiforov, E.W. Bohannan, J.A. Switzer, An electrochemical method for CuO thin film deposition from aqueous solution, Electrochemical and solid state letters, 6 (2002) C21.

[67] N. Bouazizi, R. Bargougui, A. Oueslati, R. Benslama, Effect of synthesis time on structural, optical and electrical properties of CuO nanoparticles synthesized by reflux condensation method, Adv. Mater. Lett, 6 (2015) 158-164.

[68] C.-Y. Huang, A. Chatterjee, S. Liu, S. Wu, C.-L. Cheng, Photoluminescence properties of a single tapered CuO nanowire, Applied surface science, 256 (2010) 3688-3692.

[69] Y. Yang, D. Xu, Q. Wu, P. Diao, Cu 2 O/CuO bilayered composite as a high-efficiency photocathode for photoelectrochemical hydrogen evolution reaction, Scientific reports, 6 (2016) 1-13.

[70] L. Wang, K. Zhang, Z. Hu, W. Duan, F. Cheng, J. Chen, Porous CuO nanowires as the anode of rechargeable Na-ion batteries, Nano Research, 7 (2014) 199-208.

[71] R.S. Hyam, J. Lee, E. Cho, J. Khim, H. Lee, Synthesis of copper hydroxide and oxide nanostructures via anodization technique for efficient photocatalytic application, Journal of nanoscience and nanotechnology, 12 (2012) 8396-8400.

[72] A. Aktar, S. Ahmmed, J. Hossain, A.B.M. Ismail, Solution-Processed Synthesis of Copper Oxide (Cu x O) Thin Films for Efficient Photocatalytic Solar Water Splitting, ACS omega, 5 (2020) 25125-25134.

[73] R.H.P. Devamani, M. Alagar, Synthesis and characterisation of copper II hydroxide nano particles, Nano Biomed. Eng, 5 (2013) 116-120.

[74] A. Zyoud, R.S. AlKerm, R.S. Alkerm, D. Park, M.H. Helal, G. Campet, R.W. Muthaffar, H. Kwon, H.S. Hilal, Enhanced PEC characteristics of pre-annealed CuS film electrodes by metalloporphyrin/polymer matrices, Solar Energy Materials and Solar Cells, 144 (2016) 429-437.

[75] G. Riveros, H. Gómez, R. Henríquez, R. Sshrebler, R. Cordova, R. Marotti, E. Dalchiele, Electrodeposition and characterization of ZnX (X= Se, Te) semiconductor thin films, Boletín de la Sociedad Chilena de Química, 47 (2002) 411-429.

[76] M. Dahrul, H. Alatas, Preparation and optical properties study of CuO thin film as applied solar cell on LAPAN-IPB Satellite, Procedia Environmental Sciences, 33 (2016) 661-667.

[77] Y.-F. Lim, C.S. Chua, C.J.J. Lee, D. Chi, Sol–gel deposited Cu 2 O and CuO thin films for photocatalytic water splitting, Physical Chemistry Chemical Physics, 16 (2014) 25928-25934.

Appendices

Appendix A

Important Figures and Tables

Figure (1)

Optical absorption spectra for combined EC/CB-CuO film electrodes tha are annealed then rapidly cooled.

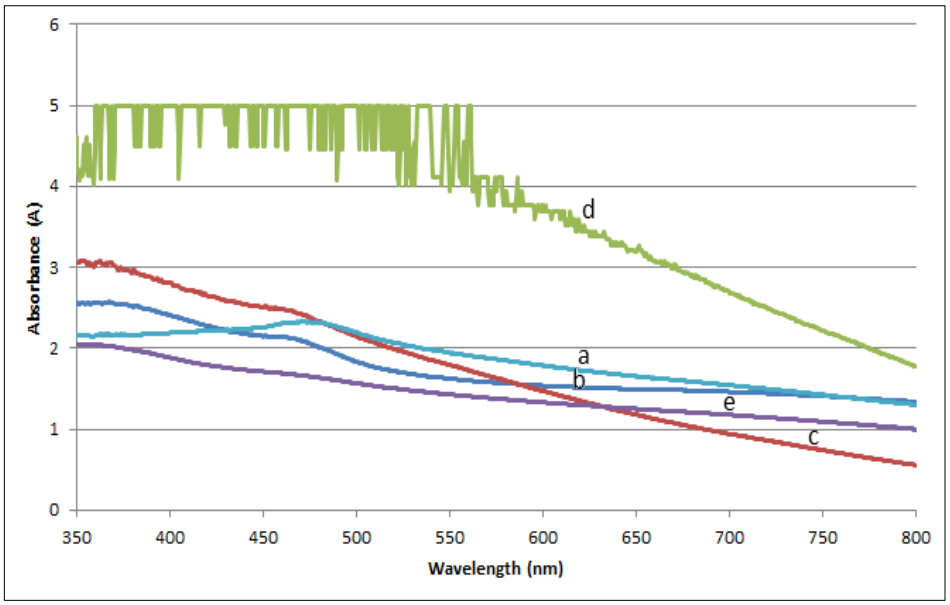

a) not annealed, b) 150℃ annealed and quickly cooled, c) 200℃ annealed and quickly cooled, d) 250℃ annealed and quickly cooled, e) 300℃ annealed and quickly cooled.

Table (1)

Band-gap values for combined EC/CB-CuO/FTO/glass films that annealed at different temperatures, rapidly cooled.

Sample	Annealing temperature °C	E_{bg} (eV)	λ_{bg} (nm)
A	Not annealed	1.95	636
B	150	1.80	689
C	200	1.70	729
D	250	1.60	755
E	300	1.40	886

Figure (2)

Optical absorption spectra for combined EC/CB-CuO film electrodes that are annealed then slowly cooled.

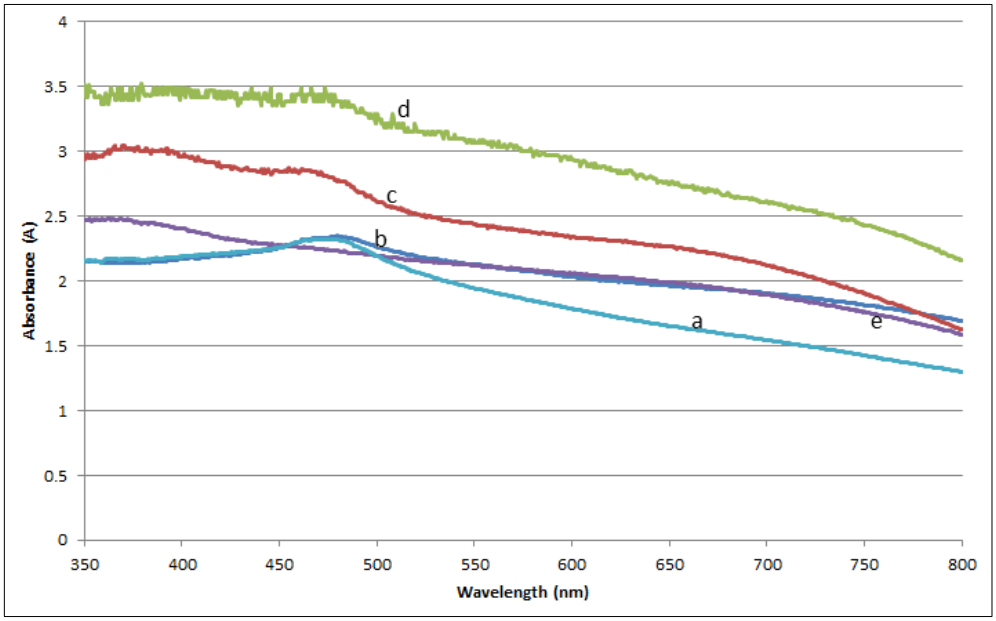

a) not annealed, b) 150℃ annealed and slowly cooled, c) 200℃ annealed and slowly cooled, d) 250℃ annealed and slowly cooled, e) 300℃ annealed and slowly cooled.

Table (2)

Values of optical band gaps for combined EC/CB-CuO/FTO/glass films annealed at various temperatures, slowly cooled.

Sample	Annealing temperature °C	E_{bg} (eV)	λ_{bg} (nm)
A	Not annealed	1.95	636
B	150	1.75	709
C	200	1.60	775
D	250	1.50	827
E	300	1.35	919

Figure (3)

SEM images for combined EC/CB-CuO thin films annealed at 300℃ annealed and a) rapidly cooled, b) slowly cooled.

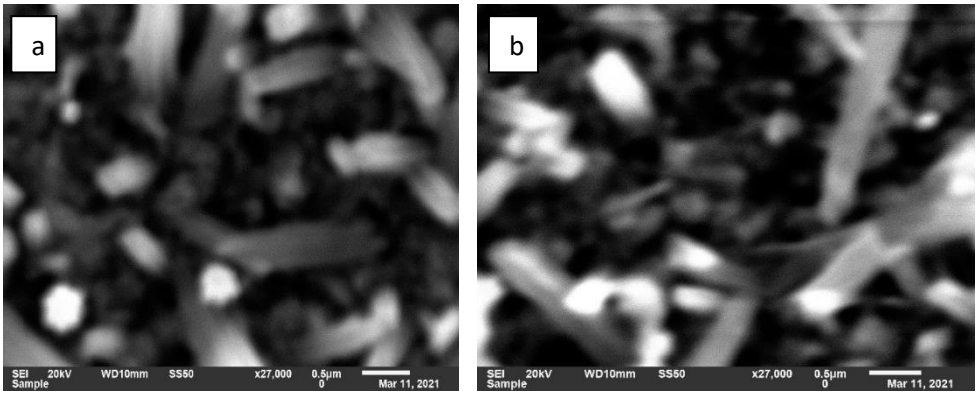

Figure (4)

Photo J-V plots measured for combined EC/CB-CuO electrodes that are annealed then quickly cooled.

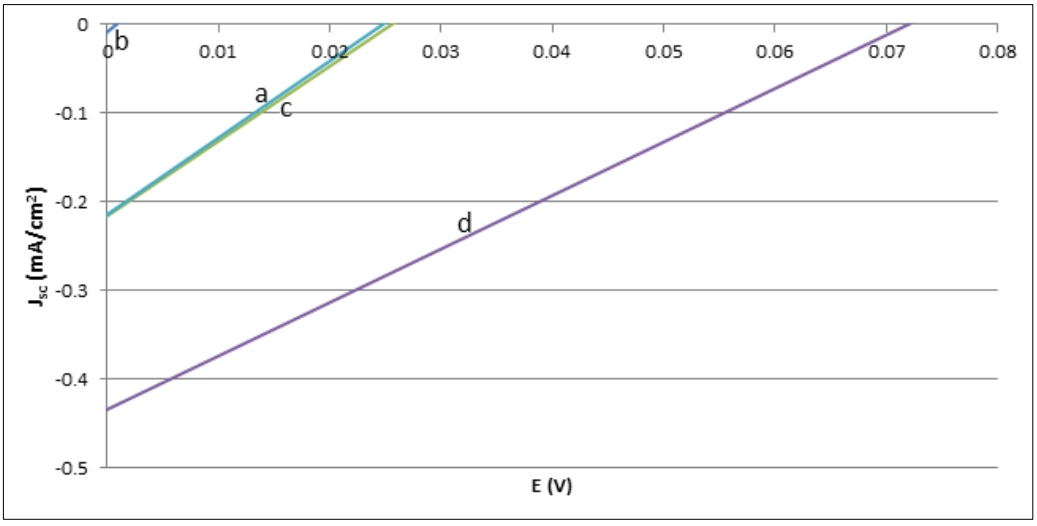

a) not annealed, b) 150℃ annealed and quickly cooled, c) 250℃ annealed and quickly cooled, d) 300℃ annealed and quickly cooled.

Table (3)

PEC characteristics for combined EC/CB-CuO/FTO/glass films annealed at various temperatures and rapidly cooled.

Sample	Annealing temperature ºC	V_{OC} (V)	J_{SC} (mA/cm^2)	ɳ %	FF%
A	Not annealed	0.025	0.21	0.15	24.76
B	150	0	0	0	0
C	250	0.026	0.21	0.015	23.81
D	300	0.072	0.43	0.085	23.74

Figure (5)

Photo J-V plots for combined EC/CB-CuO electrodes that are annealed then slowly cooled.

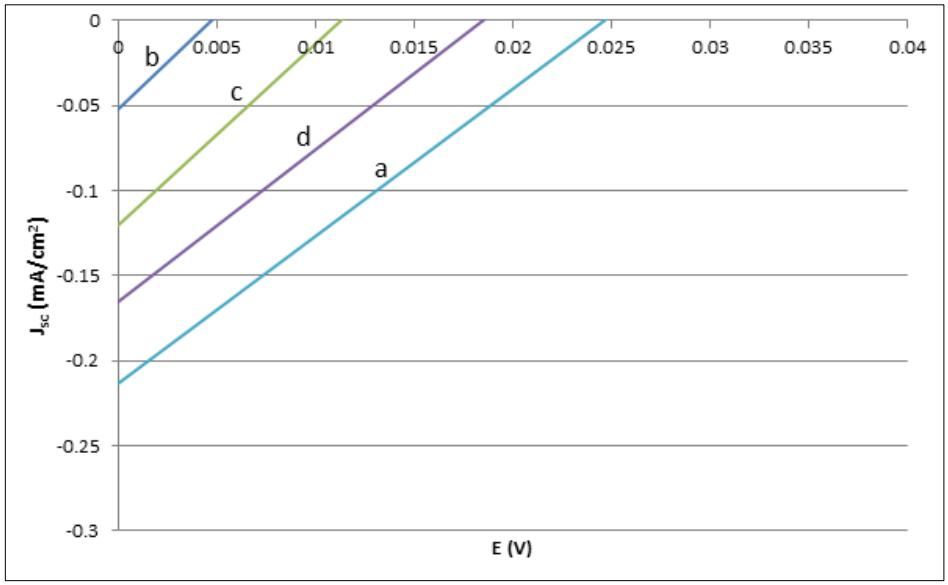

a) non-annealed, b) annealed at 150℃, slowly cooled, c) annealed at 250℃, slowly cooled, d) annealed at 300℃, slowly cooled.

Table (4)

PEC characteristics for combined EC/CB-CuO/FTO/glass films annealed at various temperatures and slowly cooled.

Sample	Annealing temperature °C	V_{OC} (V)	J_{SC} (mA/cm^2)	η %	FF%
A	Not annealed	0.025	-0.21	0.015	25.14
B	150	0.005	-0.05	0.001	25.00
C	250	0.011	-0.12	0.004	27.27
D	300	0.019	-0.16	0.007	20.72

Figure (6)

J_{sc} vs. time plots for some CuO films.

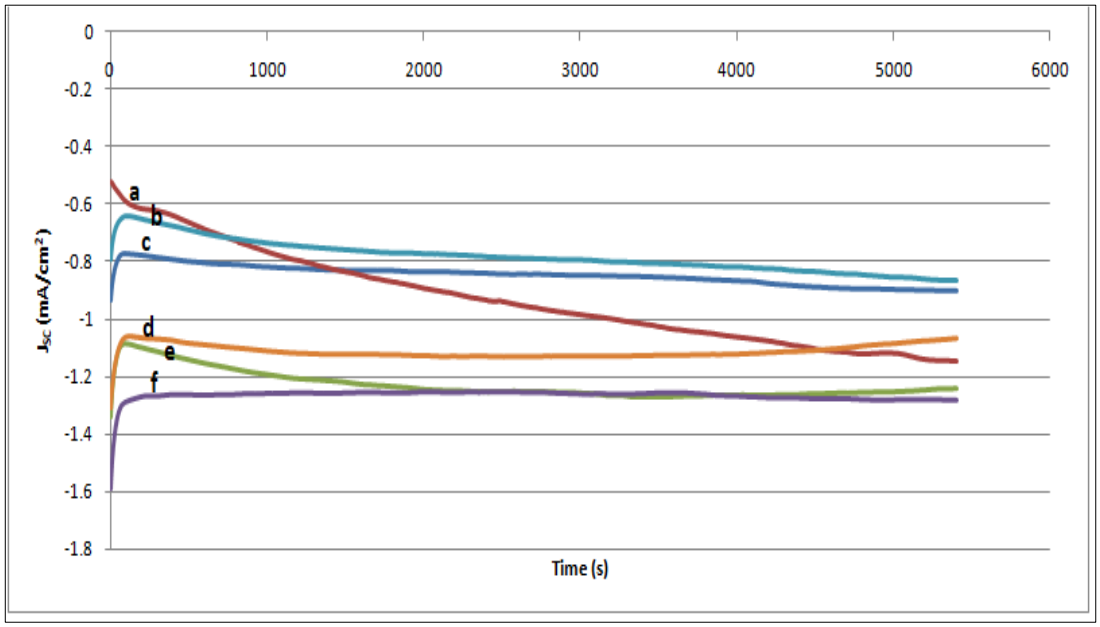

a) ECD and annealed at 150 ˚C but quickly cooled, b) ECD and annealed at 250 ˚C but slowly cooled, c) CBD and annealed at 150 ˚C rapidly cooled, d) combined EC/CB deposited and annealed at 250 ˚C slowly cooled, e)combined EC/CB deposited and annealed at 150 ˚C rapidly cooled and f) CBD and annealed at 250 ˚C slowly cooled.

Appendix B

Tauc Plots

Figure 1

Tauc plot from UV-Vis analysis of CuO/FTO/glass chemical path deposited film annealed at 150 ˚C, rapidly cooled.

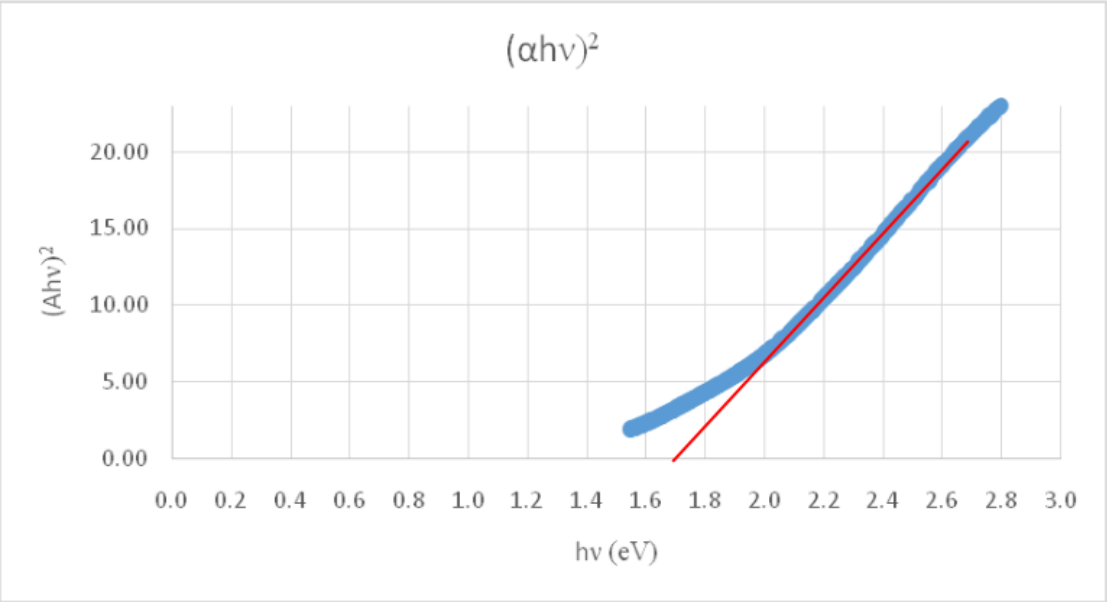

Figure 2

Tauc plot from UV-Vis analysis of CuO/FTO/glass chemical path deposited film, annealed at 200 ˚C, rapidly cooled.

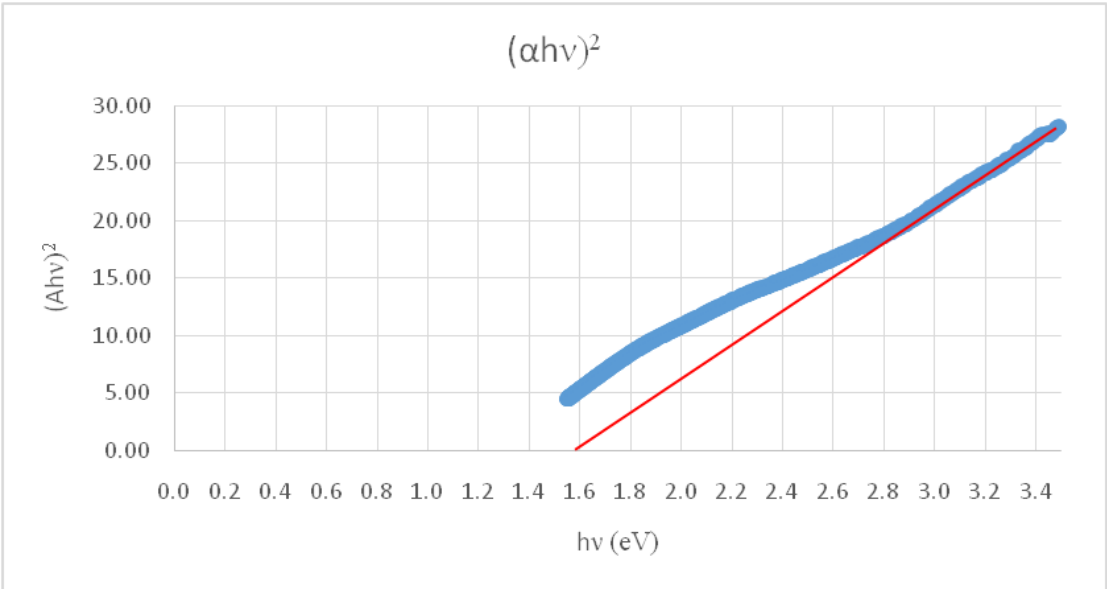

Figure 3

Tauc plot from UV-Vis analysis of CuO/FTO/glass chemical path deposited film, annealed at 250 ˚C, rapidly cooled.

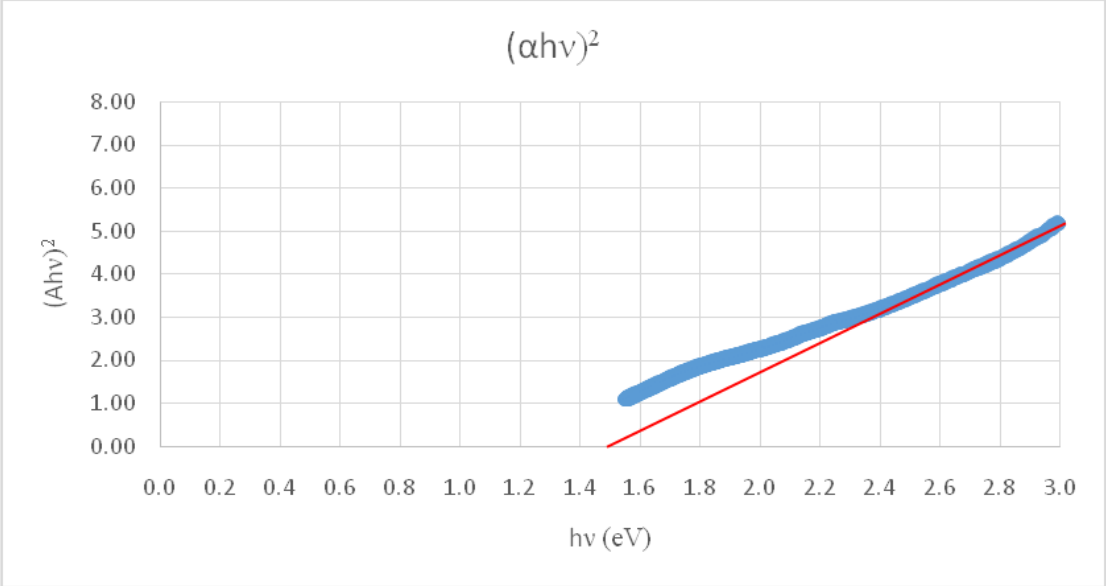

Figure 4

Tauc plot from UV-Vis analysis of CuO/FTO/glass chemical path deposited film annealed at 300 ˚C, rapidly cooled.

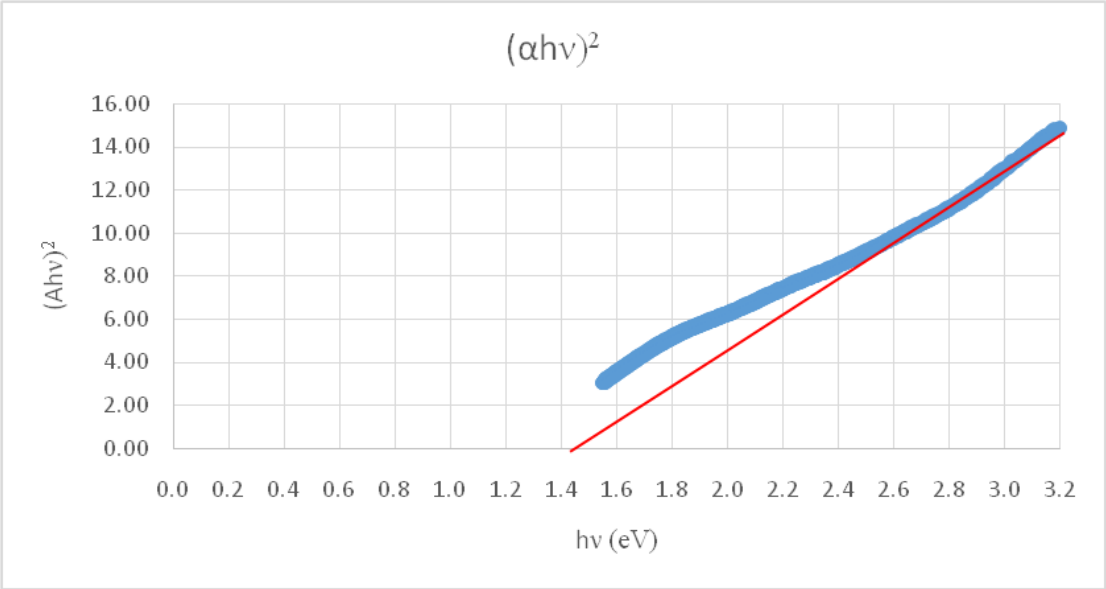

Figure 5

Tauc plot from UV-Vis analysis of CuO/FTO/glass chemical path deposited film, nonannealed.

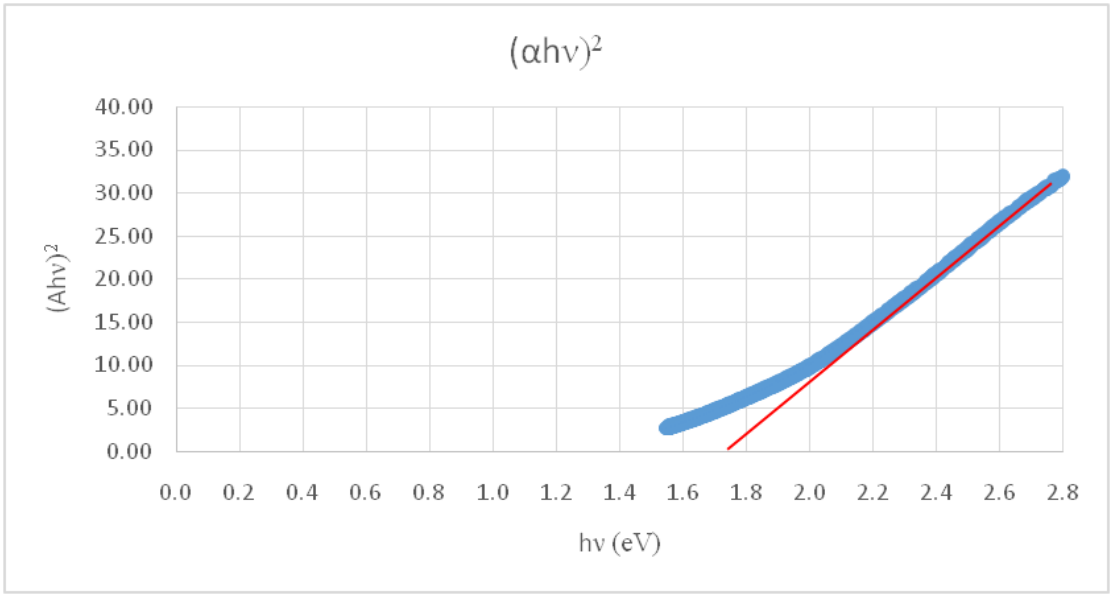

Figure 6

Tauc plot from UV-Vis analysis of CuO/FTO/glass chemical path deposited film, annealed at 150 ˚C, slowly cooled.

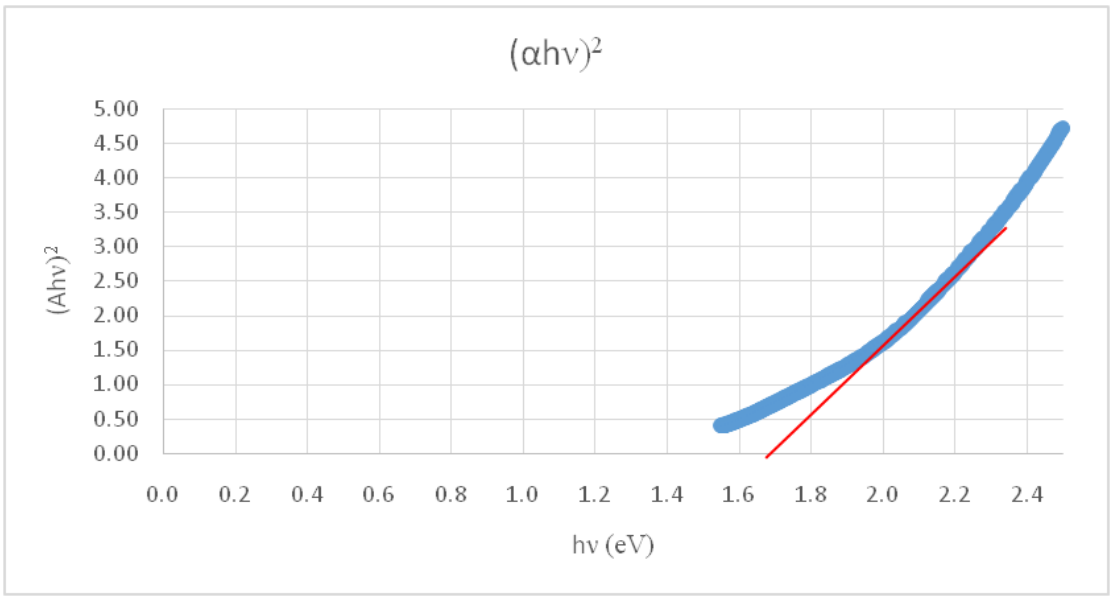

Figure 7

Tauc plot from UV-Vis analysis of CuO/FTO/glass chemical path deposited film, annealed at 200 ˚C, slowly cooled.

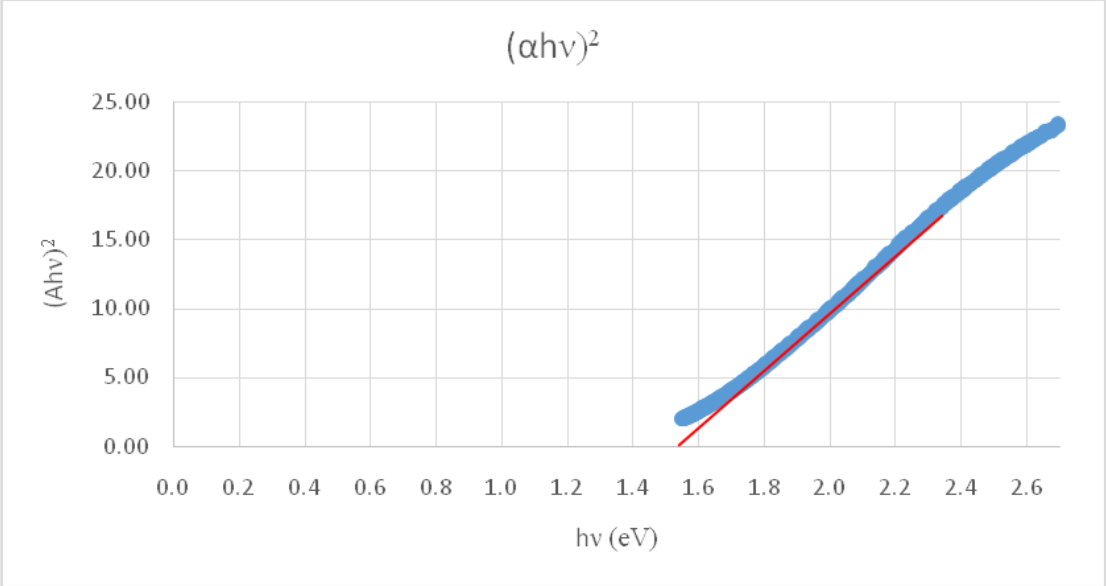

Figure 8

Tauc plot from UV-Vis analysis of CuO/FTO/glass chemical path deposited film, annealed at 250 ˚C, slowly cooled.

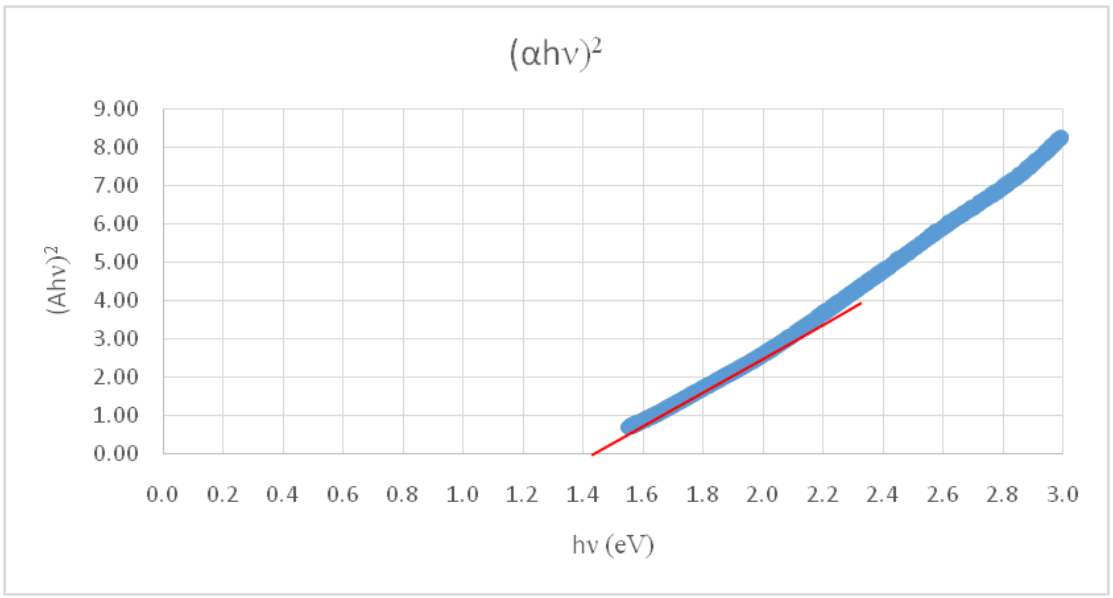

Figure 9

Tauc plot from UV-Vis analysis of CuO/FTO/glass chemical path deposited film, annealed at 300 ˚C, slowly cooled.

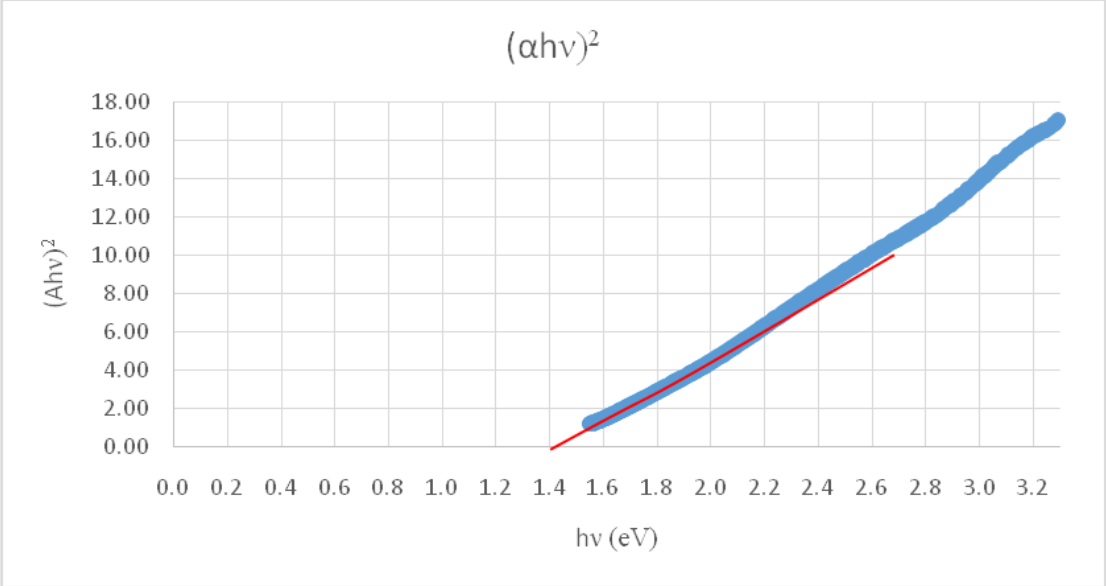

Figure 10

Tauc plot from UV-Vis analysis of CuO/FTO/glass electrodeposited film, nonannealed.

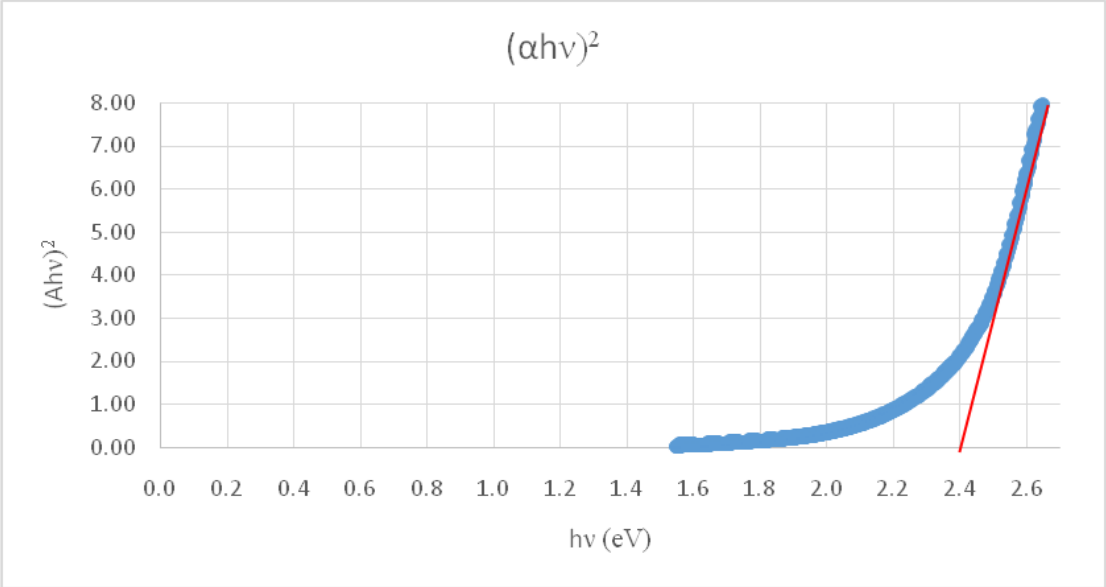

Figure 11

Tauc plot from UV-Vis analysis of CuO/FTO/glass electrodeposited film, annealed at150 ˚C, rapidly cooled.

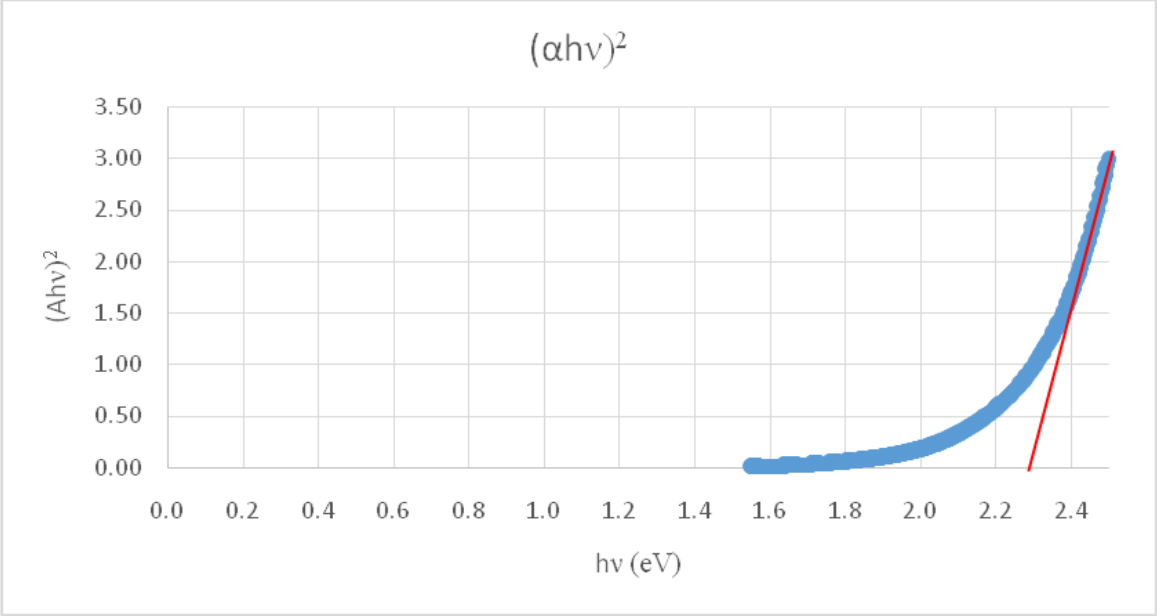

Figure 12

Tauc plot from UV-Vis analysis of CuO/FTO/glass electrodeposited film, annealed at 200 ˚C, rapidly cooled.

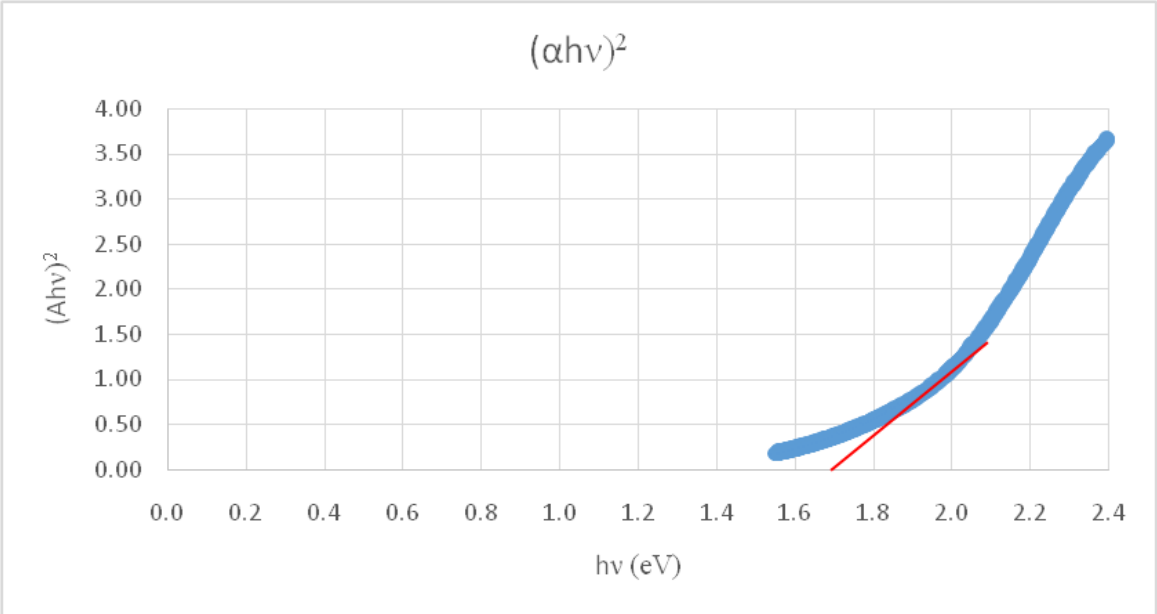

Figure 13

Tauc plot from UV-Vis analysis of CuO/FTO/glass electrodeposited film, annealed at 250 ˚C, rapidly cooled.

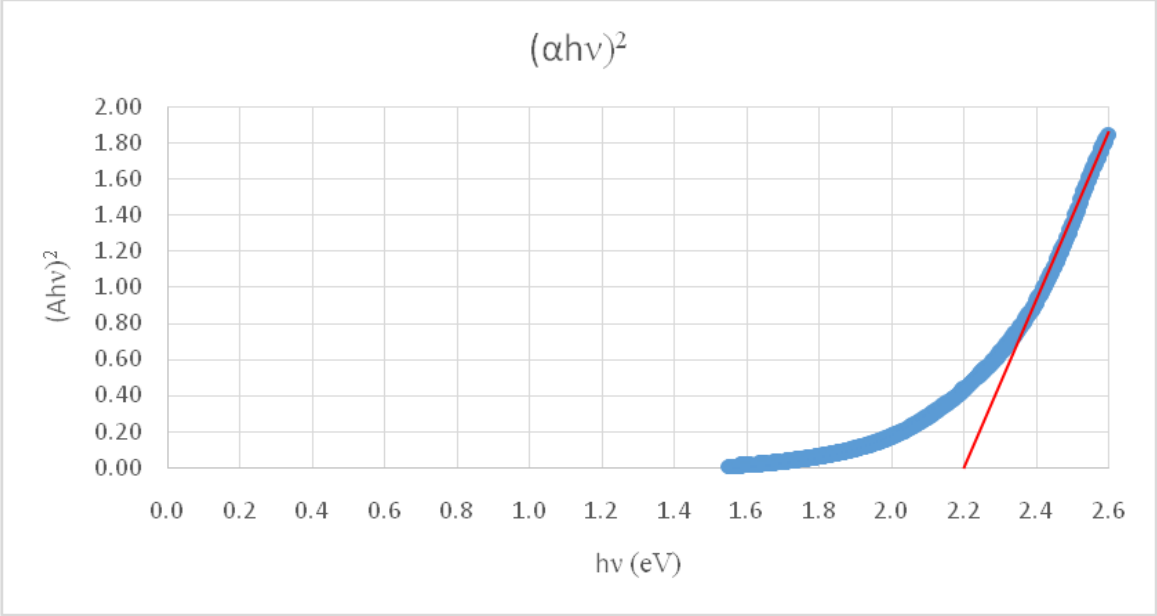

Figure 14

Tauc plot from UV-Vis analysis of CuO/FTO/glass electrodeposited film, annealed at 300 ˚C, rapidly cooled.

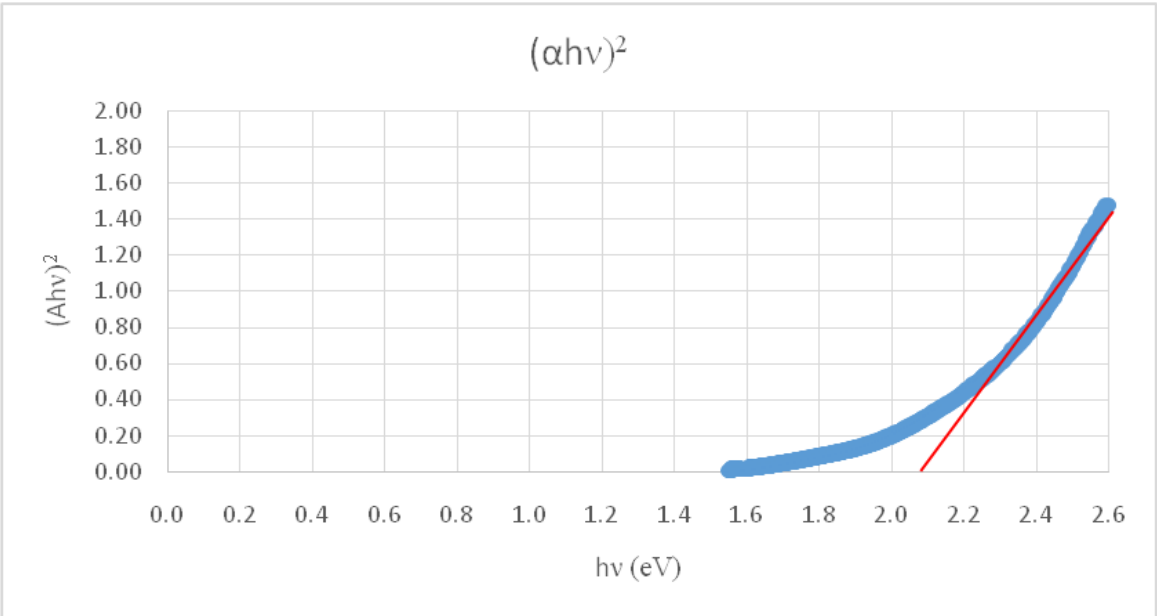

Figure 15

Tauc plot from UV-Vis analysis of CuO/FTO/glass electrodeposited film, annealed at 150 ˚C, slowly cooled.

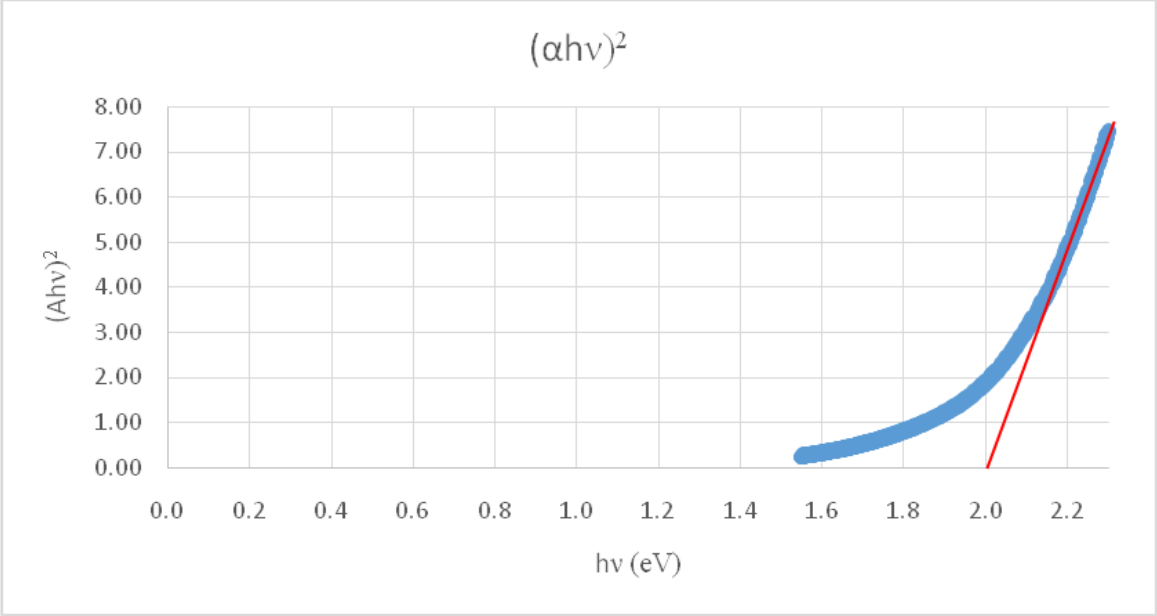

Figure 16

Tauc plot from UV-Vis analysis of CuO/FTO/glass electrodeposited film, annealed at 200 ˚C, slowly cooled.

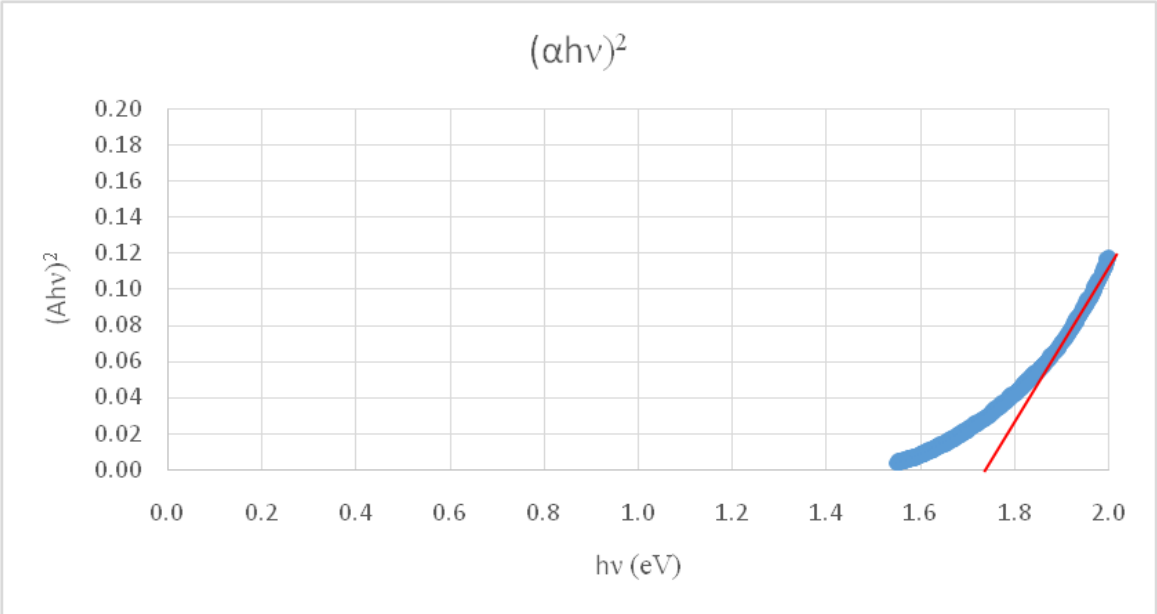

Figure 17

Tauc plot from UV-Vis analysis of CuO/FTO/glass electrodeposited film, annealed at 250 ˚C, slowly cooled.

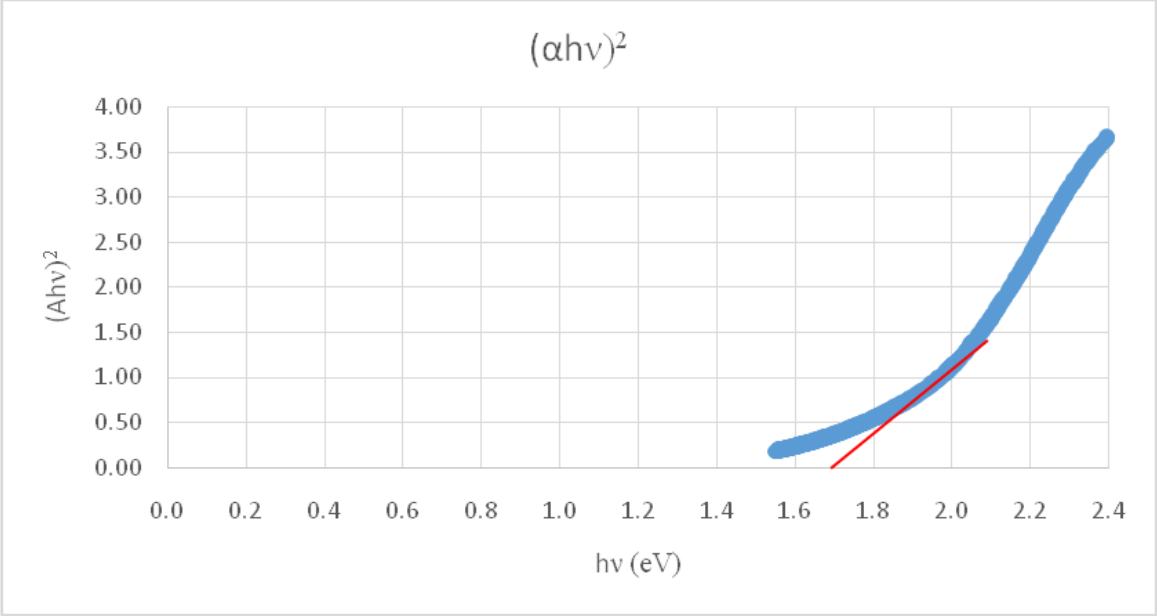

Figure 18

Tauc plot from UV-Vis analysis of CuO/FTO/glass electrodeposited film, annealed at 300 ˚C, slowly cooled.

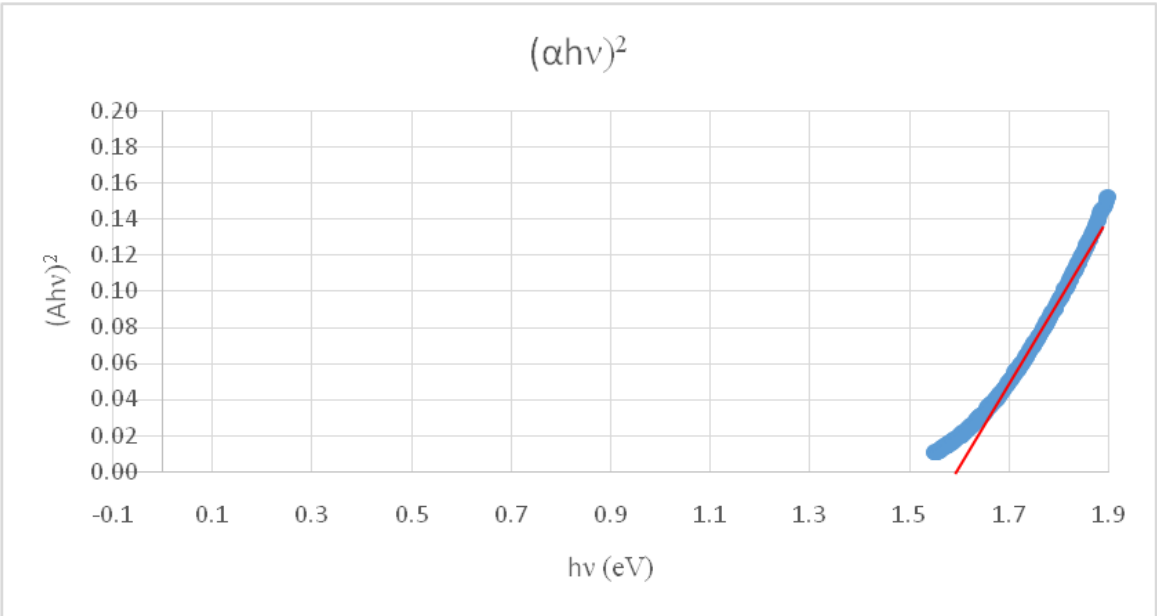

Figure 19

Tauc plot from UV-Vis analysis of CuO/FTO/glass electrodeposited film for 2 min.

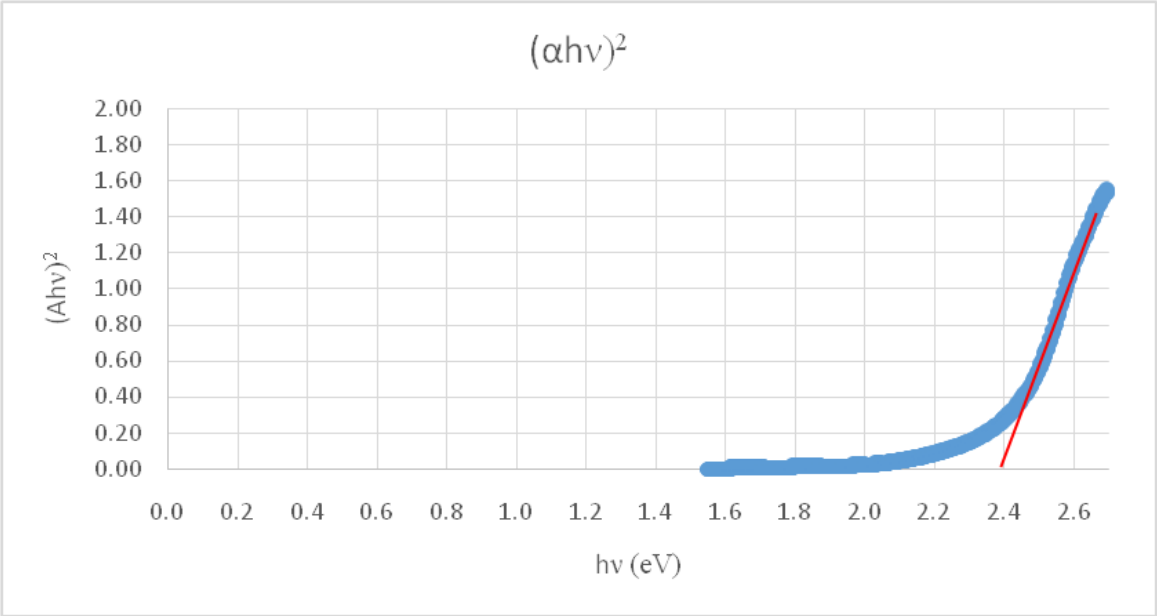

Figure 20

Tauc plot from UV-Vis analysis of CuO/FTO/glass electrodeposited film for 4 min.

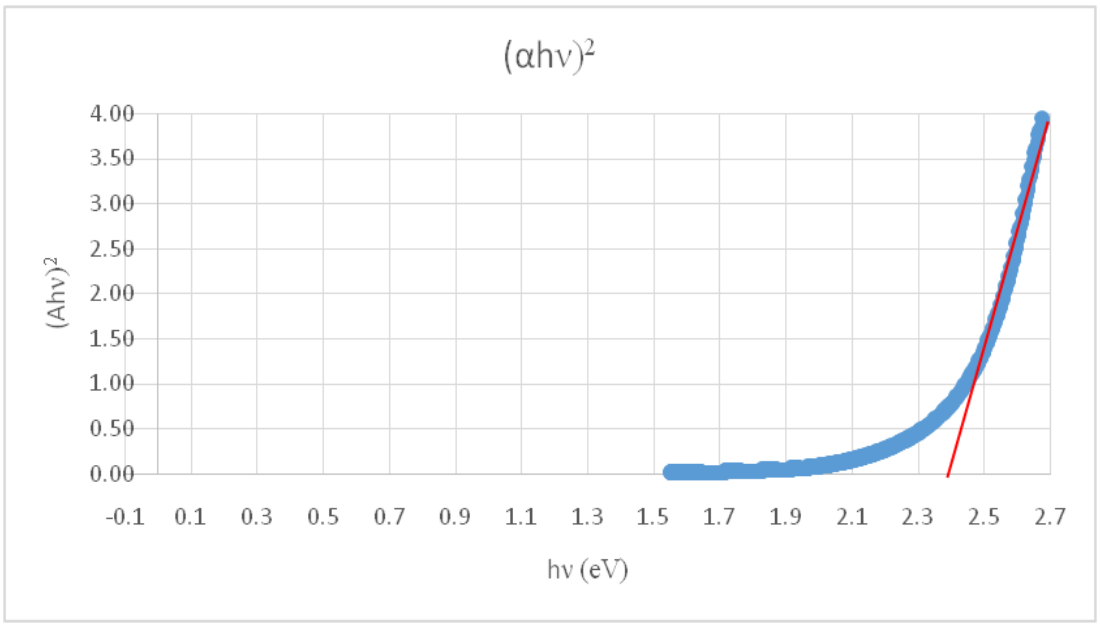

Figure 21

Tauc plot from UV-Vis analysis of CuO/FTO/glass electrodeposited film for 6 min.

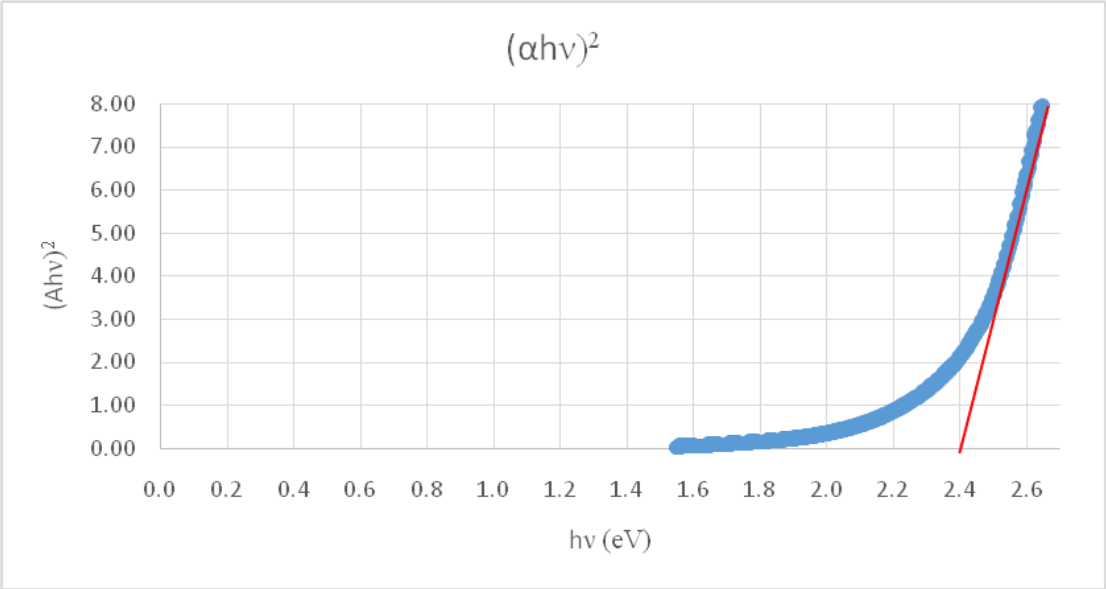

Figure 22

Tauc plot from UV-Vis analysis of CuO/FTO/glass electrodeposited film for 8 min.

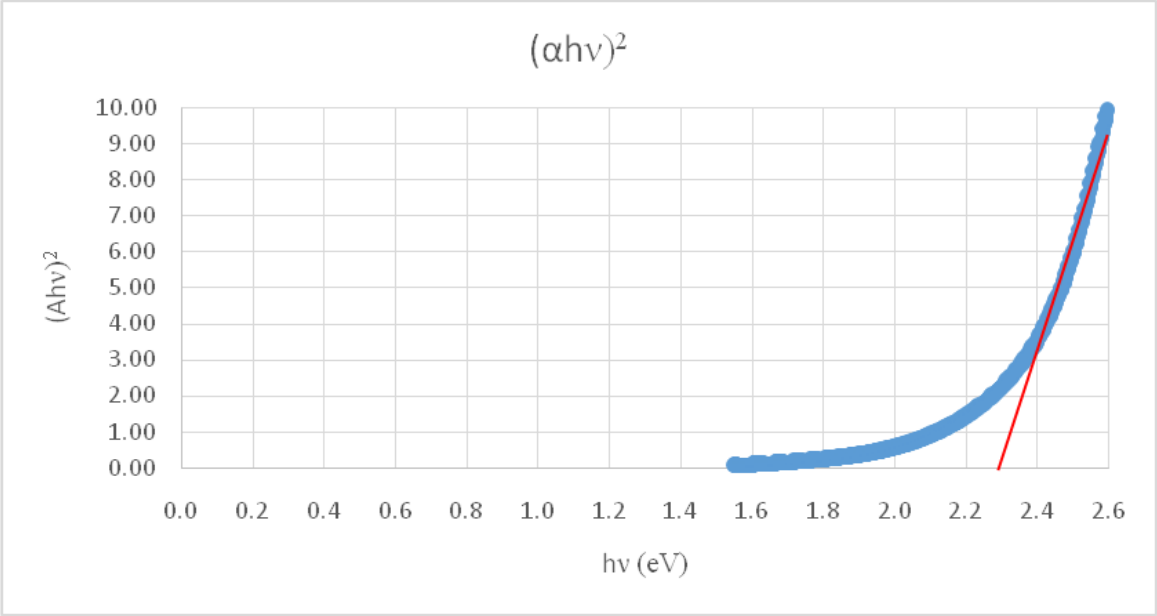

Figure 23

Tauc plot from UV-Vis analysis of CuO/FTO/glass electrodeposited film for 10 min.

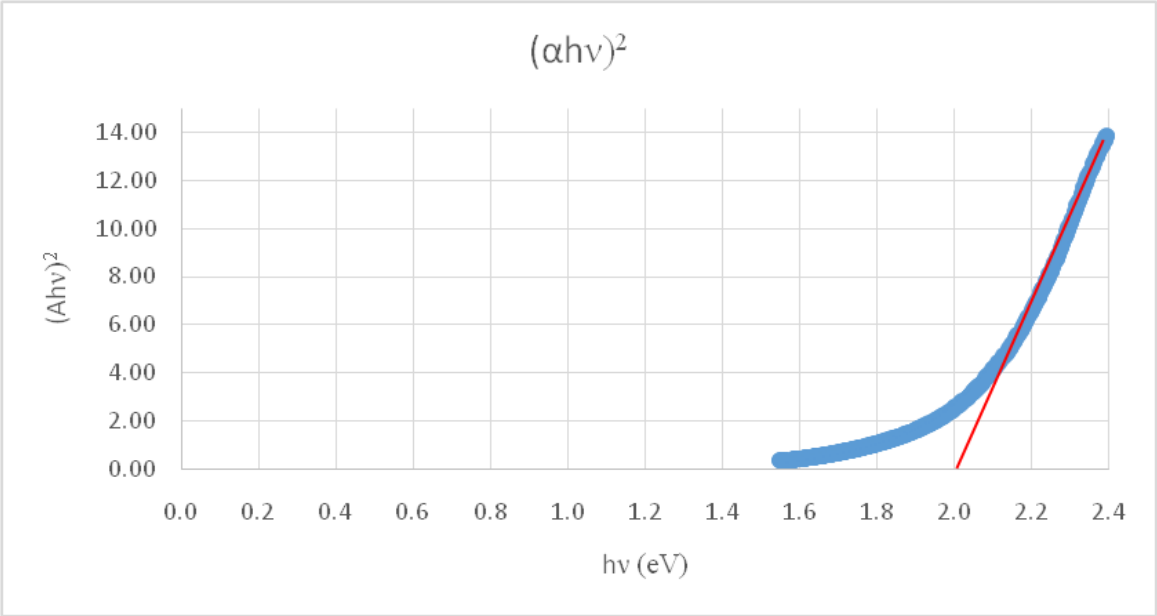

Figure 24

Tauc plot from UV-Vis analysis of CuO/FTO/glass combined electrochemical and chemical path deposition film, non annealed.

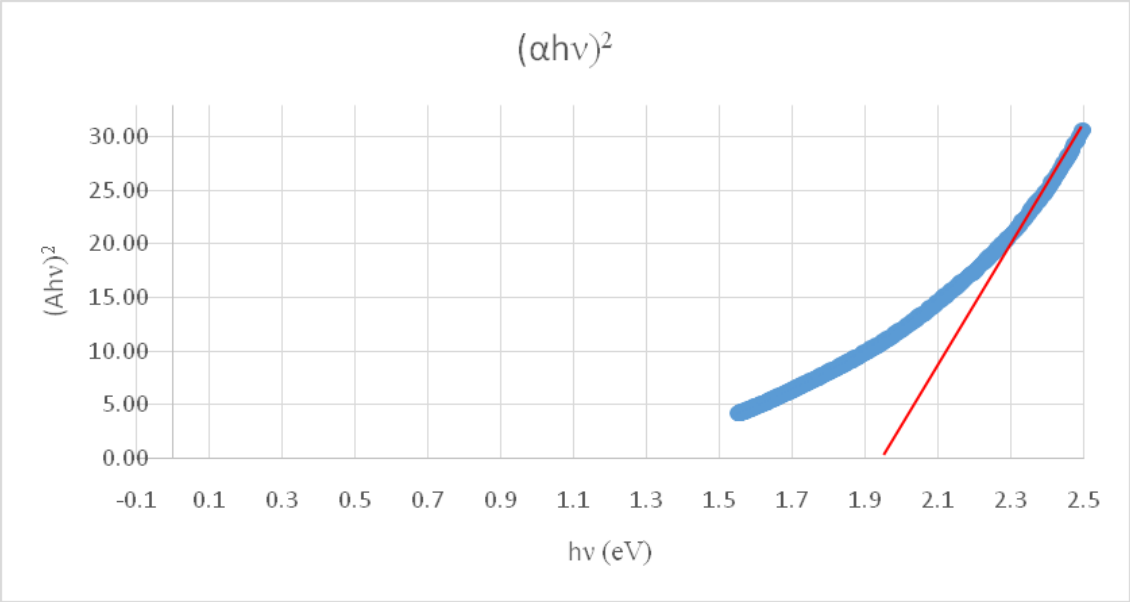

Figure 25

Tauc plot from UV-Vis analysis of CuO/FTO/glass combined electrochemical and chemical path deposition film, annealed at 150˚C, rapidly cooled.

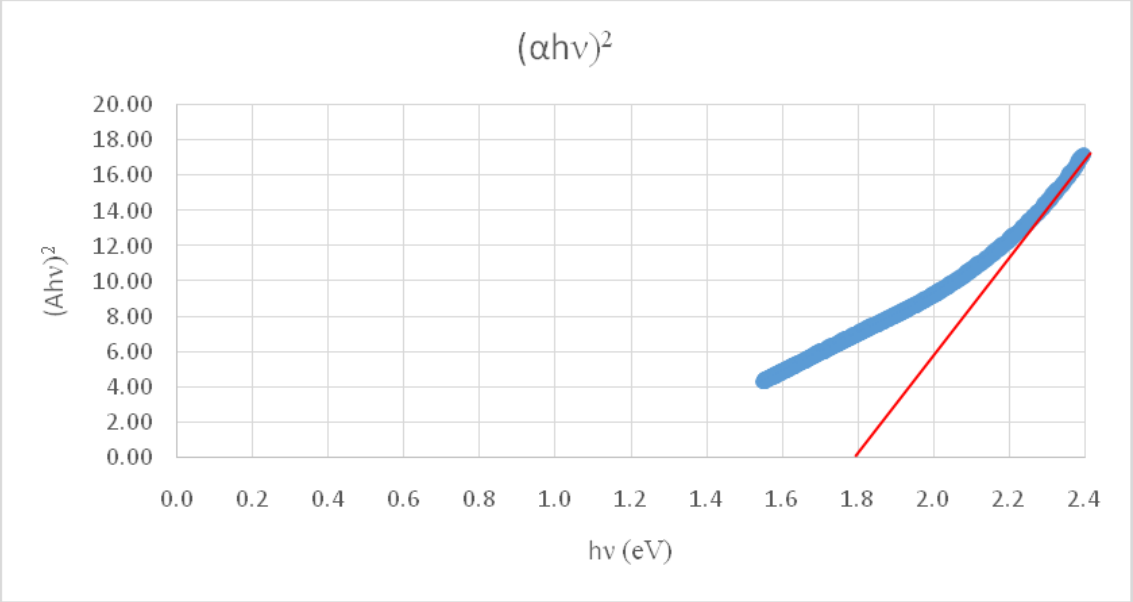

Figure 26

Tauc plot from UV-Vis analysis of CuO/FTO/glass combined electrochemical and chemical path deposition film, annealed at 200˚C, rapidly cooled.

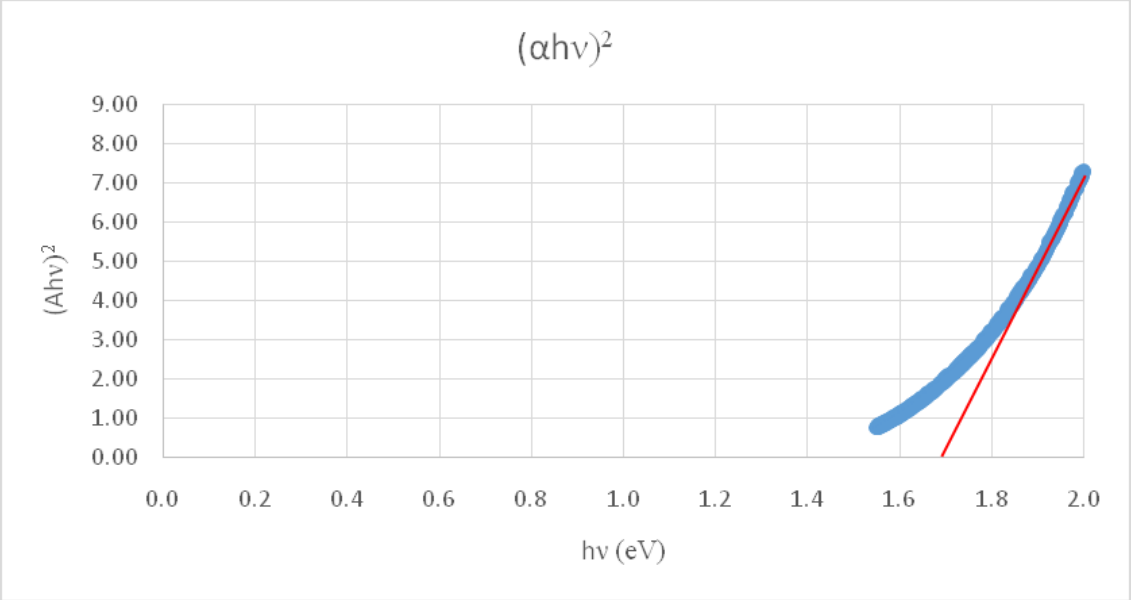

Figure 27

Tauc plot from UV-Vis analysis of CuO/FTO/glass combined electrochemical and chemical path deposition film, annealed at 250 ˚C, rapidly cooled.

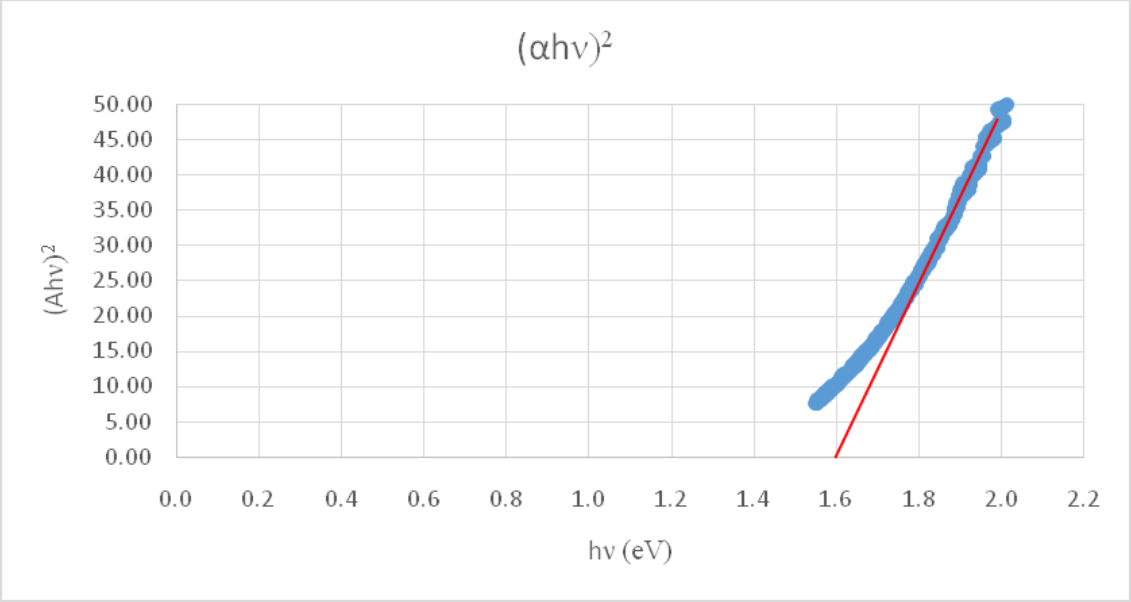

Figure 28

Tauc plot from UV-Vis analysis of CuO/FTO/glass combined electrochemical and chemical path deposition film, annealed at 300 ˚C, rapidly cooled.

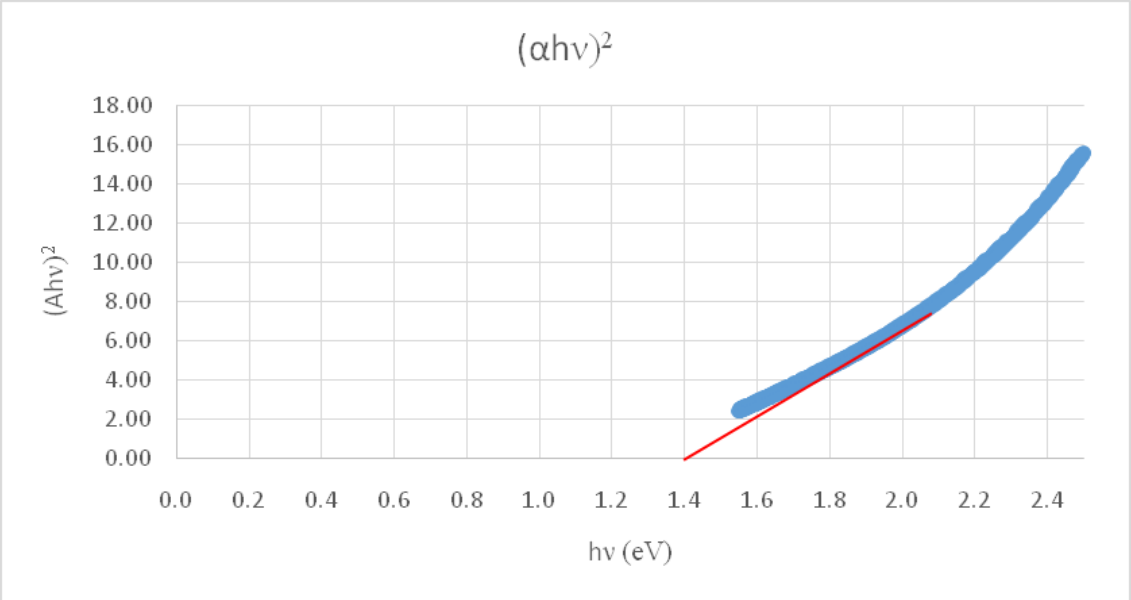

Figure 29

Tauc plot from UV-Vis analysis of CuO/FTO/glass combined electrochemical and chemical path deposition film, annealed at 150 ˚C, slowly cooled

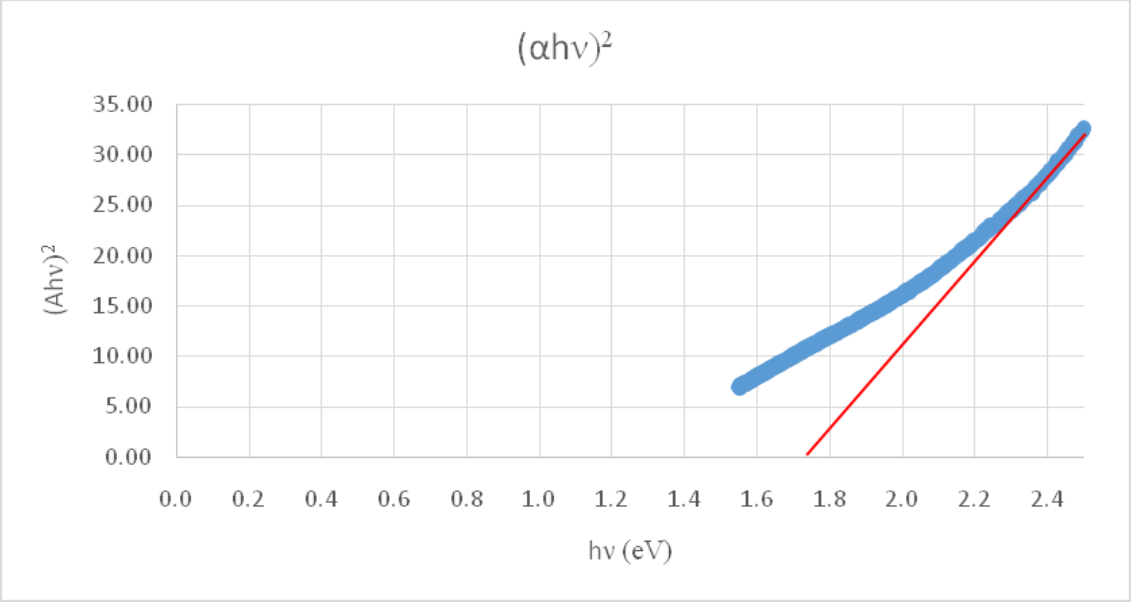

Figure 30

Tauc plot from UV-Vis analysis of CuO/FTO/glass combined electrochemical and chemical path deposition film, annealed at 200˚C, slowly cooled.

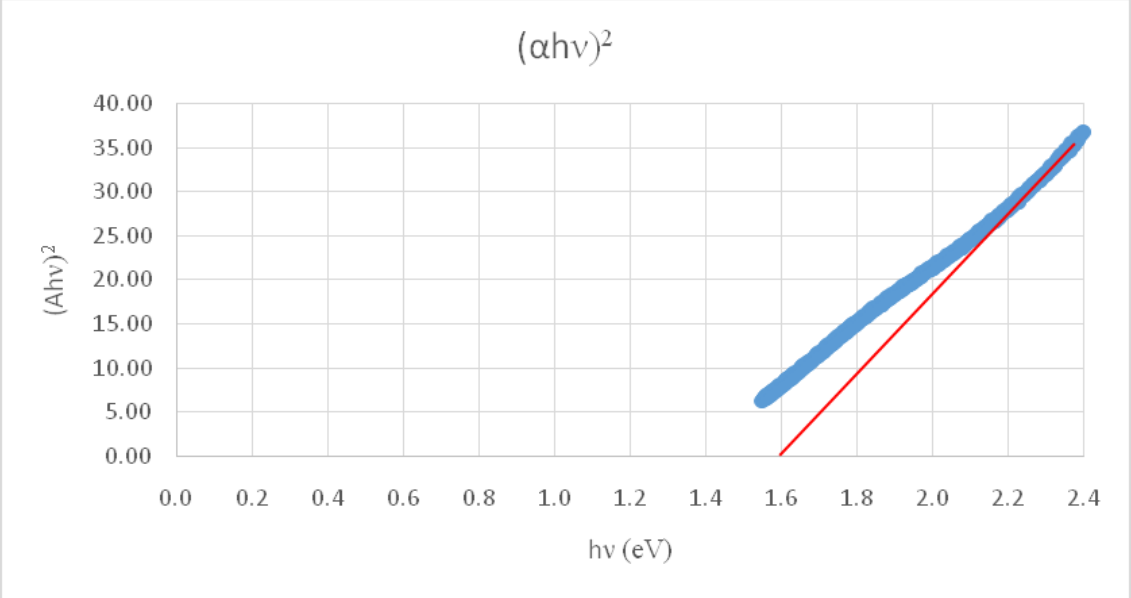

Figure 31

Tauc plot from UV-Vis analysis of CuO/FTO/glass combined electrochemical and chemical path deposition film, annealed at 250 ˚C, slowly cooled.

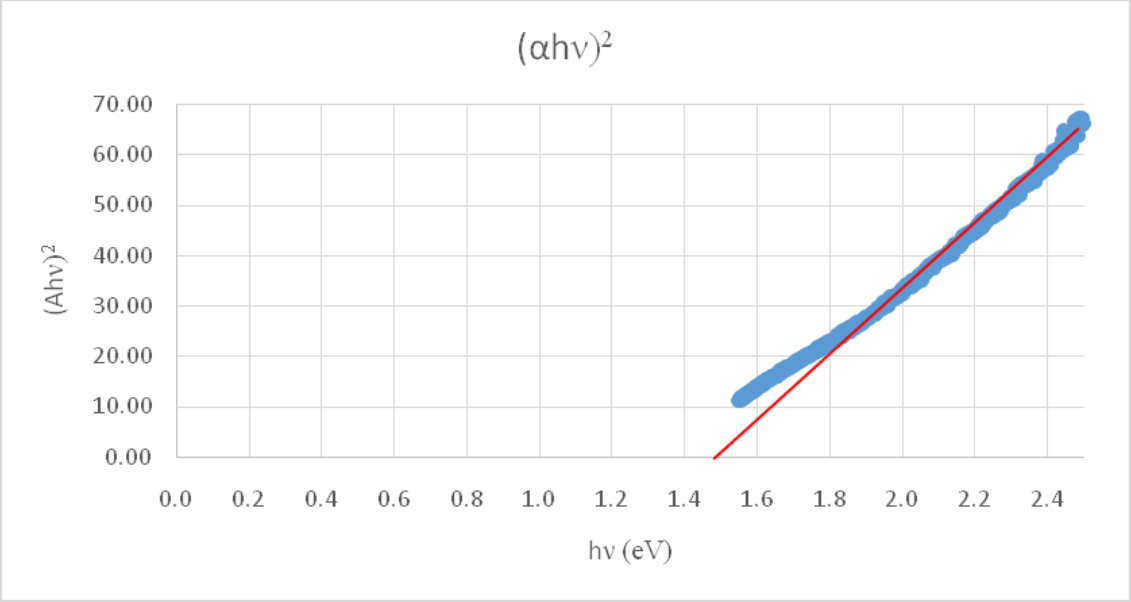

Figure 32

Tauc plot from UV-Vis analysis of CuO/FTO/glass combined electrochemical and chemical path deposition film, annealed at 300˚C, slowly cooled.

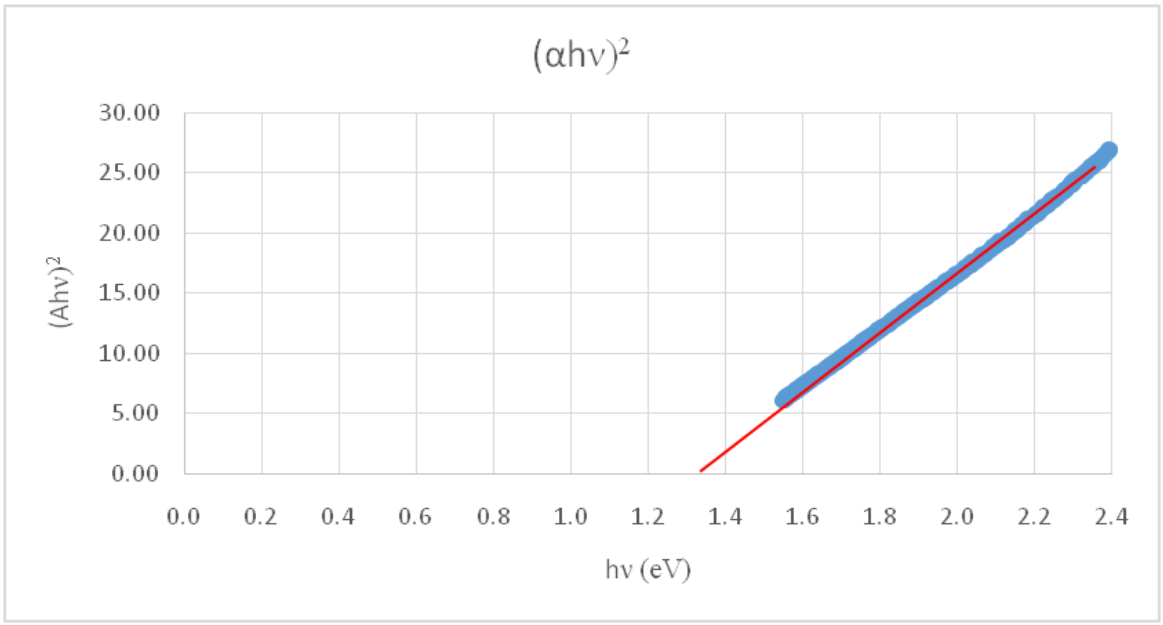

جـامعـــة النجاح الوطنية

كليـــة الدراســـات العليـــا

أفلام CuO المحضرة بالترسيب الكهروكيميائي والكيميائي المشترك

إعداد

سندس وليد "محمد علي" عمرية

إشراف

د. عاهد زيود

أ.د. حكمت هلال

قدمت هذه الرسالة استكمالا لمتطلبات الحصول على درجة الماجستير في الكيمياء من كلية الدراسات العليا في جامعة النجاح الوطنية، نابلس– فلسطين.

2022

أفلام CuO المحضرة بالترسيب الكهروكيميائي والكيميائي المشترك

إعداد

سندس وليد "محمد علي" عمرية

إشراف

د. عاهد زيود

أ.د. حكمت هلال

الملخص

خلفية الدراسة: تظهر الأفلام الرقيقة أهمية كبيرة في تكنولوجيا الطاقة الشمسية لإنتاج الكهرباء من الضوء. CuO هو أحد الأمثلة على أشباه الموصلات الشائعة التي لم تسفر عن أداء كهروضوئي عالي (PEC). هذه مشكلة يجب حلها.

الأهداف: تهدف هذه الدراسة لانتاج أفلام CuO الرقيقة ذات كفاءة عالية في تحويل الضوء إلى كهرباء. سيتم ترسيب هذه الأفلام بثلاث طرق مختلفة ثم ستتم المقارنة بين خصائص الافلام المحضرة وذلك بعد تعديلها بواسطة التسخين لدرجات حرارة مختلفة والتبريد السريع والبطيء.

المنهجية: تم استخدام ثلاث تقانات من أجل ترسيب أفلام CuO الرقيقة على شرائح زجاجية مغطاة بطبقة رقيقة وشفافة وموصلة من أكسيد القصدير المزود بالفلور FTO . الطريقة الأولى هي طريقة الترسيب الكيميائي CBD والثانية طريقة الترسيب الكهربي ECD وفي الطريقة الثالثة تم الجمع بين الترسيب الكهربي والكيميائي ECD/CBD . ثم تمت دراسة خصائص الأفلام المحضرة باستخدام عدة تقنيات تتضمن: أطياف انحراف أشعة إكس (XRD) وأطياف الإمتصاص. كما تم دراسة كفاءة هذه الأفلام في تحويل الضوء إلى كهرباء، حيث تم دراسة الصفات التالية: منحنيات كثافة تيار الإضاءة مقابل الجهد (photo J–V plots)، وكثافة تيار الدارة القصيرة (J_{sc})، وجهد الدارة المفتوح (V_{OC}) ، واستقرار هذه الخلايا أمام الضوء.

النتائج: أظهرت النتائج أن أفلام CuO المحضرة بالطرق المختلفة ذات كفاءة منخفضة نوعا ما في تحويل الضوء إلى كهرباء. وقد كانت أفلام الترسيب الكيميائي أعلى كفاءة من تلك المحضرة بالطرق الاخرى لكنها تحتاج إلى تسخين على درجات حرارة أعلى من 150 °س للتخلص من هيدروكسيد النحاس الناتج أثناء الترسيب. في المقابل فإن التسخين على درجات حرارة عالية جدا يؤثر سلبا على الأفلام لان CuO لديه حزمة فراغية band gap صغيرة (1.3–2.1 الكترون فولت). كما لوحظ أن الجمع بين طريقتي الترسيب الكهربي والكيميائي لم تحسن من صفات الأفلام على عكس التوقعات، لكن الأفلام المنتجة أظهرت استقرارا جيدا أمام الضوء في النهاية.

التوصيات: أفلام CuO المحضرة لم تعطي كفاءة عالية في تحويل الضوء إلى كهرباء عموما. الأفلام التي تم تحضيرها بطريقة الترسيب الكيميائي لديها أفضل كفاءة لكنها تحتاج إلى التسخين على درجة حرارة أكبر من150 °س للتخلص من هيدروكسيد النحاس الناتج أثناء التحضير. ولأن أكسيد النحاس لديه حزمة فراغية صغيرة نسبيا فهو حساس جدا لدرجات الحرارة المرتفعة. في المقابل أعطت الأفلام المحضرة بطريقة الترسيب الكهربي ثباتا أكبر أمام درجات الحرارة المرتفعة ولكن كفاءته أقل في تحويل الضوء إلى كهرباء. أما الأفلام المحضرة بطريقة الجمع بين الترسيب الكهربي والكيميائي فلم تعطي أداء جيدا في تحويل الضوء إلى كهرباء.

المقترحات: تحضير أفلام CuO الرقيقة مع بعض التعديلات مثل تغطيتها بأنابيب نانو الكربون متعددة الجدران (MWCNT). يمكن أيضا دراسة تأثير درجات حرارة أخرى على خصائص الأفلام المحضرة. الأفلام المحضرة بطريقة الترسيب الكهربي يمكن إعادة ترسيبها عدة مرات لتحسين الخصائص. كما يمكن استخدام بعض الشوائب وأيضا يمكن الترسيب على مادة أخرى مثل ITO.

الكلمات المفتاحية: أفلام رقيقة، ترسيب كيميائيCBD، ترسيب كهربي ECD، الجمع بين الترسيب الكهربي والكيميائي ECD/CBD، تسخين.